The Schwinger Variational Principle Applied to Molecular Photoionization

Thesis by

Maile Elizabeth Smith

In Partial Fulfillment of the Requirements
for the Degree of
Doctor of Philosophy

California Institute of Technology
Pasadena, California

1985

(Submitted September 24, 1984)

ACKNOWLEDGMENTS

The years I spent at Caltech have been some of the best of my life. I had a great (albeit low-paying) job, flexible hours, loads of vacation, and the opportunity to live in such a dynamic and interesting place as Southern California. However, my best memories will be of the people I knew and the times spent with them. Because I sometimes neglected to thank them in person, I ought to get it in writing, so they'll know how much I appreciate their friendship and kindness.

I'd like to thank Professor Vincent McKoy for putting up with me for five years. His patience, support, and advice were always appreciated and his enthusiasm and knowledge were very helpful in my research endeavors.

As my time at Caltech comes to an end, I already tend to forget the few trying and stressful periods of my stay here. Maybe that is due to the support and caring of friends like Jack Kaye, Margaret Carter, Dave Wardlaw, Chris McDade, and Puvin Pichaichanarong. With friends like these, it's hard to stay depressed for too long. I was extremely fortunate in my choice of roommates -- in Diane Hood and Laura Gilliom I not only found compatible roomates, but great friends. Lisa McElwee-White was always there as a friend and confidante; I will always be grateful to her for spending hours on end with me and for mentioning me in her thesis.

My coworkers were always a source of inspiration, information, and entertainment. I will forever be indebted to Robert Lucchese for his help and guidance, especially during my first two years of graduate school. Working with Diane Lynch on Chapter III of this thesis was a real treat. She, Tom

Gibson, and Marco Lima were extremely helpful in proofreading and discussing the material in this thesis.

There were also friends from home who were just as helpful to me during the last five years. Kay Seymer-Munday deserves a special mention for writing to me constantly with words of encouragement and news from home. Aunt Jelli was always happy to visit and spend time with me whenever I was back in the South visiting. And Granny was always there, ready for a visit, and to tell stories.

Of course the most deserving of my appreciation and love are my parents, Charles and Aimee Smith. Without their love and support I would never have finished Caltech. Maybe my greatest accomplishment over the last five years was to grow up enough so that they became my best friends.

Financial support from the National Science Foundation in the form of a predoctoral fellowship is gratefully acknowledged.

ABSTRACT

We have developed a method based upon the Schwinger Variational Principle to study molecular photoionization and electron molecule scattering. We obtain exact static-exchange solutions to the equations for the continuum orbitals within the Hartree-Fock approximation, and from these we derive cross sections and angular distributions for both of the above processes. We have applied this method to photoionization of the valence levels of three different systems.

The first application of this method is in a study of the photoionization of the valence levels of NO. For photoionization of the 5σ level we find that the magnitudes of the cross sections for the resulting $b^3\Pi$ and $A^1\Pi$ states of NO^+ are not in the statistical 3:1 ratio and that the position of the peaks in the shape resonances appear at significantly different photoelectron kinetic energies. The differences are a reflection of the sensitivity of the shape resonances to small changes in the exchange component of the molecular ion potential. We also examined photoionization of the 2π and 4σ levels of NO and found that these levels, along with the 5σ, exhibit shape resonances in the σ continuum.

Vibrationally resolved branching ratios and vibrational state-specific asymmetry parameters for photoionization of the 5σ level of CO are presented. The agreement between these results and the measured data was obscured by autoionization peaks superimposed upon the region of the spectrum in which the experiment was performed. The limited experimental data which are not obscured by autoionization, agree quite well with our

results.

Finally, a study of the photoionization of the 5σ level of CO adsorbed on a nickel surface is reported. Approximating this system by the linear triatomic molecule NiCO leads to cross sections and angular distributions which are in good agreement with experimental data. The use of polarized, highly tunable synchrotron radiation along with detection at various angles yields far more information than can be obtained from the photoionization of the same molecule in the gas phase. With this technique it is possible to determine the adsorbate geometry, resolve partial channels, and resolve the photoemisison from two degenerate orbitals of different symmetries, simply by making appropriate choice of the polarization and collection angles. Examples of these techniques are discussed.

TABLE OF CONTENTS

INTRODUCTION

The study of molecular photoionization is a rapidly growing area of current research. Emphasis is no longer placed upon the determinization of ionization potentials, but rather upon obtaining cross sections, asymmetry parameters, and vibrational branching ratios, all as functions of the energy of the incident photon. This field of research is relatively new and owes its existence to the fact that experimentalists have recently been able to tap in to the synchrotron radiation which provides a tunable, monochromatic source of photons. As more and more molecules are being studied by the experimentalists, efforts by the theoreticians to analyze and explain the results increase also. The work presented in this thesis describes our attempts to predict and interpret the results of various photoionization experiments and thus to learn more about the dynamics of this process. We present the theory behind our approach to describing this process, and then the application of this method to the photoionization of the valence orbitals of NO, CO, and NiCO.

The cross sections obtained from photoionization calculations or experiments are useful in the modeling of many physical processes. Atmospheric chemists make use of this information in any model of atmospheric composition. Photoionization is a common event in the interstellar medium, and astrophysicists need reliable cross sections upon which their models can be based. The closely related process of electron-molecule scattering is a major feature which must be well characterized before a reasonable description can be devised for energy transport in plasmas or electron impact processes in lasers. Also the phenomenon of the shape resonance, which occurs so often in these situations, is known to induce non-

Franck-Condon behavior in the branching ratios for the final vibrational states of the system. More recently photoemission studies have played a key role in probing the nature of adsorbates on metal surfaces, and in an even newer area, the process of multiphoton ionization of atoms and molecules is rapidly becoming an important probe of quantum state-specific photoelectron dynamics. In short, photoionization is a frequent occurrence that needs to be well understood.

An accurate theoretical determination of cross sections for molecular photoionization requires considerable effort. Unlike the case of atomic photoionization, the nonspherical molecular ion induces the coupling of partial waves in the continuum function. There is also the problem of devising a method to correctly describe the nonlocal exchange potential in an ab initio manner. Even the local part of the potential can sometimes be difficult to describe adequately due to numerical problems which may occur.

In Chapter I of this thesis we present our theoretical method and discuss the manner in which we address the above problems. We discuss the merits of our method and compare it to other methods used by researchers studying similar problems. The remaining chapters are concerned with the applications of this method to various facets of the photoionization problem. Chapter II contains the results of a study of the photoionization of the valence orbitals of nitric oxide, in which we examined the effects of photoionization from an open-shell molecule. This system provides a rare opportunity to study the case in which photoionization from a closed-shell orbital results in the molecular ion which can be in either of two spin states, depending upon whether the remaining electron is triplet or singlet coupled to

the electron in the original open shell. We examined the cross sections from these states and found the surprising result that they were not in the 3:1 ratio that would be expected based upon the multiplicities of the final states. Chapter III contains the results of a study of the vibrationally resolved cross sections for the photoionization of the 5σ orbital of carbon monoxide. This channel contains a shape resonance which causes non Franck-Condon branching ratios for the final vibrational states of the CO^+ ion. Finally, in Chapter IV the results of a study on the photoionization of NiCO are presented. NiCO has been found to be a good approximation for the more complicated system of CO adsorbed on a Ni surface. We fixed the direction of the molecule in space and then compared the angular distributions of the ejected electrons with those obtained experimentally for CO adsorbed on a Ni surface. For lesser-studied systems, a study of this type would be an ideal way in which to help determine the angle of bonding between the molecule and the surface.

This is by no means a complete treatise on the subject of molecular photoionization. It is hoped that the many references given at the end of each chapter will provide information not given here as well as different insights and different approaches to solutions of problems in this field.

CHAPTER I

Development of the Schwinger Variational Method Which is Suitable for Long-Range Potentials

SECTION A

Introduction

Much effort in chemical research in recent years has been directed toward understanding molecular photoionization.[1,2] This phenomenon is often observed in physical processes which occur in planetary atmospheres, plasmas, and the interstellar medium and recently photoionization has come into considerable use as a probe of the nature of adsorbates on a metal surface. The material in this chapter describes the specifics of a new theoretical approach used to predict photoionization cross sections. It is useful to initially present a brief overview of the basic concepts behind this theory. It should be noted that much of the theory presented in this chapter is applicable with only minor modifications to the similar phenomenon of electron-molecule scattering[3] which also occurs in the above processes and is of central importance in gas lasers and electron energy loss spectroscopy (EELS).

At first glance the photoionization process seems quite straightforward. An incident photon strikes a molecule and if the energy of the photon is sufficient an electron can be ejected from the molecule. Our work in this field is directed primarily toward obtaining photoionization cross sections as a function of the energy of the incident photon. The cross section for photoionization from an N-electron molecule is given by[4]

$$\sigma(E) = \frac{4\pi^2\omega}{3c} \quad < \Psi_i(\mathbf{r},\mathbf{R}) | \mu | \Psi_f(\mathbf{r},\mathbf{R}) > |^2, \qquad (1)$$

where $\Psi_i(\mathbf{r},\mathbf{R})$ is the initial-state wave function corresponding to the ground state of the molecule and Ψ_f is the final-state wave function corresponding to an (N-1)-electron ion and the continuum wave function of the photoelectron.

The coordinate $\mathbf{r}$ refers to all N electrons collectively and R is the relative position vector of the nuclei. The photon-molecule interaction is represented by the dipole operator μ and the factors c and ω are the speed of light and photon frequency. The initial state Ψ_i is easily obtained from standard electronic structure codes. Thus, all of our efforts are directed toward obtaining the continuum orbital in the final-state wave function Ψ_f. We must first develop the equation for ϕ_k, the one-electron continuum part of Ψ_f, and then outline a method for the solution of this equation.

The final state wave function in the photoionization process describes a photoelectron and a molecular ion. We solve Schrödinger's equation with the Hamiltonian

$$H = H_{ion} + T + V_{int} \tag{2}$$

where H_{ion} is the Hamiltonian of the molecular ion, T is the kinetic energy operator for the continuum electron, and V_{int} represents the interactions between the electron and molecular ion. The stationary state solutions of this Hamiltonian satisfy the time-independent Schrödinger equation

$$H \Psi_E^{\gamma} = E \Psi_E^{\gamma}. \tag{3}$$

Note that Ψ_E^{γ} is an N-particle wave function. The superscript γ represents the quantum numbers n, v, j, and s which are the electronic, vibrational, rotational, and spin states of the ion, along with S and M_s which

describe the total spin angular momentum and its $\hat{Z}$ component.

It is not possible to solve Schrödinger's equation directly for the N-particle equation Ψ_E^γ. By using the eigenfunction expansion and retaining only the first term in the expansion, we approximate Ψ_E^γ as

$$\Psi_E^\gamma = \phi_k(r;R)\ \Phi^\alpha(r_1, r_2, \ldots, r_{N-1}, R) \tag{4}$$

where Φ^α is an eigenfunction of the ionic Hamiltonian

$$H_{ion}\ \Phi^\alpha = E^\alpha \Phi^\alpha,$$

ϕ_k is the continuum orbital and α represents the quantum numbers n, v, j, and s of the ion. We allow vibration and rotation within the framework of the Born-Oppenheimer approximation and thus write

$$\Phi^\alpha(r,R) = \phi^{n,s}(r;R)\chi^{j,v}(R).$$

With this form for Φ^α in Eq. (4), we insert this into Eq. (3), multiply on the left-hand side by Φ^α and integrate over the electron coordinates $r_1, r_2, \ldots, r_{N-1}$ and the nuclear coordinates $\hat{R}$ to obtain a single-particle equation for the continuum orbital ϕ_k

$$\left[\nabla^2 - 2\ V(r;R) + k^2\right]\phi_k(r;R) = 0. \tag{5}$$

Here $V(r)$ is equal to the interaction potential V_{int} averaged over the molecular ion and k^2 is related to the energy of the continuum electron by

$$E = E^{ion} + \frac{1}{2} k^2.$$

The internuclear distance R appears as a parameter now. If we want information about ϕ_k for various bond lengths in the ion we simply insert the appropriate $V(r;R)$ into Eq. (5). The solution of Eq. (5) will provide us with the information necessary to obtain photoionization cross sections.

Up to this point the discussion of the wave functions has been based upon the incorrect assumption that the electrons are distinguishable. This was done to simplify the presentation of the theory. To account for the indistinguishability of the electrons an antisymmetrized wave function must be introduced in Eq. (4). This results in a more complicated single-particle equation

$$(\nabla^2 - 2\,V(r) + k^2)\phi_k(r) = \int 2\,V^{ex}(r,r')\phi_k(r')d^3r', \qquad (6)$$

where we have suppressed the parametric dependence of V and ϕ_k on the internuclear distance R. The left-hand side is the same as that in Eq. (5) but the exchange potential has been introduced on the right-hand side. The first thing we immediately notice is that it is a nonlocal potential; i.e., to know the value of $V^{ex}\phi_k$ at a single point, we must know the value of

$\phi_k(r)$ everywhere. If the exchange potential could be rendered separable -- that is, made into a function of r times a function of r' -- we could then obtain a solution of Eq. (6) more readily. We have chosen a separable form for this exchange potential which was originally proposed by Schwinger.[5] Because the body of this chapter concerns an adaptation of this technique, we will discuss the original theory and its merits next.

Eq. (6) can be rewritten as

$$\left(\nabla^2 - \frac{2}{r} + k^2\right)\phi_k(r) = \int d^3r'\, U(r,r')\, \phi_k(r') \qquad (7)$$

where U is equal to twice the sum of V plus V^{ex} with the long-range Coulomb interaction given by 2/r removed. Using the Coulomb Green's function defined by[6]

$$G_c^{(\pm)} = (\nabla^2 - \frac{2}{r} + k^2 \pm i\varepsilon)^{-1}$$

The solution to Eq. (7) becomes the Lippmann-Schwinger equation[6]

$$\phi_k^{(\pm)}(r) = f_k(r) + \iint d^3r_1\, d^3r_2\, G_c^{(\pm)}(r,r_1)\, U(r_1,r_2)\, \phi_k^{(\pm)}(r_2) \qquad (8)$$

where f_k is the Coulomb function corresponding to scattering from a point

charge. The + (-) refers to the outgoing- (incoming-) wave boundary conditions. The incoming-wave boundary conditions are used in photoionization calculations because the final state is a well-defined particle, not a scattered wave as is the case for outgoing-wave boundary conditions. We would like to express the kernel in Eq. (8) in a separable form

$$\int d^3r_1 \; G(r,r_1) \; U(r_1,r_2) \simeq \sum_{i=1}^{N} \alpha_i(r) \; \beta_i(r_2). \qquad (9)$$

Insertion of this separable kernel into Eq. (8) gives

$$\phi_k(r) = f_k(r) + \sum_{i=1}^{N} \alpha_i(r) < \beta_i | \phi_k >$$

which can be manipulated to obtain a closed form solution for ϕ_k

$$\phi_k(r) = f_k(r) + \sum_{i,j} \alpha_i(r) \times \left[(1 - < \beta | \alpha >)^{-1} \right]_{ij} < \beta_j | f_k >.$$

The problem now is how to choose the form for α_i and β_i for our separable potential in Eq. (9). The form we chose was originally proposed by Schwinger[5,7]

$$U^s(r,r') = \sum_{i,j} < r|U|a_i > \left[U^{-1}\right]_{ij} < a_j|U|r' >.$$

Use of this separable potential in Eq. (8) gives the closed form solution

$$\phi_k(\mathbf{r}) = f_k(\mathbf{r}) + \sum_{i,j} < \mathbf{r}|GU|a_i > \left(D^{-1}\right)_{ij} < a_j|U|f_k > \tag{10}$$

where

$$D_{ij} = < a_i|U - UGU|a_j >. \tag{11}$$

The obvious question to ask is what's so special about the Schwinger separable potential. There are other separable potentials we could use; why did we choose this particular form? The answer lies in the connection between this separable potential and the Schwinger variational principle.

The Schwinger variational expression for the T matrix is[8]

$$T_{k,k'} = < f_k|U|\phi_{k'}^{(+)} > + < \phi_k^{(-)}|U|f_{k'} > -$$

$$< \phi_k^{(-)}|U - UGU|\phi_{k'}^{(+)} >. \tag{12}$$

If we form some trial function for ϕ_k, say

$$\phi_k^{tr} = \phi_k + \delta\phi_k,$$

where $\delta\phi_k$ is some small change in the true function ϕ_k, then insertion of ϕ_k^{tr} into Eq. (12) will give a trial T matrix that differs from the exact T matrix in second order

$$T^{tr}_{k,k'} = T_{k,k'} + O(\delta\phi_k)^2 .$$

There are no first-order errors and the T matrix is variationally stable. If the trial function is chosen as a linear combination of basis functions a_i

$$\phi^{tr}_k = \sum_i c_i | a_i >$$

and is inserted into Eq. (12), then by using the fact that the T matrix is variationally stable we require

$$\frac{\partial T_{k,k'}}{\partial c_i} = 0$$

for all c_j. This results in an expression for c_i

$$c_i = \sum_j \left(D^{-1}\right)_{ij} < a_j | U | f_k >$$

where D_{ij} is defined in Eq. (11). Insertion of ϕ^{tr}_k into the Lippmann-Schwinger equation, Eq. (8), gives

$$\phi_k(r) = f_k(r) + \sum_{i,j} < r | GU | a_i > \left(D^{-1}\right)_{ij} < a_j | U | f_k > .$$

This is exactly the same form for the wave function which we obtained in Eq.

(10) where we started from the Schwinger separable potential.

It is even possible to iterate with this method.[9] This is done by augmenting the basis set $\{|a_i\rangle\}$ with the function ϕ_k obtained previously and then repeating the calculation. This iterative procedure can be performed until the wave function from the $n+1^{st}$ iteration is no different from the wave function in the n^{th} iteration.

The work presented in this chapter is a modification of the above method which yields significantly better results in fewer iterations. It is still based upon the Schwinger variational principle but the starting point is Eq. (6) rather than Eq. (7). Because only the exchange potential is nonlocal, it is the only part of the potential which must be rendered separable; the local part could be treated exactly by existing methods and thus none of it would be "lost" in an unnecessary projection onto an incomplete basis. When this method was implemented we found that iterating became unnecessary in most cases and our results converged significantly faster. The material in this chapter describes this method in more detail and presents some results which illustrate how quickly the method converges. In later chapters, we present the results of applications of this method to various problems in molecular photoionization.

References and Notes

(1) See, for example, Electron-Molecule and Photon-Molecule Collisions, T. Rescigno, V. McKoy, and B. Schneider, Eds., Plenum Press, New York (1979).

(2) See, for example, Photoabsorption, Photoionization, and Photoelectron Spectroscopy, by J. Berkowitz, Academic Press, New York (1979).

(3) For an excellent review, see the article by N. F. Lane, Rev. Mod. Phys. **52**, 29 (1980).

(4) W. J. Moore, Physical Chemistry, pp. 752-753, Prentice Hall, New Jersey (1972).

(5) S. K. Adhikari and I. H. Sloan, Phys. Rev. C **11**, 1133 (1975).

(6) L. S. Rodberg and R. M. Thaler, Introduction to the Quantum Theory of Scattering, Academic Press, New York (1967).

(7) D. K. Watson and V. McKoy, Phys. Rev. A **20**, 1474 (1979).

(8) R. G. Newton, Scattering Theory of Waves and Particles, McGraw-Hill, New York (1966).

(9) R. R. Lucchese and V. McKoy, Phys. Rev. A **24**, 770 (1981).

SECTION B

Schwinger Variational Principle Applied to Long-Range Potentials

I. INTRODUCTION

In recent years several new approaches[1-5] have been developed for studying the collisions of low-energy electrons with molecules and the related problem of molecular photoionization. In several of these methods, the use of discrete basis functions plays an important role. Of specific interest to the developments in this paper is the Schwinger variational method in which the trial scattering wave function can, in principle, be expanded exclusively in a discrete basis. It is known that the expansion of the trial wave function, in such a basis, e.g., $|\Psi\rangle = \Sigma_i c_i |a_i\rangle$, in the Schwinger variational principle is equivalent to the use of a separable potential of the form

$$V^S(\mathbf{r},\mathbf{r}') = \sum_{i,j} \langle \mathbf{r}|V|a_i\rangle \left(V^{-1}\right)_{ij} \langle a_j|V|\mathbf{r}'\rangle \qquad (1)$$

in the Lippmann-Schwinger equation.[6] Clearly the basis functions in Eq. (1) must span the range of the full potential in order for V^S to be an adequate representation of V. Applications to date have shown that for molecular targets with no strong long-range potentials,[7] e.g., H_2, N_2^+, and CO_2,[8-10] a discrete basis set approach to the Schwinger variational principle can be very effective. However, for strongly polar systems, e.g., LiH, $NO^+(2\pi^{-1})$, and $CO^+(5\sigma^{-1})$,[11-13] it is difficult to describe the long-range forces with only discrete basis functions, and we have found that continuum functions must be included in the trial function so as to obtain the correct scattering solutions particularly at low energies. For these cases and, more generally, to have a method which can provide accurate solutions where such

solutions may be required, we have developed an iterative procedure for solving the Lippmann-Schwinger equation which is based on the Schwinger variational principle.[2] In this iterative procedure appropriate continuum functions can be systematically incorporated into the basis set for the trial scattering function. Criteria for the convergence of this method have been developed.[2]

The features discussed above pertain to the Schwinger variational principle in a form in which the entire scattering potential V, including both its long- and short-range components, is projected on a basis in the separable form of Eq. (1). The Schwinger variational principle can be expressed in a form which assumes that the direct and long-range interactions will be treated exactly, e.g., by numerical integration, and only the short-range forces such as exchange effects will be projected onto a discrete basis set as in Eq. (1).[14,15] If this approach could be implemented efficiently, it could be expected to be a very effective way of applying the Schwinger method to the more difficult system such as the scattering of electrons by strongly polar molecular ions, which often arises in studies of molecular photoionization. In fact, Rescigno and Orel[5] have recently developed an approach to electron-molecule collisions in which exactly this division of the scattering potential into a long-range direct component and a short-range exchange component is made but in which the exchange component is approximated by a separable potential of the form

$$V_{ex}(\mathbf{r},\mathbf{r}') = \sum_{i,j} \langle \mathbf{r}|a_i\rangle \langle a_i|V_{ex}|a_j\rangle \langle a_j|\mathbf{r}'\rangle . \qquad (2)$$

The results of the application of this approach were impressive.[5] Exactly such a separation of the scattering potential and the subsequent representation of the exchange component by a basis set expansion of the form of Eq. (2) have been used extensively and successfully by Schneider and Collins.[3] These results certainly suggest that a similar approach within the framework of the Schwinger variational method would be very useful.

In this paper we develop an adaptation of the Schwinger variational principle for long-range potentials in which the static component of the electron-molecule interaction is treated exactly and the exchange interactions are approximated by the separable potential of the form of Eq. (1). Most importantly, we will show that the use of a separable potential of this type leads to variationally stable scattering matrices. The method also includes an iterative procedure for obtaining the converged scattering solutions systematically. Moreover, the related photoionization cross sections can be shown to be variationally stable. The method of solution is essentially based on the integral equations approach of Sams and Kouri[5,16,17] and does not require the Green's function for the static potential.[5]

In the next section we formulate our adaptation of the Schwinger potential for long-range potentials and demonstrate that the photoionization cross sections obtained with these continuum solutions are variationally stable. In Section III we will illustrate various features of our method by application to the e-$NO^+(X^1\Sigma^+)$ and e-H_2 systems. The first example is chosen as an application of the method to molecular photoionization involving a strongly polar ion while the second example has been extensively studied by several methods. The results of these applications, particularly those of the

e-NO^+ system, are very encouraging and show that the procedure converges rapidly.

II. THEORY

A. Formulation

The Schrödinger equation for electron-molecule scattering in the static-exchange approximation is

$$(\nabla^2 - U + k^2)\Psi_{\mathbf{k}}(\mathbf{r}) = 0, \tag{3}$$

where ½ U is the static-exchange potential of the target. To this equation we also add terms containing Lagrange multipliers to impose any desired orthogonality of the continuum function $\Psi_{\mathbf{k}}$ to occupied target orbitals. We can write Eq. (3) including the auxiliary orthogonality conditions as

$$(\nabla^2 - U + k^2)\Psi_{\mathbf{k}}(\mathbf{r}) = \sum_i \lambda_i \chi_i(\mathbf{r}), \tag{4}$$

where, for example, χ_i are the occupied orbitals of some closed-shell molecular target and λ_i are the Lagrange multiplers. These Lagrange multipliers play an important role in determining the photoelectron continuum functions in the frozen-core approximation.[9] By breaking the scattering potential U into its direct and exchange components, U_{dir} and U_{ex}, respectively, Eq. (4) becomes

$$(\nabla^2 - U_{dir} + k^2)\Psi_{\mathbf{k}} = U_{ex}\Psi_{\mathbf{k}} + \sum_i \lambda_i \chi_i . \tag{5}$$

The solution of Eq. (5) can be written as

$$\Psi_k = \Psi^e_k + \sum_i \lambda_i \Psi^{\chi_i} \tag{6}$$

where the functions $\Psi^e_{\mathbf{k}}$ and Ψ^{χ_i} satisfy the equations

$$\Psi^e_{\mathbf{k}} = \Psi^d_{\mathbf{k}} + G^d U_{ex} \Psi^e_{\mathbf{k}} \tag{7a}$$

and

$$\Psi^{\chi_i} = G^d \chi_i + G^d U_{ex} \Psi^{\chi_i} . \tag{7b}$$

In Eqs. (7) $\Psi^d_{\mathbf{k}}$ is the solution for the direct potential, i.e.,

$$(\nabla^2 - U_{dir} + k^2)\Psi^d_{\mathbf{k}} = 0 \tag{8}$$

and G^d is the Green's function for the static potential, i.e., $(\nabla^2 - U_{dir} + k^2 \pm i\varepsilon)^{-1}$. The orthogonality of $\Psi_{\mathbf{k}}$ to the orbitals χ_i requires that

$$\langle \chi_j | \Psi_{\mathbf{k}} \rangle = \langle \chi_j | \Psi^e_{\mathbf{k}} \rangle + \sum_i \langle \chi_j | \Psi^{\chi_i} \rangle \lambda_i = 0 \tag{9}$$

and, hence,

$$\lambda_i = -\sum_j (A^{-1})_{ij} < \chi_j | \Psi^e_k >, \tag{10}$$

where

$$A_{ij} = < \chi_i | \Psi^{\chi_j} >. \tag{11}$$

The partial wave K-matrix element associated with solutions of Eqs. (6) and (7) is given by

$$K_{\ell',\ell m} = K^d_{\ell',\ell m} - \frac{1}{k} \Big(< \Psi^d_{k\ell',m} | U_{ex} | \Psi^e_{k\ell m} > +$$

$$\sum_{i,j} \Big(< \Psi^d_{k\ell',} | \chi_i > + < \Psi^d_{k\ell',m} | U_{ex} | \Psi^{\chi_i} > \Big) (A^{-1})_{ij}$$

$$\times < \chi_j | \Psi^e_{k\ell m} > \Big), \tag{12}$$

where $K^d_{\ell\ell'm}$ is the K-matrix element for the direct potential and we have assumed the molecule is linear.

Our objective is to obtain a variationally stable expression of the Schwinger form for such K-matrix elements. We assume that we have exact values for the $K^d_{\ell\ell'}$ and $<\Psi^d_\ell | \chi_i>$ elements which can be obtained from the solution of Eq. (8). We will discuss our method for solving this equation later. We obtain a variational estimate of $K_{\ell\ell'm}$ by constructing variational estimates of the matrix elements

$$I^{(1)}_{\ell'\ell} = \langle \Psi^d_{\ell'} | U_{ex} | \Psi^e_\ell \rangle , \tag{13a}$$

$$I^{(2)}_{\ell' i} = \langle \Psi^d_{\ell'} | U_{ex} | \Psi^{\chi_i} \rangle , \tag{13b}$$

$$I^{(3)}_{i\ell} = \langle \chi_i | \Psi^e_\ell \rangle , \tag{13c}$$

$$I^{(4)}_{ij} = A_{ij} = \langle \chi_i | \Psi^{\chi_j} \rangle . \tag{13d}$$

In Eqs. (13) we have abbreviated the partial-wave designation. We can use Eqs. (6) and (7) to write the following variational expressions for these four terms[13,18-20]

$$\tilde{I}^{(1)}_{\ell'\ell} = \langle \Psi^d_{\ell'} | U_{ex} | \tilde{\Psi}^e_\ell \rangle + \langle \tilde{\Psi}^e_{\ell'} | U_{ex} | \Psi^d_\ell \rangle - \langle \tilde{\Psi}^e_{\ell'} | U_{ex} - U_{ex} G^d U_{ex} | \tilde{\Psi}^e_\ell \rangle , \tag{14a}$$

$$\tilde{I}^{(2)}_{\ell' i} = \langle \tilde{\Psi}^d_{\ell'} | U_{ex} | \tilde{\Psi}^{\chi_i} \rangle + \langle \tilde{\Psi}^e_{\ell'} | U_{ex} G^d | \chi_i \rangle - \langle \tilde{\Psi}^e_{\ell'} | U_{ex} - U_{ex} G^d U_{ex} | \tilde{\Psi}^{\chi_i} \rangle , \tag{14b}$$

$$\tilde{I}^{(3)}_{j\ell} = \langle \chi_j | \Psi^d_\ell \rangle + \langle \chi_j | G^d U_{ex} | \tilde{\Psi}^e_\ell \rangle + \langle \tilde{\Psi}^{\chi_j} | U_{ex} | \Psi^d_\ell \rangle - \langle \tilde{\Psi}^{\chi_j} | U_{ex} - U_{ex} G^d U_{ex} | \tilde{\Psi}^e_\ell \rangle , \tag{14c}$$

$$\tilde{I}^{(4)}_{ij} = \langle \chi_i | G^d | \chi_j \rangle + \langle \chi_i | G^d U_{ex} | \tilde{\Psi}^{\chi}_j \rangle + \langle \tilde{\Psi}^{\chi}_i | U_{ex} G^d | \chi_j \rangle - \langle \tilde{\Psi}^{\chi}_i | U_{ex} - U_{ex} G^d U_{ex} | \tilde{\Psi}^{\chi}_j \rangle . \quad (14d)$$

Expansion of the trial functions $\tilde{\Psi}^e$ and $\tilde{\Psi}^{\chi}$ in a basis $\{|\alpha_i\rangle\}$ and variation of the expansion parameters leads to the variationally stable expressions for these elements, i.e.,

$$\tilde{I}^{(1)}_{\ell',\ell} = \sum_{a,b} \langle \Psi^d_{\ell'} | U_{ex} | \alpha_a \rangle \left(D^{-1}\right)_{ab} \langle \alpha_b | U_{ex} | \Psi^d_{\ell} \rangle , \quad (15a)$$

$$\tilde{I}^{(2)}_{\ell',i} = \sum_{a,b} \langle \Psi^d_{\ell'} | U_{ex} | \alpha_a \rangle \left(D^{-1}\right)_{ab} \langle \alpha_b | U_{ex} G^d | \chi_i \rangle , \quad (15d)$$

$$\tilde{I}^{(3)}_{i\ell} = \langle \chi_i | \Psi^d_{\ell} \rangle + \sum_{a,b} \langle \chi_i | G^d U_{ex} | \alpha_a \rangle \left(D^{-1}\right)_{ab} \times \langle \alpha_b | U_{ex} | \Psi^d_{\ell} \rangle , \quad (15c)$$

$$\tilde{I}^{(4)}_{ij} = \langle \chi_i | G^d | \chi_j \rangle + \sum_{a,b} \langle \chi_i | G^d U_{ex} | \alpha_a \rangle \times \left(D^{-1}\right)_{ab} \langle \alpha_b | U_{ex} G^d | \chi_j \rangle , \quad (15d)$$

where $\left(D^{-1}\right)_{ab}$ is an element of the inverse of the matrix

$$D_{ab} = \langle \alpha_a | U_{ex} - U_{ex} G^d U_{ex} | \alpha_b \rangle . \quad (16)$$

Use of Eq. (15) in Eq. (12) provides a variationally stable expression for the K matrix.

Finally, insertion of a separable approximation for U_{ex} of the form

$$U_{ex}^{S} = \sum_{a,b} U_{ex} |\alpha_a > (U_{ex}^{-1})_{ab} < \alpha_b | U_{ex} \tag{17}$$

in Eq. (7) yields the wave functions

$$\psi_{k\ell}^{(0)e} = \psi_{k\ell}^{d} + \sum_{a,b} G^{d} U_{ex} |\alpha_a > (D^{-1})_{ab} < \alpha_b | U_{ex} | \psi_{k\ell}^{d} >, \tag{18a}$$

$$\psi^{(0)\chi_i} = G^{d}\chi_i + \sum_{a,b} G^{d} U_{ex} |\alpha_a > (D^{-1})_{ab} \times < \alpha_b | U_{ex} G^{d} | \chi_i >, \tag{18b}$$

which will be shown to be point-by-point variationally stable in Section IIc. Substitution of Eq. (18) in Eq. (6) gives a total scattering solution whose partial wave asymptotic form defines a K matrix identical to that obtained by using Eqs. (15) in Eq. (12).

B. Iterative Procedure

The functions in Eqs. (18) provide approximate solutions of Eq. (3). In several applications, it can be important to obtain the converged solutions of Eq. (3). A procedure for doing so begins by augmenting the initial basis $\{|\alpha_i>\}$ with the energy-dependent set of functions $S^{(0)} =$

$\{\Psi^{(0)}_{k\ell_1}, \Psi^{(0)}_{k\ell_2}, \ldots, \Psi^{(0)}_{k\ell_p}\}$ defined by the initial solutions of Eqs. (18). Here ℓ_p is the maximum partial wave retained in the expansion of $\Psi^{(0)}_k$. Eqs. (18) are now solved again with this augmented basis providing a new, and more accurate, set of solutions $S^{(1)} = \{\Psi^{(1)}_{k\ell_1}, \Psi^{(1)}_{k\ell_2}, \ldots, \Psi^{(1)}_{k\ell_p}\}$. Repetition of this procedure with a new basis consisting of the set of functions $\{|\alpha_i\rangle\}$ and $S^{(1)}$ leads to a more converged set of solutions $S^{(2)} = \{\Psi^{(2)}_{k\ell_1}, \Psi^{(2)}_{k\ell_2}, \ldots, \Psi^{(2)}_{k\ell_p}\}$. These functions are the converged solutions of Eq. (3) when the set of $S^{(n+1)}$ functions is equal to the $S^{(n)}$ set.[2]

C. Variational Stability of Photoionization Cross Sections

An important objective of our work is to use these continuum solutions to obtain molecular photoionization cross sections. The relevant one-electron matrix element is given by

$$M = \langle \phi_i | \mu | \Psi_k \rangle = \langle R | \Psi_k \rangle , \qquad (19)$$

where ϕ_i is the orbital from which ionization occurs, Ψ_k is the photoelectron continuum function, and μ is the dipole moment operator. We now show that our approximate continuum solutions obtained above provide variationally stable estimates of Eq. (19). For convenience we keep the same notation as in the preceding section, although in actual applications to photoionization one must redefine the Green's function and the scattering potential of Eq. (1) due to the presence of the Coulomb potential. From Eqs. (6), (7), (10), and (19), we obtain

$$M = \langle R|\Psi_k^d\rangle + \langle R|G^d U_{ex}|\Psi_k^e\rangle + \sum_{i,j} (\langle R|G^d|\chi_i\rangle + \langle R|G^d U_{ex}|\Psi^{\chi_i}\rangle) \times (A^{-1})_{ij} \langle \chi_j|\Psi_k^e\rangle . \quad (20)$$

To obtain a variational expression for the matrix element M, we need, in addition to the variational estimates of $I_{i\ell}^{(3)}$ and $I_{ij}^{(4)}$, given by Eqs. (14), variational expressions for $I_\ell^{(5)}$ and $I_i^{(6)}$ where

$$I_\ell^{(5)} = \langle R|G^d U_{ex}|\Psi_\ell^e\rangle \quad (21a)$$

and

$$I_i^{(6)} = \langle R|G^d U_{ex}|\Psi^{\chi_i}\rangle , \quad (21b)$$

where we again use a partial-wave designation for the continuum function, Ψ^e. Variational functionals for $I_\ell^{(5)}$ and $I_i^{(6)}$ can be written as

$$\tilde{I}_\ell^{(5)} = \langle R|G^d U_{ex}|\tilde{\Psi}_\ell^e\rangle + \langle \tilde{\Psi}^R|U_{ex}|\Psi_\ell^d\rangle - \langle \tilde{\Psi}^R|U_{ex} - U_{ex}G^d U_{ex}|\tilde{\Psi}_\ell^e\rangle \quad (22a)$$

and

$$\tilde{I}_i^{(6)} = \langle R|G^d U_{ex}|\tilde{\Psi}^{\chi_i}\rangle + \langle \tilde{\Psi}^R|U_{ex}G^d|\chi_i\rangle - \langle \tilde{\Psi}^R|U_{ex} - U_{ex}G^d U_{ex}|\tilde{\Psi}^{\chi_i}\rangle , \quad (22b)$$

where $\tilde{\Psi}^R$ is a variational trial function for Ψ^R and

$$\psi^R = G^d R + G^d U_{ex} \psi^R . \tag{23}$$

As before, we expand the trial functions $\tilde{\psi}^R$, $\tilde{\psi}^{\chi i}$, and $\tilde{\psi}^e_\ell$ in the basis $\{|\alpha_i\rangle\}$ to obtain the variational expressions for $\tilde{I}^{(5)}_\ell$ and $\tilde{I}^{(6)}_i$, i.e.,

$$\tilde{I}^{(5)}_\ell = \sum_{a,b} \langle R|G^d U_{ex}|\alpha_a\rangle \left(D^{-1}\right)_{ab} \times \langle \alpha_b|U_{ex}|\psi^d_\ell\rangle \tag{24a}$$

and

$$\tilde{I}^{(6)}_i = \sum_{a,b} \langle R|G^d U_{ex}|\alpha_a\rangle \left(D^{-1}\right)_{a,b} \langle \alpha_b|U_{ex}G^d|\chi_i\rangle . \tag{24b}$$

Use of Eqs.(15c), (15d), and (24) in Eq. (20) leads to a variationally stable expression for the matrix element M. However, insertion of Eqs. (18) for ψ^e_ℓ and $\psi^{\chi i}$ directly into Eq. (19) gives the identical expression for this matrix element, showing that our procedure provides a variationally stable estimate of M.

Finally, we note that $\tilde{I}^{(5)}_\ell$ and $\tilde{I}^{(6)}_i$ are exactly the matrix elements found in Eqs. (18), with $\langle R|$ replaced by $\langle r|$. This indeed confirms that the wave functions we obtain are variationally stable.

D. Computational Approach

To evaluate the variational expressions of Eqs. (15) and (24) it is necessary to solve for the partial-wave static solution, $\Psi^d_{k\ell m}$, and functions of the form

$$\Psi^u(\mathbf{r}) = \langle \mathbf{r}|G^d|u\rangle, \tag{25}$$

where $|u\rangle$ may be either $U_{ex}|\alpha\rangle$ or $|\chi_i\rangle$. Procedures for evaluating $U_{ex}|\alpha\rangle$ have been given elsewhere.[20] The functions $\Psi^d_{k\ell m}$ and Ψ^u satisfy the integral equations

$$\Psi^d_{k\ell m} = S_{k\ell m} + G^0 U_{dir}\Psi^d_{k\ell m} \tag{26}$$

and

$$\Psi^u = G^0 u + G^0 U_{dir}\Psi^u, \tag{27}$$

respectively, where $S_{k\ell m}$ is the free-particle solution and G^0 the free-particle Green's function. Partial-wave expansions are first made in Eqs. (26) and (27) and the resulting coupled equations then converted to a set of Volterra integral equations. Volterra integral equations have been used extensively in related applications[5,16,17,21] and techniques for their numerical solution have been discussed elsewhere.[5,17,21] In fact, our approach is very similar to what has been used recently by Rescigno and Orel.[5] First, we consider Eq. (26). The partial-wave function $\Psi^d_{\ell\ell' m}$, defined by the expansion

$$\Psi^{d}_{k\ell m}(\mathbf{r}) = \sum_{\ell'} \Psi^{d}_{\ell\ell' m}(r) Y_{\ell' m}(\hat{r}), \tag{28}$$

is obtained from Eq. (29), i.e.,

$$[\Psi^{d}] = [\phi^{d}][M_2^{-1}], \tag{29}$$

where

$$(M_2)_{\ell'\ell} = \delta_{\ell'\ell} + \frac{1}{k} \sum_{\ell''} \int_0^{\infty} g_{\ell'} U^{dir}_{\ell'\ell''} \phi^{d}_{\ell''\ell} \, dr \tag{30}$$

and $\phi^{d}_{\ell\ell'}$ satisfies the Volterra integral equation

$$\begin{aligned} \phi^{d}_{\ell\ell'}(r) = {} & f_{\ell}(r)\delta_{\ell\ell'} + \frac{1}{k} \sum_{\ell''} f_{\ell}(r) \\ & \times \int_0^{r} g_{\ell}(r') U^{dir}_{\ell\ell''}(r') \phi^{d}_{\ell''\ell'}(r') \, dr' \\ & - \frac{1}{k} \sum_{\ell''} g_{\ell}(r) \int_0^{r} f_{\ell}(r') U^{dir}_{\ell\ell''}(r) \phi^{d}_{\ell''\ell'}(r') \, dr'. \end{aligned} \tag{31}$$

In Eqs. (29) and (30) f_{ℓ} and g_{ℓ} are the Riccati-Bessel and Riccati-Neumann functions, respectively, and we have suppressed the subscripts k and m for convenience. It is well known that placing Eq. (30) on a quadrature mesh provides a noniterative propagation scheme for outward integration of the equations.[17,21] The associated K matrix, i.e., $[K^{d}]$, is given by

$$[K^d] = [M_1][M_2^{-1}], \tag{32}$$

where

$$(M_1)_{\ell',\ell} = -\frac{1}{k}\sum_{\ell''}\int_0^\infty f_{\ell'}\, U^{dir}_{\ell',\ell''}\,\phi^d_{\ell''\ell}\, dr \tag{33}$$

and $(M_2)_{\ell'\ell}$ is given in Eq. (30).

To maintain accuracy, numerical stabilization procedures had to be carried out at various grid points as the solutions were propagated outward. These procedures have been described in detail elsewhere.[17,21,22]

The solution of Eq. (27) is obtained in a similar way by transforming the equation for Ψ^u to a Volterra-type integral equation for ϕ^u. In partial-wave form, for each inhomogeneity u, we have

$$\Psi^u_\ell = \phi^u_\ell + \sum_{\ell'}\phi^d_{\ell\ell'}\, C_{\ell'\ell}, \tag{34}$$

where, in matrix notation

$$[C] = [M_3^{-1}][M_4] \tag{35}$$

with

$$(M_3)_{\ell\ell'} = -\left(\delta_{\ell\ell'} + \frac{1}{k}\sum_{\ell''}\int_0^\infty g_\ell\, U^{dir}_{\ell\ell''}\,\phi^d_{\ell''\ell'}\, dr\right) \tag{36a}$$

and

$$(M_4)_\ell = \frac{1}{k}\sum_{\ell'}\int_0^\infty g_\ell\, U^{dir}_{\ell\ell'}\,\phi^u_{\ell'}\, dr. \tag{36b}$$

The function $\phi_\ell^u(r)$ satisfies the integral equation

$$\phi_\ell^u(r) = -\frac{1}{k}\int_0^\infty f_\ell(r_<)g_\ell(r_>)u_\ell(r')dr'$$

$$+\frac{1}{k}\sum_{\ell'} f_\ell(r)\int_0^r g_{\ell'} U_{\ell\ell'}^{dir}\phi_{\ell'}^u dr'$$

$$-\frac{1}{k}\sum_{\ell'} g_\ell(r)\int_0^r f_{\ell'} U_{\ell\ell'}^{dir}\phi_{\ell'}^u dr'. \qquad (37)$$

Again the usefulness of this equation becomes apparent when it is placed on a quadrature mesh.

In the numerical integrations we used the ordinary Simpson's rule cyclically, and then used Simpson's "3/8 rule" for integrals which ended on a midpoint of an ordinary Simpson's rule quadrature. Knirk[23] has shown this quadrature scheme should be generally more accurate than the overlapped Simpson's rule or the trapezoidal rule.

III. APPLICATIONS

To illustrate our procedure we first studied the photoionization cross section for the 2π level of NO leading to the $X^1\Sigma^+$ state of NO^+. We primarily looked at the $2\pi \rightarrow k\sigma$ component of this cross section which is shape-resonant enhanced.[12,24,25] We have studied this system recently and it provides a good example of difficulties which can arise in obtaining the electronic continuum of strongly polar ions in resonance regions.

The rotationally unresolved, fixed-nuclei photoionization cross section is given by

$$\sigma(R) = \frac{4\pi^2\omega}{3c} \; | \; < \Psi_i(\mathbf{r};R) | \mu | \Psi_f(\mathbf{r};R) > \; |^2, \qquad (38)$$

where μ is the dipole moment operator and ω the photon frequency. In Eq. (38) $\Psi_i(\mathbf{r},R)$ is the initial state of the molecule and Ψ_f the final ionized state. For Ψ_i we used the self-consistent field (SCF) wave function and for the (N-1) bound electrons of Ψ_f we use the ground-state SCF orbitals, i.e., the frozen-core approximation. The continuum orbital is a solution of the one-particle Schrödinger equation with the static-exchange potential of this ion. Details of the SCF basis, quadrature grids, and partial-wave expansions have been given previously.[12] In these studies the dipole moment of the molecular ion with respect to the center of mass of the system is 1.27D.[12] We also assume the experimental ionization potential of 9.3 eV.

To illustrate the performance of the method and to compare it with the iterative Schwinger variational approach, we have carried out calculations with three different initial basis sets. These are given in Table I and consist of six, twelve, and eighteen Cartesian and spherical Gaussian functions defined as

$$\phi(\mathbf{r})^{\alpha,\ell,m,n} = N_c (x-A_x)^{\ell} (y-a_y)^{m} (z-A_z)^{n} e^{-\alpha|\mathbf{r}-\mathbf{A}|^2} \qquad (39)$$

and

$$\phi(\mathbf{r})^{\alpha,\ell,m} = N_s |\mathbf{r}-\mathbf{A}|^{\ell} e^{-\alpha|\mathbf{r}-\mathbf{A}|^2} Y_{\ell m}(\Omega_{\mathbf{r}-\mathbf{A}}), \qquad (40)$$

respectively. There are slight differences in the respective basis sets for the two methods. We have found that basis functions are needed at the center of

mass in the iterative Schwinger method to represent the direct component of the scattering potential. However, in the present method where only the exchange potential is projected on a basis, higher-order Gaussian functions on the nuclei are more effective than those at the center of mass.

Our results are given in Table II. There we show some $^2\Sigma$ K-matrix elements, the $k\sigma$ eigenphase sums, and the $2\pi \rightarrow k\sigma$ photoionization cross section at a photon energy of 14 eV which corresponds to the peak of the shape resonance in this channel.[12] At this photon energy the photoelectron kinetic energy is 4.7 eV. We chose this example since it is generally more difficult to obtain converged K matrices and photoionization cross sections in resonant regions than at nonresonant energies. The results show that, even starting with the very small basis of six functions, the present method gives essentially the converged results after one iteration. The Schwinger method, in which the entire potential is projected onto the basis, gives much poorer results at this level. It is important to note, however, that with just six basis functions and no iterative improvement, the present method provides a good estimate of the photoionization cross section. This is a consequence of the variational stability of these cross sections. At the L^2 level, the differences between the two methods become smaller as the size of the basis sets increases but, as expected, the present method yields more accurate results. With these larger basis sets, the differences between these two methods become quite small once the wave functions are improved iteratively. Away from the resonant energies in the $2\pi \rightarrow k\sigma$ channel and for the nonresonant $2\pi \rightarrow k\pi$ and $k\delta$ channels, the present method performs extremely well

providing accurate cross sections at the L^2 level with just six basis functions. For these channels and with these small basis sets, the cross sections obtained with the Schwinger method would change by as much as 40% with iteration.

As a next example we obtain some $^2\Sigma_g$ K-matrix elements and eigenphase sums for e-H_2 at $k^2 = 0.25$ in the static-exchange approximation. This system is simple and has been extensively studied previously. We chose this system so as to compare the present method both with the iterative Schwinger procedure[2] and the method of Rescigno and Orel.[5] Our present method is very similar to theirs[5] and differs essentially only in the use of a different separable representation of the exchange potential, i.e., the use of Eq. (1) instead of Eq. (2). As we have shown earlier, the use of the separable potential of the form of Eq. (2) leads to a variationally stable formulation. For the comparison of these results for this simple system obtained by the different approaches we do not believe it is necessary to present extensive numerical details.

For these studies of e-H_2 we use an SCF target wave function constructed from a (5s2p) basis discussed previously.[2] This basis gives an SCF energy of -1.1330 a.u. and a quadrupole moment of 0.452 a.u. We chose two small scattering basis sets containing two and four σ_g functions, respectively. The basis functions are given in Table III. The results of these calculations are given in Table IV and show that with only two basis functions the present method already provides quite accurate K-matrix elements at the L^2 level. With this same basis and without any iterations the Schwinger method gives much poorer results. With four basis

functions the differences between these two methods at the L^2 level remain significant. However, after one iteration, the two methods give essentially the same results. The iterated results in Table IV are almost identical to the converged K matrices at this energy. For comparison, with their choice of Eq. (2) for the separable representation of the exchange potential, Rescigno and Orel[5] obtained values for K_{00}, K_{02}, and K_{22} of -1.490, 0.012, and 0.0148. These calculations[5] used the present (5s2p) SCF basis, i.e., $7\sigma_g$ functions, to form the separable representation of the potential. Larger basis sets in the present method without iterations and in their studies[5] can both provide the converged K matrices directly.

IV. CONCLUSIONS

We have developed an adaptation of the Schwinger variational principle which is particularly well suited for treating long-range potentials. The method treats the direct component of the interaction potential exactly by numerical procedures but assumes a separable representation of the Schwinger type for the exchange potential. The method includes an iterative procedure for systematically obtaining converged solutions of the corresponding Lippmann-Schwinger equation. The approach should be particularly useful in obtaining continuum solutions of strongly polar ions which are required in related studies of resonant molecular photoionization cross sections. The method, moreover, provides variationally stable estimates of these photoionization cross sections. In this regard, applications of the method to the photoionization of the 2π level of NO gave encouraging results and suggest that the approach can be quite useful in other related applications.

References and Notes

(1) L. A. Collins, W. D. Robb, and M. A. Morrison, Phys. Rev. A. **21**, 488 (1980).

(2) R. R. Lucchese, D. K. Watson, and V. McKoy, Phys. Rev. A. **22**, 421 (1980).

(3) B. I. Schneider and L. A. Collins, Phys. Rev. A **24**, 1264 (1981); L. A. Collins and B. I. Schneider, ibid. **24**, 2387 (1981); **27**, 101 (1983).

(4) M.-T. Lee, K. Takatsuka, and V. McKoy, J. Phys. B. **14**, 4115 (1981).

(5) T. N. Rescigno and A. E. Orel, Phys. Rev. A **24**, 1267 (1981).

(6) W. H. Miller, J. Chem. Phys. **50** 407 (1969).

(7) This does not include the special case of the Coulomb potential.

(8) D. K. Watson, R. R. Lucchese, V. McKoy, and T. N. Rescigno, Phys. Rev. A **21**, 738 (1980).

(9) R. R. Lucchese, G. Raseev, and V. McKoy, Phys. Rev. A **25**, 2572 (1982).

(10) R. R. Lucchese and V. McKoy, Phys. Rev. A **25**, 1963 (1982).

(11) D. K. Watson, T. N. Rescigno, and V. McKoy, J. Phys. B **14**, 1875 (1981).

(12) M. E. Smith, R. R. Lucchese, and V. McKoy, J. Chem. Phys. **79**, 1360 (1983).

(13) R. R. Lucchese and V. McKoy, Phys. Rev. A **28**, 1382 (1983).

(14) R. G. Newton, Scattering Theory of Waves and Particles (McGraw-Hill, New York, 1966), p. 193.

(15) R. K. Nesbet, Electron-Atom Scattering Theory (Plenum, New York, 1980), p. 64.

(16) W. N. Sams and D. J. Kouri, J. Chem. Phys. **51**, 4809 (1969); **51**, 4815 (1969).

(17) M. A. Morrison, N. F. Lane, and L. A. Collins, Phys. Rev. A **15**, 2186 (1977).

(18) R. G. Newton, Scattering Theory of Wave and Particles (McGraw-Hill, New York, 1966), p. 317.

(19) S. G. Mikhlin, Variational Methods in Mathematic Physics (MacMillan, New York, 1964).

(20) R. R. Lucchese and V. McKoy, Phys. Rev. A **21**, 112 (1980).

(21) M. A. Morrison, in Electron-Molecule and Photon-Molecule Collisions, edited by T. N. Rescigno, V. McKoy, and B. Schneider (Plenum, New York, 1979), p. 15.

(22) T. N. Rescigno and A. E. Orel, Phys. Rev. A **25**, 2402 (1982).

(23) D. L. Knirk, J. Comp. Phys. **21**, 371 (1976).

(24) S. Wallace, D. Dill, and J. Dehmer, J. Chem. Phys. **76**, 1217 (1982).

(25) J. J. Delaney, I. H. Hillier, and V. R. Saunders, J. Phys. B **15**, 1477 (1982).

TABLE I. Starting Gaussian basis sets for the ^{2} continuum of the e-$NO^+(X^1\Sigma^+)$ system.

Basis Set	Present Method Center	ℓ	m	n	α	Iterative Schwinger Method Center	ℓ	m	n	α
I	Nuclei[a]	0	0	0	4.0	Nuclei	0	0	0	4.0
		0	0	0	0.5		0	0	0	0.5
		0	0	1	1.0		0	0	1	1.0
II	Nuclei	0	0	0	8.0	Nuclei	0	0	0	8.0
		0	0	0	2.0		0	0	0	2.0
		0	0	0	0.5		0	0	0	0.5
		0	0	1	1.0		0	0	1	1.0
		0	0	1	0.25		0	0	1	0.25
		0	0	2	0.5	c.m.[b]	1	0		1.0
							2	0		1.0
III	Nuclei	0	0	0	8.0	Nuclei	0	0	0	8.0
		0	0	0	4.0		0	0	0	4.0
		0	0	0	2.0		0	0	0	2.0
		0	0	0	1.0		0	0	0	1.0
		0	0	0	0.5		0	0	0	0.5
		0	0	1	2.0		0	0	1	1.0
		0	0	1	1.0		0	0	1	0.25
		0	0	1	0.25	c.m.	1	0		1.0
		0	0	2	0.5		2	0		1.0
							3	0		1.0
							4	0		1.0

[a]Basis functions on the nuclei are Cartesian Gaussians. [b]Center of mass. Functions here are always spherical Gaussians.

TABLE II. Comparison of the $^2\Sigma$ K-matrix elements, σ eigenphase sums, and the $2\pi \rightarrow k\sigma$ photoionization cross sections at a photoelectron kinetic energy of 4.7 eV for the e-NO^+ system obtained by the present method and the iterative Schwinger method.

	Basis Set I[a]		Basis Set II		Basis Set III	
	L^2[a]	Iterated[b]	L^2	Iterated	L^2	Iterated
$K_{(\ell,\ell')}$						
0,0	-0.224	0.091	-0.045	0.094	0.069	0.094
0,1	0.625	-0.524	-0.439	-0.526	-0.518	-0.526
1,1	31.451	-1.585	-2.467	-1.549	-1.740	-1.546
0,2	0.884	0.534	0.564	0.535	0.536	0.535
1,2	11.006	-1.154	-1.343	-1.145	-1.177	-1.145
2,2	3.579	-0.529	-0.595	-0.525	-0.553	-0.524
δ sum[c]	1.616	-0.498	-0.806	-0.489	-0.576	-0.488
σ_i[d]	1.336	1.501	1.328	1.509	1.472	1.513
			Iterative Schwinger Method			
0,0	13.346	-0.273	-0.043	0.103	-0.033	0.096
0,1	14.671	-1.285	-0.397	-0.551	-0.524	-0.534
1,1	16.582	-2.764	-2.729	-1.507	-2.471	-1.521
0,2	-2.554	-0.121	0.603	0.532	0.553	0.535
1,2	-2.901	-1.571	-1.209	-1.135	-1.122	-1.144
2,2	0.564	-0.864	-0.423	-0.524	-0.370	-0.523
δ sum	-1.076	-0.853	-0.869	-0.488	-0.748	-0.479
σ_i	0.798	0.524	1.239	1.342	1.277	1.524

[a]Discrete basis functions only. See Table I. [b]One iteration only. [c]In radians. [d]In megabarns (1 Mb = 10^{-18} cm^2).

TABLE III. Starting basis sets for the $^2\Sigma_g$ continuum of e-H_2. All functions are centered on the nuclei. All are Cartesian Gaussian functions defined in Eq. (39).

Basis Set	ℓ	m	n	α
I	0	0	0	0.5
	0	0	1	0.5
II	0	0	0	1.0
	0	0	0	0.3
	0	0	1	1.0
	0	0	1	0.3

TABLE IV. Comparison of the $^2\Sigma_g$ K-matrix elements and eigenphase sums for e-H_2 at $k^2 = 0.25$ a.u.

Basis Set		Present Method L^2	Present Method Iterated	Iterative Schwinger Method L^2	Iterative Schwinger Method Iterated
I	$K_{(\ell, \ell')}$				
	(0,0)	-1.721	-1.546	0.690	-1.549
	(0,2)	0.019	0.013	-0.028	-0.014
	(2,2)	0.014	0.016	0.002	0.016
	δ sum	-1.026	-0.976	0.606	-0.975
II	(0,0)	-1.598	-1.546	-2.079	-1.545
	(0,2)	0.016	0.013	0.004	0.013
	(2,2)	0.015	0.016	0.004	0.016
	δ sum	-0.992	-0.976	-1.118	-0.974

CHAPTER II

Photoionization of the Valence Levels of Nitric Oxide

SECTION A

Introduction

The photoionization of nitric oxide has been a subject of great interest in the last few years. From a practical point of view, this topic is of interest in atmospheric chemistry where NO^+ is a major component in many reactions.[1] NO^+ is found in the D, E, and F_1 regions of the ionophere which extend from roughly 80 to 120 km in altitude. From a theoretical point of view the photoionization of NO posed new difficulties which were not encountered in photoionization studies of closed-shell molecules. Furthermore, existing theoretical and experimental studies for the NO system are in poor agreement with each other.

To resolve the observed discrepancies between the experimental results of Southworth et al.[2] and the theoretical values of Wallace et al.[3] and Delaney et al.,[4] we applied our theoretical methods[5,6] based upon the Schwinger variational principle[7] to the photoionization of the valence levels of NO. We studied the 2π orbital using the Iterative Schwinger Method of Lucchese et al.[5] and then for the 4σ and 5σ orbitals applied a new adaptation of this method[6] which is well suited to the study of polar ions with large dipole moments. The theoretical results of Wallace et al.[3] were obtained with the Continuum Multiple Scattering Method[7] which employs a semi-empirical, muffin tin type of potential and local approximation to the exchange interaction. Delaney et al.[4] employed an ab initio method, the Stieltjes-Tchebycheff Moment Theory, but failed to converge their calculations and obtained cross sections which oscillated wildly -- a very unphysical result. The differences between these results and the experiments were so large that we were prompted to study this system.

In the molecular orbital picture the ground state electronic configura-

tion of NO is

$$(1\sigma)^2(2\sigma)^2(3\sigma)^2(4\sigma)^2(5\sigma)^2(1\pi)^4(2\pi)^1\ X^2\Pi.$$

We considered the following one-electron ionization processes from the ground state of NO

$$(2\pi \rightarrow k\sigma)^2\Sigma^+ \quad (2\pi \rightarrow k\pi)^2\Pi \quad (2\pi \rightarrow k\delta)^2\Delta$$
$$(5\sigma \rightarrow k\sigma)^2\Pi \quad (5\sigma \rightarrow k\pi)^2\Sigma^+,\ ^2\Sigma^-,\ ^2\Delta$$
$$(4\sigma \rightarrow k\sigma)^2\Pi \quad (4\sigma \rightarrow k\pi)^2\Sigma^+,\ ^2\Sigma^-,\ ^2\Delta.$$

Photoionization out of the 2π orbital leads to the $X^1\Sigma^+$ ground state of NO^+. However, photoionization out of the 5σ (4σ) orbital can lead to either the $b^3\Pi$ ($c^3\Pi$) or the $A^1\Pi$ ($B^1\Pi$) states of NO^+, depending upon whether the remaining electron in the photoionized orbital is triplet or singlet coupled to the electron in the 2π orbital.

In this chapter we report the first theoretical results for photoionization from the 5σ orbital of NO in which separate calculations were performed for the two final states of the molecular ion. We report cross sections for photoionization leading to the $b^3\Pi$ and the $A^1\Pi$ states of NO^+. We found the somewhat surprising result that the relative magnitudes of these cross sections do not exhibit the 3:1 ratio that would be expected based upon simple spin statistics. We also found that the $5\sigma \rightarrow k\sigma$ shape resonance appeared at different electron kinetic energies in the two calculations. These results were also observed experimentally. In the previous calculations on this

system[3,4] a "spin-averaged" ion was constructed from 3/4 of the triplet ion and 1/4 of the singlet ion. The scattering calculation was performed for an electron in the field of this ficticious ion and then the cross section was partitioned into a 3:1 ratio for the triplet and singlet states. This approximation inherently forces the $5\sigma \rightarrow k\sigma$ shape resonance to occur at the same electron kinetic energy for the two processes. Thus, this method leads to cross sections which, by the very nature of the approximation, cannot exhibit the above-mentioned anomalous properties.

The work presented in this chapter is our attempt to present accurate static-exchange cross sections for photoionization of the 4σ, 5σ, and 2π orbitals of NO. We found that we differed from many of the theoretical results previously reported and we discuss the reasons for these differences. We compare our results to experimental cross sections and find reasonable agreement between the two. Our multiplet-resolved cross sections for photoionization from the 5σ orbital are presented and their relationship to the spin-averaged cross sections is discussed.

References and Notes

(1) M. Nicolet and A. C. Aikin, J. Geophys. Res. **65**, 1469 (1960).

(2) S. Southworth, C. M. Truesdale, P. H. Korbin, D. W. Lindle, D. W. Brewer, and D. A. Shirley, J. Chem. Phys. **76**, 143 (1982).

(3) S. Wallace, D. Dill, and J. L. Dehmer, J. Chem. Phys. **76**, 1217 (1982).

(4) J. J. Delaney, I. H. Hillier, and V. R. Saunders, J. Phys. B **15**, 1477 (1982).

(5) R. R. Lucchese, G. Raseev, and V. McKoy, Phys. Rev. A **25**, 2572 (1982).

(6) M. E. Smith, R. R. Lucchese, and V. McKoy, Phys. Rev. A **29**, 1857 (1984).

(7) J. L. Dehmer and D. Dill, "The Continuum Multiple-Scattering Approach to Electron-Molecule Scattering and Molecular Photoionization," in Electron-Molecule and Photon-Molecule Collisions, T. N. Rescigno, V. McKoy, and B. Schneider, Eds. (Plenum Press, New York-London, 1979).

SECTION B

Studies of the Photoionization Cross Section of the 2π Level of Nitric Oxide

I. INTRODUCTION

Theoretical studies of molecular photoionization, which yield cross sections and photoelectron angular distributions, can provide an important probe of molecular electronic structure and dynamics.[1] With the tunable continuum provided by synchrotron radiation, the spectral variation of these cross sections and angular distributions can now be studied over a wide continuous range of incident photon energy. Such data have already shown that shape resonances play an important role in molecular photoionization.[2]

Recently, the photoionization cross sections of nitric oxide have been measured using both synchrotron radiation[3] and the (e, 2e) pseudophoton technique.[4] The measured cross sections for photoionization out of the 2π level show two resonant-like features at photon energies of 19 and 29 eV with the feature at 29 eV being very broad. This partial cross section has also been studied recently by the Stieltjes-Tchebycheff moment theory (STMT) approach[5] and by the continuum multiple-scattering method (MSM).[6] In this paper, we present photoionization cross sections and asymmetry parameters for the 2π level of NO which are obtained from the direct solution of the e + NO^+ collisional equations at the static-exchange level. These cross sections differ significantly from those obtained by the STMT approach; in particular, the nonresonant $2\pi \rightarrow k\pi$ and $2\pi \rightarrow k\delta$ contributions to this partial cross section do not show the sharp structure seen in the STMT results[5] at photon energies between 13 and 17 eV. Our calculated cross sections also suggest that the broad feature at a photon energy of 29 eV is nonresonant and arises from the energy dependence of the $2\pi \rightarrow k\pi$ and $2\pi \rightarrow k\delta$ dipole matrix elements. However, this feature is not as pronounced in the calculated cross

sections as is observed experimentally and, moreover, our cross sections are smaller than the measured cross sections in this region. At the equilibrium geometry our calculated cross sections show a σ-shape resonance around 14 eV which is about 5 eV below the feature in the measured cross section, which has been attributed to this shape resonance.[3,6] The implication and a probable explanation of this difference are discussed.

II. THEORY AND CALCULATIONAL DETAILS

The rotationally unresolved, fixed-nuclei photoionization cross section is given by

$$\sigma_{i,f}(R) = \frac{4\pi^2\omega}{3c} \; | < \Psi_i(\mathbf{r},R) \; | \; \mu \; | \; \Psi_f(\mathbf{r},R) > |^2, \qquad (1)$$

where μ is the dipole moment operator and ω the photon frequency. In Eq. (1), $\Psi_i(\mathbf{r},R)$ is the initial state of the molecule and $\Psi_f(\mathbf{r},R)$ the final ionized state. For $\Psi_i(\mathbf{r},R)$ we use the ground state SCF wave function and for the (N-1) bound electrons of $\Psi_i(\mathbf{r},R)$ we use the ground state SCF orbitals, i.e., the frozen-core approximation. The continuum orbital in $\Psi_f(\mathbf{r},R)$ for the ejected electron is a solution of the one-particle Schrödinger equation with the static-exchange potential V_{N-1} of the ion. The continuum orbital satisfies the equation

$$\left(-\frac{1}{2}\nabla^2 + V_{N-1}(\mathbf{r},R) - \frac{k^2}{2} \right) \Psi_k(\mathbf{r},R) = 0, \qquad (2)$$

where $k^2/2$ is the kinetic energy of the ejected electron.

The partial wave component of Ψ_k, $\Psi_{k\ell m}$ then satisfies the Lippmann-Schwinger equation

$$\Psi^{(-)}_{k\ell m} = \phi_{k\ell m} + G_C^{(-)} U \Psi^{(-)}_{k\ell m}, \tag{3}$$

where $G_C^{(-)}$ is the Coulomb Green's function with incoming-wave boundary conditions, $\phi_{k\ell m}$ the regular Coulomb function, and U = 2V where V is the potential of the molecular ion with the Coulomb component removed. We have recently developed an iterative approach to the solution of the Lippmann-Schwinger equation which is based on the Schwinger variational principle.[7] Applications[8,9] have shown that the method is a very effective approach to electron-molecular ion collisions at energies where partial wave coupling due to nonspherical potentials and exchange effects are important. Details have been discussed elsewhere.[7] In this approach, we first solve the Lippmann-Schwinger equation by assuming an approximate separable form for the scattering potential U, i.e.,

$$U(\mathbf{r},\mathbf{r}') \simeq U^s(\mathbf{r},\mathbf{r}') = \sum_{i,j} \langle \mathbf{r}|U|\alpha_i \rangle \times (U^{-1})_{ij} \langle \alpha_j|U|\mathbf{r}' \rangle, \tag{4}$$

where the matrix $(U^{-1})_{ij}$ is the inverse of the matrix $U_{ij} = \langle\alpha_i|U|\alpha_j\rangle$. The functions α_i are initially chosen to be discrete basis functions such as Cartesian or spherical Gaussian functions. The solution of

equation (3) for the potential U^s is simply

$$\Psi^{(0)}_{k\ell m}(\mathbf{r}) = \phi_{k\ell m} + \sum_{i,j} \langle \mathbf{r}|G_C U|\alpha_i\rangle (D^{-1})_{ij} \times \langle a_j|U|\phi_{k\ell m}\rangle , \quad (5)$$

where the matrix $(D^{-1})_{ij}$ is the inverse of the matrix

$$D_{ij} = \langle \alpha_i| U - UG_C U|\alpha_j\rangle . \quad (6)$$

The solutions $\Psi^{(0)}_{k\ell m}$ provide the initial estimates of the photoionization cross sections which are, at this stage, variationally stable. However, these functions $\Psi^{(0)}_{k\ell m}$ are solutions of the Lippmann-Schwinger equation for separable potential U^s, and not for the actual scattering potential U. To obtain more accurate and, if necessary, converged solutions of Eq. (3) we have developed a method to iteratively improve the solutions of Eq. (5) $\Psi^{(0)}_{k\ell m}$. The procedure contains criteria which allow one to determine when the exact solutions of the scattering problem have been obtained.[10] Such solutions provide increasingly accurate estimates of both the photoionization cross section and photoelectron asymmetry parameters.

We have used this procedure to study the photoionization out of the 2π level of NO at the static-exchange frozen-core approximation.[8] The target wave function was constructed from the same (5s,3p,1d) contracted Cartesian Gaussian basis set as used in the STMT calculations of Ref. 5. The SCF energy of NO at the ground state equilibrium separation of 2.173 a.u. in this basis is -129.269 a.u. All matrix elements are evaluated by a single-center expansion and the radial integrals are computed by Simpson's rule.[11]

To assume convergence we truncated these expansions as follows:

(i) Maximum partial wave retained in the expansion of the scattering function = $\ell_{max} = 20$.

(ii) Maximum partial wave retained in the expansion of the scattering function in the exchange matrix elements = $\ell_{max}^{ex} = 20$.

(iii) Maximum partial wave retained in the expansion of $1/r_{12}$ in the direct potential (not including the nuclear terms) = $\lambda_{max} = 20$. We always include $2\lambda_{max}$ terms in the expansion of the nuclear potential.

(iv) Maximum partial wave in the expansion of the i^{th} occupied orbital in the exchange matrix elements = ℓ_i^{ex}. These values of ℓ_i^{ex} are chosen so that the orbitals are normalized to better than 0.99 and range from 20 for the 1σ orbital to 10 for the 1π orbital.

This truncation of the partial wave expansions should assure convergence of the calculated matrix elements and cross sections. For example, reduction of the expansion parameters to $\ell_{max} = 16$, $\lambda_{max} = 16$, $\ell_{max}^{ex} = 16$, $\ell_i^{ex}(1\sigma) = 16$, and $\ell_i^{ex}(1\pi) = 6$ leads to changes of about 3% in the eigenphase sum and less than 0.5 eV in the position of the resonance. In the nonresonant regions this error was considerably smaller. All radial integrands were

expanded on a grid of 800 points extending out to 64 a.u. The smallest step size in this grid was 0.01 a.u., which was used out to 2 a.u., and the largest step size was 0.16 a.u.

The photoionization cross sections reported here were calculated with continuum wave functions obtained after one or two steps in the iterative procedure.[10] In general, the cross sections obtained with the uniterated scattering functions, i.e., the $\Psi^{(0)}_{k\ell m}$ of Eq. (5), were accurate to within 2% in the nonresonant regions and to within 15% in the resonance region. The starting basis sets for these calculations contained a total of 18 Gaussian functions for the $k\sigma$ and $k\pi$ channels and 17 for the $k\delta$ channel.

III. RESULTS AND DISCUSSION

Figure 1 shows our calculated results for the $2\pi \rightarrow k\sigma$, $2\pi \rightarrow k\pi$, and $2\pi \rightarrow k\delta$ components of the fixed-nuclei (R = 2.173 a.u.) photoionization cross sections for the 2π level of NO. The photon energy scale assumes an ionization potential of 9.3 eV. The $2\pi \rightarrow k\sigma$ component of the cross section is very clearly enhanced by a shape resonance centered at about 5 eV of photoelectron kinetic energy. The calculated eigenphases show a very strong mixing of the p and f waves in this region. These results also show that the $2\pi \rightarrow k\pi$ and $k\delta$ cross sections are non-shape resonant. Their enhancement around a photon energy of 24 eV is due to the general energy dependence of the dipole matrix elements for the 2π valence level. The $2\pi \rightarrow k\pi$ and $k\delta$ components will hence be insensitive to changes in the internuclear distance.

Figure 2 shows the $2\pi \rightarrow k\sigma$, $k\pi$, and $k\delta$ photoionization cross sections of Delaney et al.[5] using six-point Tchebycheff imaging procedure.[12] A comparison of our results in Figure 1 with those of Figure 2 show that our $2\pi \rightarrow k\pi$ and $k\delta$ cross sections do not show the sharp structure seen between 13 and 17 eV in the results of the Tchebycheff imaging procedure.[5] Moreover, the general shape of the $k\pi$ and $k\delta$ cross sections of the imaging procedure[5] is substantially different from those of the present calculations. We note that these calculations are both done at the static-exchange level using the same molecular ion potential. These results suggest that the sharp structure in these $k\pi$ and $k\delta$ cross sections[5] is spurious and may, in fact, be due to the inclusion of insufficient or unconverged moments of the oscillator strength distribution in these calculations.[13]

In Figure 3 we compare our calculated 2π photoionization cross sections with the experimental results obtained by synchrotron radiation[3] and (e, 2e)[4] measurements. Figure 3 also includes the cross sections obtained by the Tchebycheff imaging procedure[5] and the continuum multiple scattering method.[6] The multiple scattering cross sections are vibrationally averaged while the other calculated results are for the nuclei fixed at R = 2.173 a.u.

The shape resonance feature is evident around 14 eV in our calculated cross section. The experimental data[3] extend only down to photon energies of 16 eV and, moreover, shows a feature at around 18 eV which has been attributed to the shape-resonant σ continuum.[3,6] The vibrationally averaged cross sections of the multiple scattering method do show a weak resonant feature around 19 eV. Our experience suggests that vibrational averaging of the fixed-nuclei cross sections for the $\nu = 0$ level will not shift the resonant

feature from its present position of 14 eV up to around 19 eV.[14] As a quantitative check we calculated the $2\pi \rightarrow k\sigma$ fixed-nuclei cross sections at an internuclear distance of 2.003 a.u., the equilibrium value of the ion. As expected, the resonance feature was broadened and shifted to higher energy ($\sim$19 eV) but its peak value was essentially unchanged. Vibrational averaging of such cross sections will not move the position of the resonance peak significantly away from its value at the equilibrium internuclear distance of 2.173. Studies of the vibrationally resolved photoionization cross sections down to 12 eV of photon energy can help clarify the origin of these features. The role of autoionizing states in this region should also be explored.

Our results show a very broad feature between 20 and 32 eV which is nonresonant and simply due to the dependence of the $2\pi \rightarrow k\pi$ and $k\delta$ dipole matrix elements on photon energy. The calculated cross sections do not adequately account for the broad resonance-like feature observed experimentally around 29 eV. Vibrational averaging is not expected to have any significant effect on these nonresonant cross sections and a numerical test carried out at R = 2.003 a.u. confirmed this. We also note that the cross sections obtained in this energy region by the Tchebycheff imaging technique[5] lie well below the experimental values.[3] Moreover, this feature is also not seen in the continuum multiple scattering results.[6] These results suggest that the broad enhancement of the cross section around 28 eV could be due to unresolved bands of autoionizing lines converging to a higher ionic level. Vibrationally resolved studies in this region are clearly needed.

In Figure 4 we compare our calculated photoelectron asymmetry parameters with the measured values. Although the results account for the

rise of these parameters with energy, the calculated values are too high. Measurements of these parameters below 16 eV will be useful in view of the predicted behavior between 10 and 16 eV.

IV. CONCLUSIONS

The results of these studies show that the broad feature in the measured cross section for the 2π level of NO around 29 eV is not due to a shape resonance and that the possible role of autoionization in this region should be examined. Our results also predict that the shape resonance due to the σ continuum is located around 14 eV which is about 5 eV below the feature in the measured cross sections which has been attributed to a shape resonance.[3,6] We have also shown that the sharp structure in the $k\pi$ and $k\delta$ components of the photoionization cross sections between 13 and 17 eV seen in the Tchebycheff imaging results[5] is spurious. Extension of the present measurements to photon energies below 16 eV and vibrationally resolved studies of these photoionization cross sections are clearly needed.

References and Notes

(1) J. Berkowitz, Photoabsorption, Photoionization, and Photoelectron Spectroscopy (Academic, New York, 1979).

(2) See, for example, J. B. West, A. C. Parr, B. E. Cole, D. L. Ederer, R. Stockbauer, and J. L. Dehmer, J. Phys. B **13**, L105 (1980).

(3) S. Southworth, C. M. Truesdale, P. H. Korbin, D. W. Lindle, D. W. Brewer, and D. A. Shirley, J. Chem. Phys. **76**, 143 (1982).

(4) C. E. Brion and K. H. Tan. J. Electron Spectrosc. Relat. Phenom. **23**, 1 (1981).

(5) J. J. Delaney, I. H. Hillier, and V. R. Saunders, J. Phys. B **15**, 1477 (1982).

(6) S. Wallace, D. Dill, and J. L. Dehmer, J. Chem. Phys. **76**, 1217 (1982).

(7) R. R. Lucchese and V. McKoy, Phys. Rev. A **24**, 770 (1981).

(8) R. R. Lucchese, G. Raseev, and V. McKoy, Phys. Rev. A **25**, 2572 (1982).

(9) R. R. Lucchese and V. McKoy, Phys. Rev. A **26**, 1406 (1982).

(10) R. R. Lucchese, D. K. Watson, and V. McKoy, Phys. Rev. A **22**, 421 (1980).

(11) R. R. Lucchese and V. McKoy, Phys. Rev. A **21**, 112 (1980).

(12) J. J. Delaney, V. R. Saunders, and I. H. Hillier, J. Phys. B **14**, 819 (1981).

(13) P. W. Langhoff, C. T. Corcoran, J. S. Sims, F. Weinhold, and R. M. Glover, Phys. Rev. A **14**, 1042 (1976).

(14) R. R. Lucchese and V. McKoy, Phys. Rev. A **26**, 1406 (1982).

FIGURE CAPTIONS

Figure 1: Components of the calculated photoionization cross section for the 2π level of NO in the present work: (---) $2\pi \rightarrow k\sigma$, (—) $2\pi \rightarrow k\pi$, (— — —) $2\pi \rightarrow k\delta$.

Figure 2: Components of the calculated photoionization cross section for the 2π level of NO, from Ref. 5, using the Tchebycheff imaging technique: (---) $2\pi \rightarrow k\sigma$, (—) $2\pi \rightarrow k\pi$, (— — —) $2\pi \rightarrow k\delta$.

Figure 3: A comparison of 2π photoionization cross sections in NO: (—) present fixed-nuclei (R = 2.173 a.u.) results, (---) Tchebycheff imaging results of Delaney et al. (Ref. 5), (— — —) vibrationally averaged results of the continuum multiple scattering model (Ref. 6), + synchrotron radiation measurements of Ref. 3, θ (e, 2e) measurements of Ref. 4.

Figure 4: A comparison of asymmetry parameters for 2π photoionization of NO: (—) present work using the fixed nuclei approximation, (---) vibrationally averaged results of the MSM (Ref. 6), Δ synchrotron radiation experiments of Ref. 3.

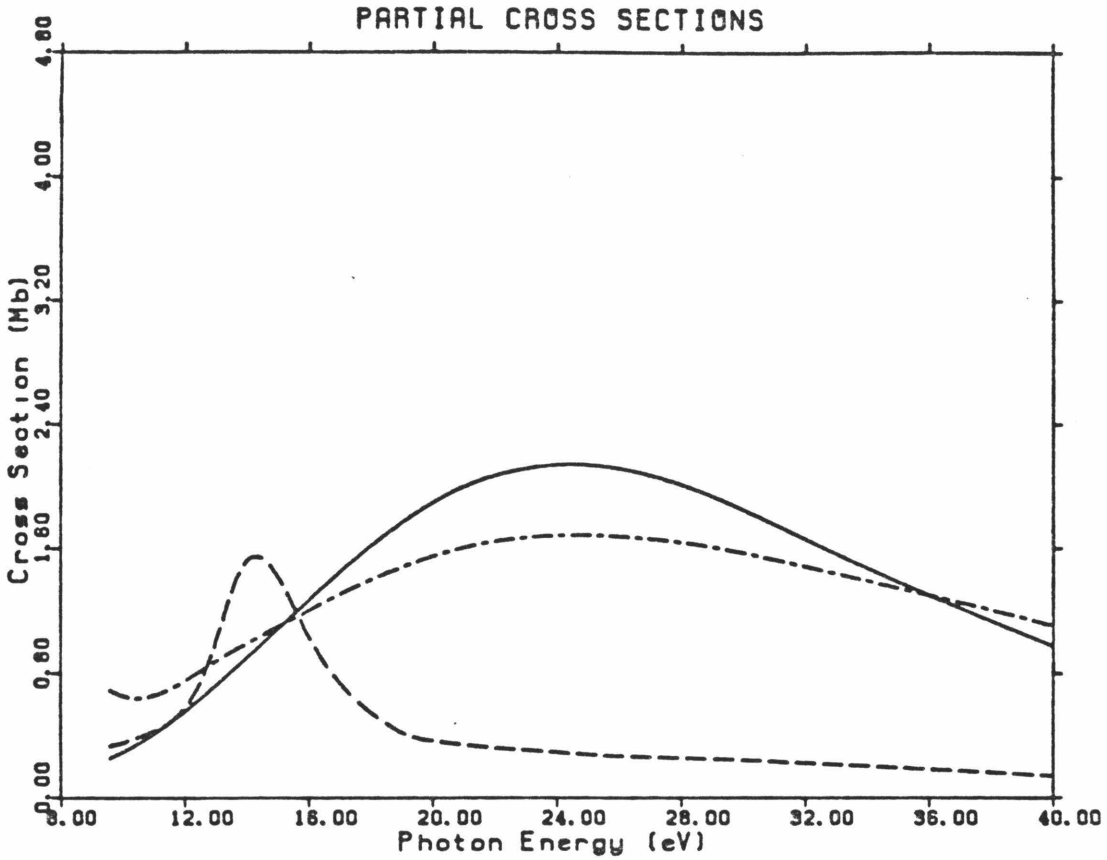
PARTIAL CROSS SECTIONS
Cross Section (Mb)
0.00
0.80
1.60
2.40
3.20
4.00
4.80
8.00
12.00
16.00
20.00
24.00
28.00
32.00
36.00
40.00
Photon Energy (eV)

FIGURE 1.

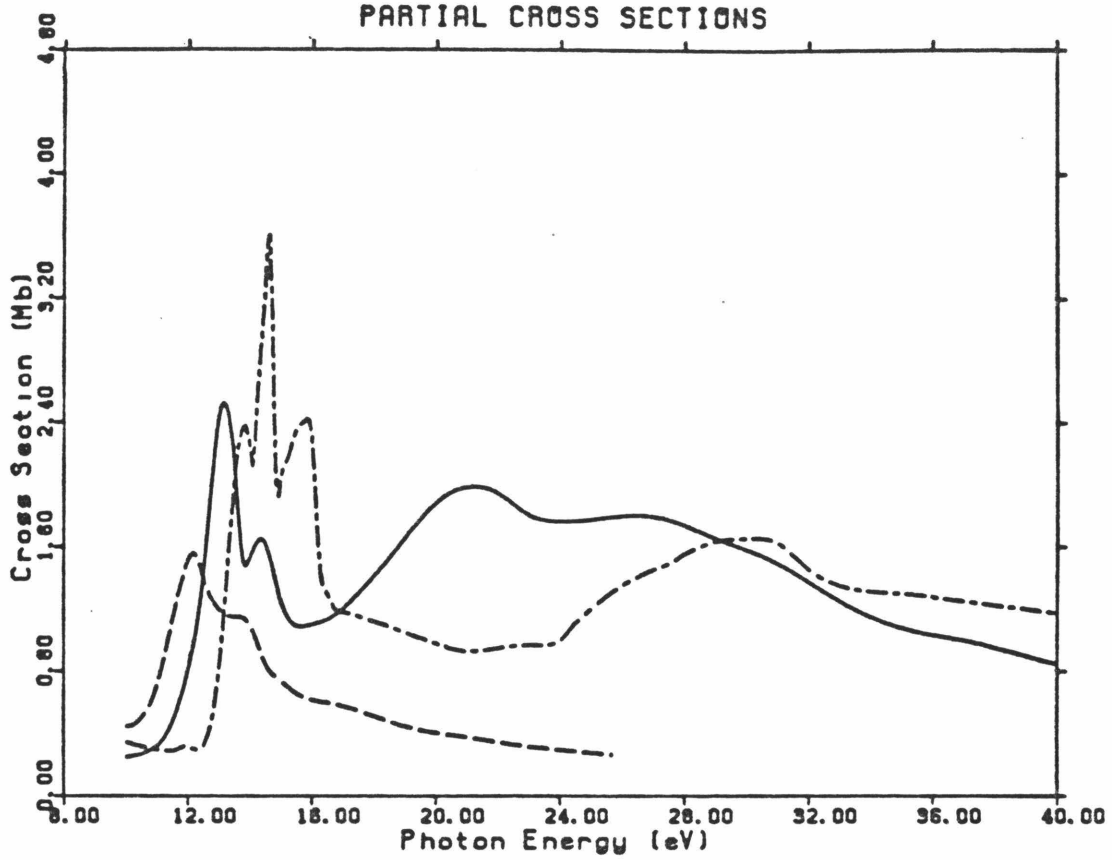
PARTIAL CROSS SECTIONS
Cross Section (Mb)
0.00
0.80
1.60
2.40
3.20
4.00
4.80
8.00
12.00
16.00
20.00
24.00
28.00
32.00
36.00
40.00
Photon Energy (eV)

FIGURE 2.

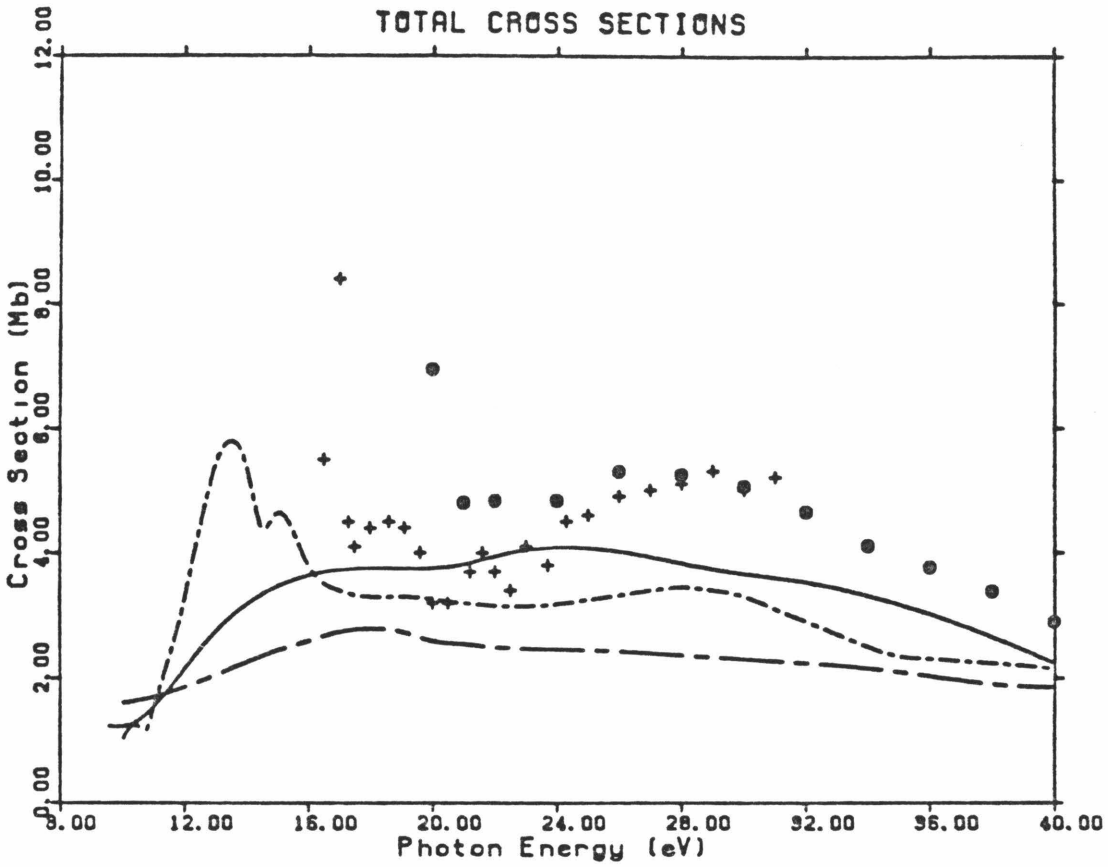
TOTAL CROSS SECTIONS
Cross Section (Mb)
0.00
2.00
4.00
6.00
8.00
10.00
12.00
8.00
12.00
16.00
20.00
24.00
28.00
92.00
96.00
40.00
Photon Energy (eV)

FIGURE 3.

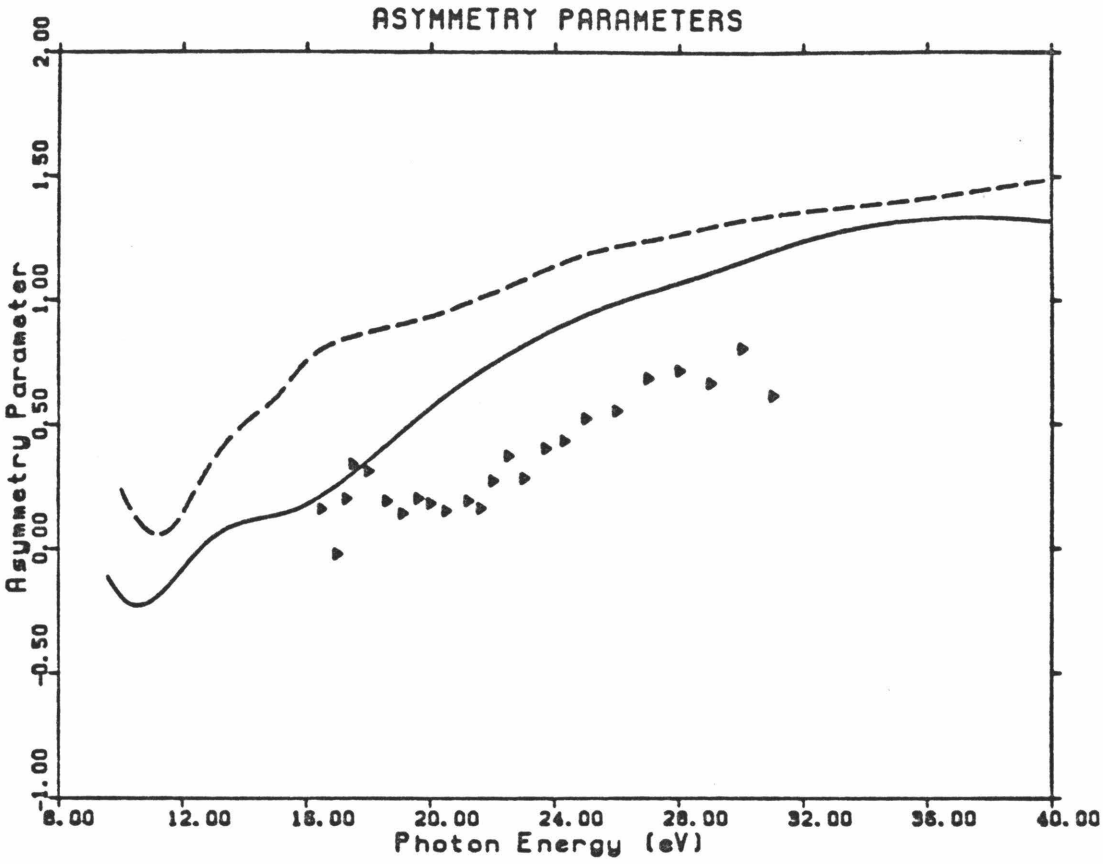
ASYMMETRY PARAMETERS
Asymmetry Parameter
2.00
1.50
1.00
0.50
0.00
-0.50
-1.00
8.00
12.00
16.00
20.00
24.00
28.00
32.00
36.00
40.00
Photon Energy (eV)

FIGURE 4.

SECTION C

Shape Resonant Features in the Photoionization Spectrum of the 5σ and 4σ Levels of NO

I. INTRODUCTION

Shape resonances in the σ continuum are known to play an important role in the photoionization of many diatomic and linear polyatomic molecules.[1-3] These resonances and their effects on the cross sections, angular distributions, and vibrational branching ratios have been extensively characterized by synchrotron radiation studies.[1,4] Several approaches to the calculation of molecular photoionization cross sections have also been used to carry out related theoretical studies on these resonance processes. These approaches include the Stieltjes-Tchebycheff Moment Theory method (STMT),[5] the Continuum Multiple-Scattering Model (CMSM),[6] and several methods for the direct solution of the Hartree-Fock equations for the photoelectron continuum orbital.[7-12] Although the more general features of the resonant cross sections obtained by these different methods are similar for many systems, some physically important trends in the differences between these various results can be identified. For example, the muffin-tin approximation and local potential of the CMSM can lead to much larger vibrational averaging effects and deviations from Franck-Condon behavior than do normal static-exchange calculations.[10,13,14] In some cases the STMT studies have excessively broadened and even smoothed away pronounced resonance structure seen in calculations which directly use photoelectron continuum functions.[10,13] These results suggest a certain sensitivity of shape resonant photoionization cross sections to both the potentials and techniques used in their determination.

With some exceptions such as O_2,[15] most systems studied to date have been closed-shell molecules.[1,3,4] The photoionization spectra of such

molecules show no multiplet structure and, from the point of view of theory, the molecular ion potential seen by the photoelectron is of a particularly simple form. For this and other reasons discussed below, the photoionization spectra of NO, an open-shell molecule with a $(1\sigma)^2(2\sigma)^2(3\sigma)^2(4\sigma)^2(5\sigma)^2(1\pi)^4(2\pi)^1$, $^2\Pi$ ground state electron configuration, should be particularly interesting. Ionization of the 2π level leads to the $X^1\Sigma^+$ closed-shell ground ionic state of NO^+, whereas removal of the 5σ or 4σ electron leads to the $b^3\Pi$ and $A^1\Pi$ terms or the $c^3\Pi$ and $B^1\Pi$ terms, respectively. Removal of the 1π electron gives rise to six terms.[16] Separate synchrotron radiation studies have determined the cross sections for production of the $X^1\Sigma^+$, $b^3\Pi$, and $c^3\Pi$ states,[17] the $c^3\Pi$ and $B^1\Pi$ states,[18] and the $b^3\Pi$ and $A^1\Pi$ states[19] of the NO^+ ion. These cross sections for photoionization of the 2π, 5σ, and 4σ orbitals exhibit the shape resonance feature expected in the σ continuum. Moreover, in their recent measurements, Morin et al.[19] actually determined multiplet-specific cross sections for the $b^3\Pi$ and $A^1\Pi$ ions which show resonant peaks at quite different photoelectron kinetic energies. This difference in the photoionization cross section for the two multiplets arises from the different exchange potentials seen by the photoelectron in the two cases and clearly reflects the sensitivity of shape-resonant cross sections to the choice of the potential.

Related theoretical studies have shown that the σ shape resonance feature in photoionization of the 2π level is obscured by the large nonresonant $2\pi \rightarrow k\pi$ and $2\pi \rightarrow k\delta$ contributions to this cross section.[20-22] Vibrational averaging significantly dampened the resonant component in the

CMSM cross sections for this level.[20] Cross sections obtained with the Hartree-Fock photoelectron continuum orbitals showed no indication of such pronounced vibrational effects.[22] The overall agreement between these calculated cross sections and the experimental data, however, is not very good and, in particular, the broad feature between photon energies of 20 and 40 eV is not accounted for by these models.[20-22] The STMT cross sections for photoionization of the 5σ and 4σ levels[21] were obtained using a multiplet-averaged potential for the molecular ion and also showed some sharply structured features similar to those seen in the 2π results and which are presumably artifacts of their calculation.[22,23]

In this paper we present photoionization cross sections for production of the $b^3\Pi$, $A^1\Pi$, $c^3\Pi$, and $B^1\Pi$ states of NO^+, arising from the ionization of the 5σ and 4σ orbitals of NO. In our studies we use Hartree-Fock photoelectron continuum orbitals. For the 5σ level we use both multiplet-specific and multiplet-averaged molecular ion potentials, but for the 4σ level only the multiplet-averaged potential is used. The multiplet-specific and multiplet-averaged potentials lead to significantly different $A^1\Pi$ cross sections reflecting the sensitivity of this resonant cross section to the nonlocal component of the molecular ion potentials since these two potentials differ only in their exchange parts. These differences are much smaller in the $b^3\Pi$ cross sections as would be expected from the 3:1 weighting of the triplet to singlet states in the multiplet-averaged potential. Although the overall shapes of the calculated and measured photoionization cross sections are similar, there are some important differences. For example, the resonance peak in the calculated $b^3\Pi$ cross section occurs at a significantly

higher energy than is seen experimentally. This discrepancy, however, is much less pronounced for the $A^1\Pi$ cross sections. Photoelectron asymmetry parameters for both the 5σ and 4σ levels are also discussed.

An outline of this paper is as follows. In the next section we give a brief outline of our method for obtaining the photoelectron continuum orbitals. In this section we also discuss the multiplet-specific static-exchange potentials used in these calculations. We then present the results of our studies of the photoionization of the 5σ and 4σ levels of NO along with a comparison of these results with those of other theoretical methods and available experimental data.

II. THEORETICAL DEVELOPMENTS

A. Solution of the Equations

The rotationally unresolved, fixed-nuclei, photoionization cross section is given by

$$\sigma = \frac{4\pi^2\omega}{3c} \left| < \Psi_i(\mathbf{r};R) | \boldsymbol{\mu} | \Psi_f(\mathbf{r},R) > \right|^2$$

where $\boldsymbol{\mu}$ is the dipole moment operator and ω is the photon frequency. In this expression Ψ_i represents the initial state of the molecule with N bound electrons and Ψ_f the final state with a photoelectron in the electronic continuum. For Ψ_i we use the Hartree-Fock wave function. For Ψ_f we use the frozen core approximation in which the orbitals containing the N-1 bound electrons of the ion are constrained to be identical to those of Ψ_i. The continuum orbital satisfies a one-electron Schrödinger equation

of the form

$$(\nabla^2 - U_{dir} - U_{ex} + k^2)\phi_k = \sum_{i=1}^{n} \lambda_i \chi_i \qquad (1)$$

where the λ_i are Lagrange multipliers which enforce the orthogonality of ϕ_k to the n occupied orbitals χ_i, and U_{dir} and U_{ex} are twice the local and nonlocal components of the molecular ion potential. The potential of Eq. (1) is nonspherical and nonlocal and several methods for solving such equations have recently been developed.[7-12] In this work we solve Eq. (1) for the photoelectron continuum function ϕ_k by a method in which the direct potential U_{dir} is treated exactly by numerical integration and the exchange or nonlocal component is approximated by a separable potential of the Schwinger form[12]

$$U_{ex} \simeq \sum_{ij}^{m} U_{ex}|\alpha_i\rangle \left(U_{ex}^{-1}\right)_{ij} \langle \alpha_j| U_{ex} \qquad (2)$$

where the α_i are chosen to be Cartesian Gaussian functions. This approach to the solution of these equations for molecular electronic continuum orbitals is ideally suited to the study of strongly polar molecular ions. The details of the method have been discussed previously[12] and here we present only a brief review. The solution of Eq. (1) can be written as

$$\phi_k = \phi_k^e + \sum_i \lambda_i \phi^{\chi_i} \qquad (3)$$

where the functions $\phi_{\mathbf{k}}^{e}$ and ϕ^{χ_i} satisfy the integral equations

$$\phi_{\mathbf{k}}^{e} = \phi_{\mathbf{k}}^{d} + G^{d}U_{ex}\Phi_{\mathbf{k}}^{e} \tag{4a}$$

and

$$\phi^{\chi_i} = G^{d}\chi_i + G^{d}U_{ex}\phi^{\chi_i}. \tag{4b}$$

The function $\phi_{\mathbf{k}}^{d}$ in Eq. (4a) is the solution for the direct potential, i.e.,

$$(\nabla^2 - U_{dir} + k^2)\phi_{\mathbf{k}}^{d} = 0 \tag{5}$$

and G^d is the Green's function for this potential, i.e., $(\nabla^2 - U_{dir} + k^2 \pm i\varepsilon)^{-1}$. In the solution of Eqs. (4) U_{ex} is approximated by the separable form of Eq. (2). The resulting equations along with Eq. (5) are the expanded in partial waves and numerically integrated. The solutions obtained are the exact solutions of Eq. (1), but with U_{ex} approximated as in Eq. (2). Although these solutions can be iteratively improved to yield converged solutions of Eq. (1),[12] we have found that in general it is not necessary to obtain such solutions and in these studies we used the solutions of Eq. (1) with a suitable Gaussian basis in Eq. (2).

Finally, the Hartree-Fock photoionization cross sections obtained with these photoelectron continuum orbitals can also be shown to be variationally stable.[12]

B. Computational Details

We have used this procedure to study the photoionization cross sections and photoelectron angular distributions for the 5σ and 4σ orbitals of NO within the frozen-core approximation. The SCF wave function for NO was obtained with a (5s, 3p, 1d) basis of contracted Cartesian Gaussian functions. This same basis was used previously by Delaney et al.[21] in their STMT study of these photoionization cross sections. At the ground state equilibrium internuclear distance of 2.173 a.u. the SCF energy in this basis was -129.269 a.u.

The partial wave expansions used in the solution of Eqs. (4) and (5) were truncated at sufficiently high values so as to ensure adequate convergence of the photoionization cross sections. For example, the maximum partial wave retained in the expansion of the scattering basis, i.e., the α_i's of Eq. (2), was 24. This was also the maximum partial wave retained in both the expansion of the scattering basis in the exchange matrix elements and in the expansion of $1/r_{ij}$ in the direct potential. In the expansion of the nuclear potential we retained partial waves up to $\ell_{max} = 48$. In the expansion of the target orbitals in the exchange matrix elements, the maximum partial wave was chosen so that the corresponding orbital normalization was better than 0.99, e.g., $\ell_i^{ex} = 20$ and 10 for the 1σ and 2π orbitals, respectively, and the ℓ_i^{ex} for the other orbitals were between these values.

The Gaussian basis set used in the separable representation of the potential in Eq. (2) contained fourteen functions all centered on the nuclei. The basis is shown in Table I. The radial integration grid extended out to 64

a.u. and contained 320 points. The integration step size ranged from 0.02 near the nuclei to 0.5 a.u. beyond 14 a.u.

C. The Scattering Potentials

Photoionization of the 5σ orbitals of NO produces NO^+ ions in both the $b^3\Pi$ and $A^1\Pi$ states with ionization potentials of 16.6 and 18.3 eV, respectively. The electronic configuration of these ions is $(\text{core})(5\sigma)^1(2\pi)^1$ where (core) represents all of the electrons in closed shells. The molecular ion potentials seen by the photoelectron are obviously different for the two final states of the ion and hence the photoelectron continuum orbitals are multiplet-specific. Since these multiplet-specific potentials differ only in their exchange parts, one does not normally expect a great sensitivity of the calculated photoionization cross sections to the choice of potential. Identical potentials are hence generally used for the different multiplet channels. This assumption, which has been made in previous studies of 5σ photoionization of NO,[20,21] leads to cross sections that are exactly in the multiplet ratio as a function of kinetic energy, e.g., 3:1 in this case. Although multiplet-averaged potentials can be expected to work well in nonresonant channels, important features such as the peak position in shape resonant cross sections may be poorly reproduced by such potentials. Photoionization of the 5σ and 4σ orbitals of NO provides an excellent example to illustrate these effects. In fact, we will see that these multiplet-specific cross sections have resonance peaks at significantly different photoelectron kinetic energies, a feature which is completely masked by multiplet-averaged potentials.

The final state wave functions for photoionization from the 5σ orbital leading to the $b^3\Pi$ state of NO^+ are

$$\Psi(^2\Pi) = \frac{1}{\sqrt{6}} \{ 2|(\text{core})(5\sigma)(2\pi_+)(\overline{k\sigma})| - |(\text{core})(\overline{5\sigma})(2\pi_+)(k\sigma)| - |(\text{core})(5\sigma)(\overline{2\pi}_+)(k\sigma)| \} \quad (6a)$$

$$\Psi(^2\Sigma^+) = \frac{1}{\sqrt{12}} \{ 2|(\text{core})(5\sigma)(2\pi_+)(\overline{k\pi}_-)| - |(\text{core})(\overline{5\sigma})(2\pi_+)(k\pi_-)| - |(\text{core})(5\sigma)(\overline{2\pi}_+)(k\pi_-)| + 2|(\text{core})(5\sigma)(2\pi_-)(\overline{k\pi}_+)| - |(\text{core})(\overline{5\sigma})(2\pi_-)(k\pi_+)| - |(\text{core})(5\sigma)(\overline{2\pi}_-)(k\pi_+)| \} \quad (6b)$$

$$\Psi(^2\Sigma^-) = \frac{1}{\sqrt{12}} \{ 2|(\text{core})(5\sigma)(2\pi_+)(\overline{k\pi}_-)| - |(\text{core})(\overline{5\sigma})(2\pi_+)(k\pi_-)| - |(\text{core})(5\sigma)(\overline{2\pi}_+)(k\pi_-)| - 2|(\text{core})(5\sigma)(2\pi_-)(\overline{k\pi}_+)| + |(\text{core})(\overline{5\sigma})(2\pi_-)(k\pi_+)| + |(\text{core})(5\sigma)(\overline{2\pi}_-)(k\pi_+)| \} \quad (6c)$$

$$\Psi(^2\Delta) = \frac{1}{\sqrt{6}} \{ 2|(\text{core})(5\sigma)(2\pi_+)(\overline{k\pi}_+)| - |(\text{core})(\overline{5\sigma})(2\pi_+)(k\pi_+)| - |(\text{core})(5\sigma)(\overline{2\pi}_+)(k\pi_+)| \} \quad (6d)$$

where a bar over an orbital denotes a β spin function and absence of a bar implies an α spin function. With these wave functions the static-exchange single-particle Schrödinger equations satisfied by these continuum orbitals can be derived straightforwardly[11]

$$^2\Pi: \quad P(f + \sum_{\text{core}} (2J_i - K_i) + J_{5\sigma} + J_{2\pi} + \tfrac{1}{2} K_{5\sigma} + \tfrac{1}{2} K_{2\pi} - \varepsilon)P|k\sigma\rangle = 0 \quad (7a)$$

$$^2\Sigma^+: \quad P(f + \sum_{\text{core}} (2J_i - K_i) + J_{5\sigma} + J_{2\pi} + \tfrac{1}{2} K_{5\sigma} + \tfrac{1}{2} K_{2\pi} + S''_{2\pi} + \tfrac{1}{2} S'_{2\pi} - \varepsilon)P|k\pi_+\rangle = 0 \quad (7b)$$

$$^2\Sigma^-: \quad P(f + \sum_{\text{core}} (2J_i - K_i) + J_{5\sigma} + J_{2\pi} + \tfrac{1}{2} K_{5\sigma} + \tfrac{1}{2} K_{2\pi} - S''_{2\pi} - \tfrac{1}{2} S'_{2\pi} - \varepsilon)P|k\pi_+\rangle = 0 \quad (7c)$$

$$^2\Delta: \quad P(f + \sum_{\text{core}} (2J_i - K_i) + J_{5\sigma} + J_{2\pi} + \tfrac{1}{2} K_{5\sigma} + \tfrac{1}{2} K_{2\pi} - \varepsilon)P|k\pi_+\rangle = 0. \quad (7d)$$

In these equations J_i and K_i represent the usual Coulomb and exchange operators and P is a projection operator which ensures the necessary

orthogonality of the continuum orbital to the occupied orbitals.[11] Their effect is equivalent to the Lagrange multipliers of Eq. (1). The operators S" and S' are defined by

$$S''_{\pi}\phi^{+}(\mathbf{r}_1) = \phi^{-}(\mathbf{r}_1) \int d^3\mathbf{r}_2 [\pi^{-}(\mathbf{r}_2)]^{*} \frac{1}{r_{12}} \pi^{+}(\mathbf{r}_2)$$

and

$$S'_{\pi}\phi^{+}(\mathbf{r}_1) = \pi^{+}(\mathbf{r}_1) \int d^3\mathbf{r}_2 [\pi^{-}(\mathbf{r}_2)]^{*} \frac{1}{r_{12}} \phi^{-}(\mathbf{r}_2)$$

and f is given by

$$f_i = -\frac{1}{2}\nabla_i^2 - \sum_{\alpha}^{\text{nuclei}} \frac{Z_{\alpha}}{r_{i\alpha}} .$$

The kinetic energy of the photoelectron is given by ε.

The final-state wave functions for photoionization of the 5σ orbital leading to the $A^1\Pi$ state of NO^+ are likewise

$$\Psi(^2\Pi) = \frac{1}{\sqrt{2}} \{ |(\text{core})(5\sigma)(\overline{2\pi}_+)(k\sigma)| - |(\text{core})(\overline{5\sigma})(2\pi_+)(k\sigma)| \} \qquad (8a)$$

$$\Psi(^2\Sigma^+) = \frac{1}{2} \{ |(\text{core})(5\sigma)(\overline{2\pi}_+)(k\pi_-)| - |(\text{core})(\overline{5\sigma})(2\pi_+)(k\pi_-)| + |(\text{core})(5\sigma)(\overline{2\pi}_-)(k\pi_+)| - |(\text{core})(\overline{5\sigma})(2\pi_-)(k\pi_+)| \} \qquad (8b)$$

$$\Psi(^2\Sigma^-) = \frac{1}{2}\{|(\text{core})(5\sigma)(\overline{2\pi}_+)(k\pi_-)| - |(\text{core})(\overline{5\sigma})(2\pi_+)(k\pi_-)| - |(\text{core})(5\sigma)(\overline{2\pi}_-)(k\pi_+)| + |(\text{core})(\overline{5\sigma})(2\pi_-)(k\pi_+)|\} \quad (8c)$$

$$\Psi(^2\Delta) = \frac{1}{\sqrt{2}}\{|(\text{core})(5\sigma)(\overline{2\pi}_+)(k\pi_+)| - |(\text{core})(\overline{5\sigma})(2\pi_+)(k\pi_+)|\} \quad (8d)$$

and the related single-particle Schrödinger equations for the continuum orbitals are

$$^2\Pi: \quad P(f + \sum_{\text{core}}(2J_i - K_i) + J_{5\sigma} + J_{2\pi} - \tfrac{1}{2}K_{5\sigma} - \tfrac{1}{2}K_{2\pi} - \varepsilon)P|k\sigma\rangle = 0 \quad (9a)$$

$$^2\Sigma^+: \quad P(f + \sum_{\text{core}}(2J_i - K_i) + J_{5\sigma} + J_{2\pi} - \tfrac{1}{2}K_{5\sigma} - \tfrac{1}{2}K_{2\pi} + S''_{2\pi} - \tfrac{1}{2}S'_{2\pi} - \varepsilon)P|k\pi_+\rangle = 0 \quad (9b)$$

$$^2\Sigma^-: \quad P(f + \sum_{\text{core}}(2J_i - K_i) + J_{5\sigma} + J_{2\pi} - \tfrac{1}{2}K_{5\sigma} - \tfrac{1}{2}K_{2\pi} - S''_{2\pi} + \tfrac{1}{2}S'_{2\pi} - \varepsilon)P|k\pi_+\rangle = 0 \quad (9c)$$

$$^2\Delta: \quad P\Big(f + \sum_{core}(2J_i - K_i) + J_{5\sigma} + J_{2\pi} - \tfrac{1}{2}K_{5\sigma} - \tfrac{1}{2}K_{2\pi} - \varepsilon\Big)P|k\pi_+\rangle = 0. \qquad (9d)$$

The molecular ion potentials of Eqs. (7) and (9) which are appropriate for the $b^3\Pi$ and $A^1\Pi$ ions of NO^+ differ essentially in their exchange components. Due to the sensitivity of resonant photoionization cross sections to nonlocal potentials, these differences are sufficient to lead to significant nonstatistical behavior of these multiplet-specific cross sections.

To obtain a multiplet-averaged potential we start with a final state wave function which is a linear combination of the wave functions of Eqs. (6) and (8) with a 3:1 weighting, respectively. These two wave functions are the appropriate final state wave functions for ionization leading to the $b^3\Pi$ and $A^1\Pi$ ions. This combination of wave functions results in a set of final state wave functions in which the 5σ electron is singlet coupled to the continuum electron. With this form for the wave function, the resulting single-particle equations for the continuum orbitals can be derived

$$^2\Pi: \quad P\Big(f + \sum_{core}(2J_i - K_i) + J_{5\sigma} + J_{2\pi} + K_{5\sigma} - \tfrac{1}{2}K_{2\pi} - \varepsilon\Big)P|k\sigma\rangle = 0 \qquad (10a)$$

$$^2\Sigma^+: \quad P\Big(f + \sum_{core}(2J_i - K_i) + J_{5\sigma} + J_{2\pi} + K_{5\sigma} - \tfrac{1}{2}K_{2\pi} + S''_{2\pi} - \tfrac{1}{2}S'_{2\pi} - \varepsilon\Big)P|k\pi_+\rangle = 0 \qquad (10b)$$

$$^2\Sigma^-: P(f + \sum_{core}(2J_i - K_i) + J_{5\sigma} + J_{2\pi} + K_{5\sigma} - \frac{1}{2}K_{2\pi} - S''_{2\pi} + \frac{1}{2}S'_{2\pi} - \varepsilon)P|k\pi_+> 0 \quad (10c)$$

$$^2\Delta: P(f + \sum_{core}(2J_i - K_i) + J_{5\sigma} + J_{2\pi} + K_{5\sigma} - \frac{1}{2}K_{2\pi} - \varepsilon)P|k\pi_+> = 0. \quad (10d)$$

The photoionization cross sections obtained with the continuum solutions of these equations will be referred to as the multiplet-averaged cross sections.

These photoelectron orbitals from Eqs. (7), (9), and (10) are used to evaluate the dipole length and velocity matrix elements which are needed to obtain the photoionization cross sections and angular distributions.[11] We note that the $^2\Sigma^+$ and $^2\Sigma^-$ wave functions in these equations do not define final states in which the photoelectron has a well defined m_ℓ projection on the molecular axis. To obtain the asymmetry parameters we, hence, work with linear combinations of these states in which the m_ℓ of the photoelectron is ± 1.

III. RESULTS AND DISCUSSION

A. Ionization of the 5σ Level

In Figure 1 we show the calculated photoionization cross sections leading to both the $b^3\Pi$ and $A^1\Pi$ states of NO^+. The photon energy scale assumes ionization potentials of 16.6 and 18.3 eV, respectively.[16] The pronounced resonance feature in these cross sections is due to the well-known shape resonance in the σ continuum.[17-21] Before comparing with available

experimental data, we note that these results indicate the significant nonstatistical multiplet behavior of these cross sections. Specifically the resonance maxima for the $b^3\Pi$ and $A^1\Pi$ ions occur at photoelectron kinetic energies of about 8.8 and 5.2 eV, respectively. This behavior arises from differences in the exchange component of the appropriate molecular ion potentials and so it is obviously not seen in studies using a multiplet-averaged potential.[20,21] Figure 2 shows the $b^3\Pi$ and $A^1\Pi$ photoionization cross sections obtained with the multiplet-averaged and multiplet-specific potentials. As expected, the differences between these pairs of cross sections are much larger for the $A^1\Pi$ state than for the $b^3\Pi$ state. In Figure 2 we have not included the multiplet-averaged static-exchange 5σ photoionization cross sections previously reported by Delaney et al.[21] These results were obtained with the STMT method and showed irregular structure which is presumably spurious and due to the imaging procedure used.[21] This spurious structure was also seen in the cross sections for the 2π level.[21,22]

In Figure 3 we compare our calculated cross sections, both length and velocity forms, for the $b^3\Pi$ state with the experimental data of Southworth et al.[17] These measured cross sections were obtained using synchrotron radiation. The calculated cross sections show a resonance maximum about 2 eV higher than is seen experimentally. Moreover, the peak height of our resonance is larger and its width is narrower than observed. We note however, that there is a significant difference between the peak values of the length and velocity forms of this resonant cross section. This difference again emphasizes the importance of electron correlation effects on resonant

cross sections.[11,23] Vibrational averaging would tend to reduce and broaden these cross sections[24] but the agreement between these fixed-nuclei static-exchange photoionization cross sections and the experimental data is obviously poorer for NO than for N_2[11] and CO.[23] In these cases the resonance features all arise from the σ shape resonant continuum. These differences reflect the more complex open-shell structure of NO^+. In Figure 3 we also show the fixed-nuclei cross section obtained with the CMSM.[20] This model gives a resonance width which is narrower than is seen in our static-exchange results, but the resonance positions are about the same. Vibrational averaging leads to significant,[20] but probably excessive,[13] broadening of these fixed-nuclei CMSM cross sections.

The vibrationally resolved ($v' = 0, 1$) photoionization cross sections for the $b^3\Pi$ and $A^1\Pi$ ions are also being studied by Morin et al.[19] Although preliminary unnormalized results have been published for these cross sections,[19] it seems advisable not to reproduce these results in our figures at this time.[24] Some comments, however, are in order. Although the observed resonance positions are lower than our calculated ones, the resonance feature does occur at about 3 eV higher kinetic energy in the $b^3\Pi$ than in the $A^1\Pi$ state of NO^+. The underlying resonance structure in these $b^3\Pi$ cross sections also appears narrower than in the data of Southworth et al.[17] Moreover, the unnormalized cross sections for the $v' = 0$ and $v' = 1$ levels of the $b^3\Pi$ channel indicate substantial non-Franck-Condon behavior.

Figure 4 shows our calculated photoelectron asymmetry parameters for the $b^3\Pi$ state along with those of the CMSM[20] and the measured values of Southworth et al.[17] The structure in these parameters between 17 and 22 eV

is due to autoionization which is not included in our model. Although the agreement between our calculated values and the experimental measurements is reasonable, it is again poor compared with the behavior seen in photoionization of related levels of N_2[11] and CO.[23]

B. Ionization of the 4σ Level

Photoionization of the 4σ level leads to the $c^3\Pi$ and $B^1\Pi$ states of NO^+. Unfortunately, the assignment of these states in the photoelectron spectrum is still controversial. One assignment associates both the $c^3\Pi$ and $B^1\Pi$ states with the band at 21.7 eV.[16] An alternative assignment puts the $c^3\Pi$ state at 21.7 eV and suggests that the $B^1\Pi$ state is strongly modified by configuration interaction and shifted to 22.7 eV.[25] In view of these uncertainties and significant discrepancies between experimental data, we obtained the photoionization cross sections for these channels using only the multiplet-averaged potential.

In Figure 5 we show our calculated cross sections for the $c^3\Pi$ state along with the CMSM results[20] and the experimental data of Southworth et al.[17] and Gustafsson and Levinson.[18] The photon energy scale assumes an ionization potential of 21.7 eV. The shape resonance feature is again evident in these cross sections. Our calculated cross sections are in better agreement with the synchrotron radiation data of Gustafsson and Levinson.[18] There is also a significant difference between the length and velocity forms of these cross sections. However, the synchrotron radiation data of Southworth et al.,[17] in which the cross section is substantially lower than that of ref. 18, are apparently in better agreement with the (e, 2e)

data.[17,26] Some further experimental studies of these cross sections could be very helpful. Figure 6 shows our calculated asymmetry parameters, those of the CMSM,[20] and the experimental data of Southworth et al.[17] The agreement between our calculated results and the measured asymmetry parameter is at best fair. The calculated asymmetry parameters for this level are expectedly quite similar to those of the 5σ level. The measured values show a deep minimum which is not seen in the data for the 5σ level.

Figure 7 shows our calculated cross sections for the $B^1\Pi$ level. In this figure we have assumed an ionization potential of 22.7 eV. Since we have used a multiplet-averaged potentials, the cross sections for these states and those of the $c^3\Pi$ state are in a 1:3 ratio. Again, the agreement between the calculated and measured photoionization cross sections is quite good.

IV. CONCLUSIONS

We have studied the cross sections for photoionization of the 5σ and 4σ levels of NO. These cross sections for the $b^3\Pi$ $(5\sigma^{-1})$ and $A^1\Pi$ $(5\sigma^{-1})$ states show nonstatistical multiplet-specific effects which arise from the sensitivity of the σ shape resonance in these channels to the exchange component of the potential seen by the photoelectron. Specifically, the resonance peak in the $A^1\Pi$ cross section appears at a kinetic energy about 3 eV lower than in the $b^3\Pi$. This result certainly emphasizes the importance of using the correct potentials in studies of shape resonance features in molecular photoionization.

This multiplet-specific effect has also been observed experimentally,[19] although the resonances actually occur at lower energies than predicted. The calculated peak heights of these resonance cross sections are somewhat larger than the data of Southworth et al.[17] which, however, appear smaller than the preliminary data of Morin et al.[19] The agreement here for these resonant cross sections in NO is certainly not as good as we have seen in related processes in N_2[11] and CO.[23] These differences are due in part to the complex open-shell structure of NO and suggest that studies beyond the Hartree-Fock approximation are needed. We note that in photoionization of the 2π level leading to the closed-shell $X^1\Sigma^+ NO^+$ ion, substantial discrepancies between the calculated and observed cross sections were also seen.[22]

After the completion of this paper the results of STMT studies of the photoionization cross sections for the $b^3\Pi$ and $A^1\Pi$ $(5\sigma^{-1})$ states were published.[27] These results also show multiplet-specific behavior for these cross sections, which was very similar to what we have seen. However, although the same model is used in these two studies, the resonance features in the STMT calculations are significantly broader than in our cross sections of Figure 1. Moreover, the resonance position is at a somewhat lower energy. These sorts of differences between photoionization cross sections obtained with numerical single-center photoelectron continuum orbitals and from STMT studies have been seen previously in many systems.[10,28,29] The underlying reasons for this behavior have been discussed extensively elsewhere.[2,4,10,30]

ACKNOWLEDGMENTS

This material is based upon work supported by the National Science Foundation under Grant NO. CHE-8218166. One of us (M.E.S.) acknowledges the support of a National Science Foundation predoctoral fellowship, and thanks Dr. Marvin Goodgame for several enlightening discussions. The research reported in this paper made use of the Dreyfus-NSF Theoretical Chemistry Computer which was funded through grants from the Camille and Henry Dreyfus Foundation, the National Science Foundation (Grant No. CHE-78-20235) and the Sloan Fund of the California Institute of Technology. We also acknowledge the National Center for Atmospheric Research for allowing us the use of their computing facilities.

References and Notes

(1) J. L. Dehmer, D. Dill, and A. C. Parr, in Photophysics and Photochemistry in the Vacuum Ultraviolet, Eds. S. P. McGlynn, G. L. Findley, and R. Huebner (Riedel Publishing Co., Holland, 1984) in press.

(2) See for example, D. Lynch, V. McKoy, and R. R. Lucchese, in Symposium on Resonances in Electron-Molecule Scattering, van der Waals Complexes, and Reactive Chemical Dynamics, Ed. D. G. Truhlar, 1984 National ACS Meeting, St. Louis, MO (ACS Symposium Series 263, 1984).

(3) P. W. Langhoff, N. Padial, G. Csanak, T. N. Rescigno, and B. V. McKoy, J. Chem. Phys. **77**, 590 (1980).

(4) See, for example, V. McKoy, T. A. Carlson, and R. R. Lucchese, J. Phys. Chem. **88**, 3188 (1984).

(5) P. W. Langhoff, in Electron-Molecule and Photon-Molecule Collisions, Eds. T. N. Rescigno, B. V. McKoy, and B. Schneider (Plenum Press, New York, 1979), pp. 183-224.

(6) D. Dill and J. L. Dehmer, J. Chem. Phys. **61**, 692 (1974).

(7) G. Raseev, H. LeRouzo, and H. Lefebre-Brion, J. Chem. Phys. **72**, 5701 (1980).

(8) W. D. Robb and L. A. Collins, Phys. Rev. A **22**, 2474 (1980).

(9) T. N. Rescigno and A. E. Orel, Phys. Rev. A **24**, 1267 (1982).

(10) B. I. Schneider and L. A. Collins, Phys. Rev. A **29**, 1695 (1984).

(11) R. R. Lucchese, G. Raseev, and V. McKoy, Phys. Rev. A **25**, 2572 (1982).

(12) M. E. Smith, V. McKoy, and R. R. Lucchese, Phys. Rev. A **29**, 1857

(1984).

(13) R. R. Lucchese and V. McKoy, Phys. Rev. A **26**, 1992 (1982).

(14) R. R. Lucchese and V. McKoy, J. Phys. B **14**, L629 (1981).

(15) See for example, P. Morin, I. Nenner, M. Y. Adam, M. J. Hubin-Franskin, J. Delwiche, H. Lefebre-Brion and A. Giusti-Suzor, Chem. Phys. Lett. **92**, 609 (1982). See also A. Gerwer, C. Asaro, B. V. McKoy, and P. W. Langhoff, J. Chem. Phys. **72**, 713 (1980). No multiplet-specific potentials were used in these studies of Gerwer et al.

(16) O. Edqvist, L. Asbrink, and E. Lundholm, Z. Naturforsch A **26**, 1407 (1971).

(17) S. Southworth, C. M. Truesdale, P. H. Kobrin, D. W. Lindle, W. D. Brewer, and D. A. Shirley, J. Chem. Phys. **76**, 143 (1982).

(18) T. Gustafsson and H. J. Levinson, Chem. Phys. Lett. **78**, 28 (1981).

(19) P. Morin, M. Y. Adam, P. Lablanquie, I. Nenner, M. J. Hubin-Franskin, and J. Delwiche, "Vacuum Ultraviolet Radiation Physics, Vol. VII," Proceedings of the 7th International Conference (Israel Physical Society, 1983), p. 613.

(20) S. Wallace, D. Dill, and J. L. Dehmer, J. Chem. Phys. **76**, 1217 (1982).

(21) J. J. Delaney, I. H. Hillier, and V. R. Saunders, J. Phys. B **15**, 1477 (1982).

(22) M. E. Smith, R. R. Lucchese, and V. McKoy, J. Chem. Phys. **79**, 1360 (1983).

(23) R. R. Lucchese and V. McKoy, Phys. Rev. A **28**, 1382 (1983).

(24) M. Y. Adam (private communication).

(25) H. Lefebre-Brion, Chem. Phys. Lett. **9**, 463 (1971).

(26) C. E. Brion and K. H. Tan, J. Electron Spectrosc. Relat. Phenom. **23**, 1 (1981).

(27) M. R. Hermann, S. R. Langhoff, and P. W. Langhoff, Chem. Phys. Lett. **109**, 150 (1984).

(28) R. R. Lucchese and V. McKoy, J. Phys. Chem. **85**, 2166 (1981).

(29) B. I. Schneider and L. Collins (private communication).

(30) D. L. Lynch and V. McKoy, Phys. Rev. A (accepted for publication) 1985.

TABLE I. Scattering Basis Sets Used in the Schwinger Potential.[1]

Symmetry of Solution	(ℓ,m,n)	Exponents[2]
σ	(0,0,0)	8.0, 4.0, 2.0, 1.0, 0.5
	(0,0,1)	1.0, 0.25
π	(1,0,0)	8.0, 4.0, 2.0, 1.0, 0.5
	(1,0,1)	1.0, 0.25

[1]These functions are centered on both Nitrogen and Oxygen. [2]The Cartesian Gaussians are defined by

$$\phi(\mathbf{r})^{\alpha,\ell,m,n,\mathbf{A}} = N(x-A_x)^{\ell}(y-A_y)^{m}(z-A_z)^{n}e^{-\alpha|\mathbf{r}-\mathbf{A}|^2}$$

FIGURE CAPTIONS

Figure 1: Multiplet-specific cross sections for the $b^3\Pi$ and $A^1\Pi$ states of NO^+: (—), present results in the dipole-dipole-length form; (– –), present results in the dipole-velocity form.

Figure 2: Dipole-length cross sections for the $b^3\Pi$ and $A^1\Pi$ states of NO^+: (—), present results with a multiplet-specific potential; (– –), present results with a multiplet-averaged potential.

Figure 3: Photoionization cross sections for the $b^3\Pi$ state of NO^+: (—), present results for a multiplet-specific potential in the dipole-length approximation; (– –), present results for a multiplet-specific potential in the dipole-velocity approximation; (– – –), multiplet-averaged potential in the CMSM of Ref. 20; (+), experimental results of Ref. 17.

Figure 4: Asymmetry parameters for the $b^3\Pi$ state of NO^+: (—), present results for a multiplet-averaged potential in the dipole-length approximation; (– – –), present result for a multiplet-averaged potential in the dipole-velocity approximation; (– – –), multiplet-averaged potential in the CMSM of Ref. 20; (+) experimental results of Ref. 17.

Figure 5: Photoionization cross sections for the $c^3\Pi$ state of NO^+: (——), present results for a multiplet-averaged potential in the dipole-length approximation; (– –), present results for a multiplet-averaged potential in the dipole-velocity approximation; (– – –), multiplet-averaged potential in the CMSM of Ref. 20; (+), experimental results of Ref. 17; (x), experimental results of Ref. 18.

Figure 6: Asymmetry parameters for the $c^3\Pi$ state of NO^+: (——), present results for a multiplet-averaged potential in the dipole-length approximation; (– –), present results for a multiplet-averaged potential in the dipole-velocity approximation; (– – –), multiplet-averaged potential in the CMSM of Ref. 20; (+), experimental results of Ref. 17.

Figure 7: Photoionization cross sections for the $B^1\Pi$ state of NO^+: (——), present results for a multiplet-averaged potential in the dipole-length approximation; (– –), present results for a multiplet-averaged potential in the dipole-velocity approximation; (– – –) multiplet-averaged potential in the CMSM of Ref. 20; (+), experimental results of Ref. 18.

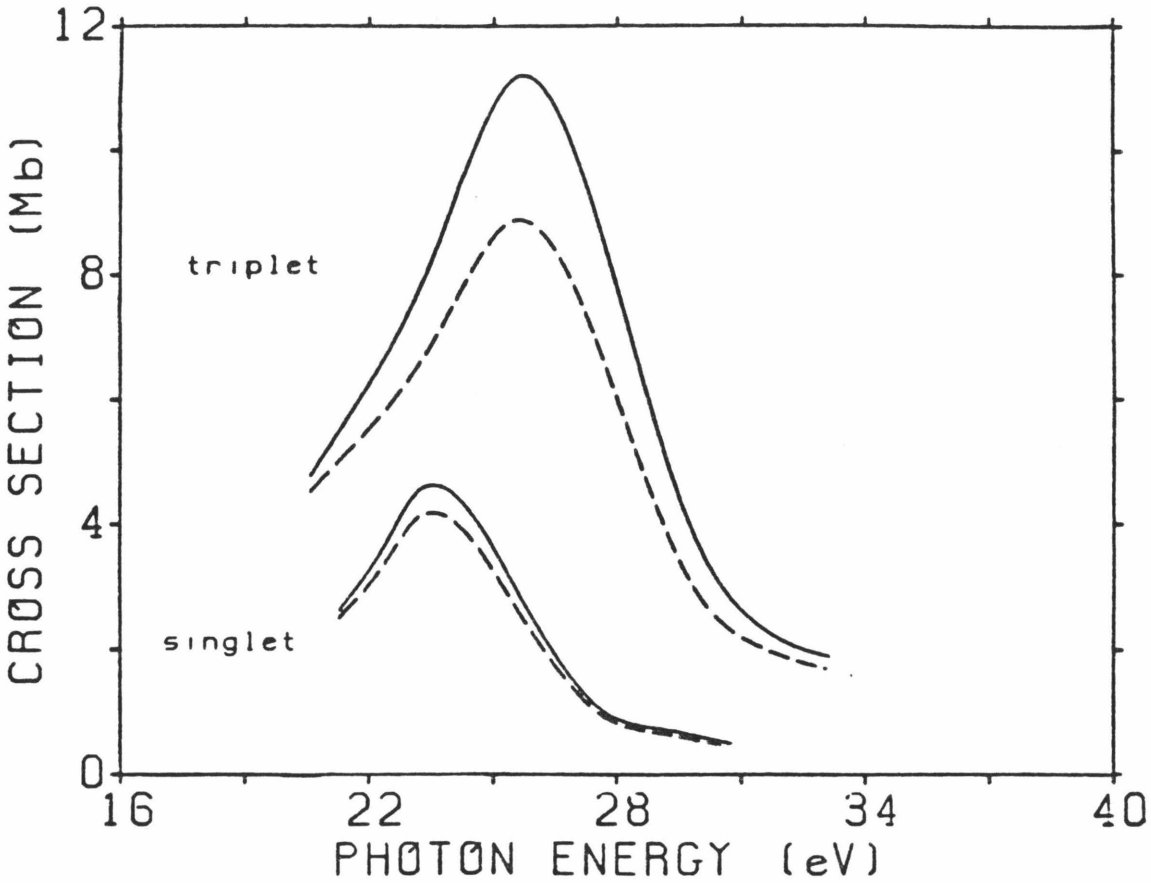
12
8
4
0
CROSS SECTION (Mb)
triplet
singlet
16
22
28
34
40
PHOTON ENERGY (eV)

FIGURE 1.

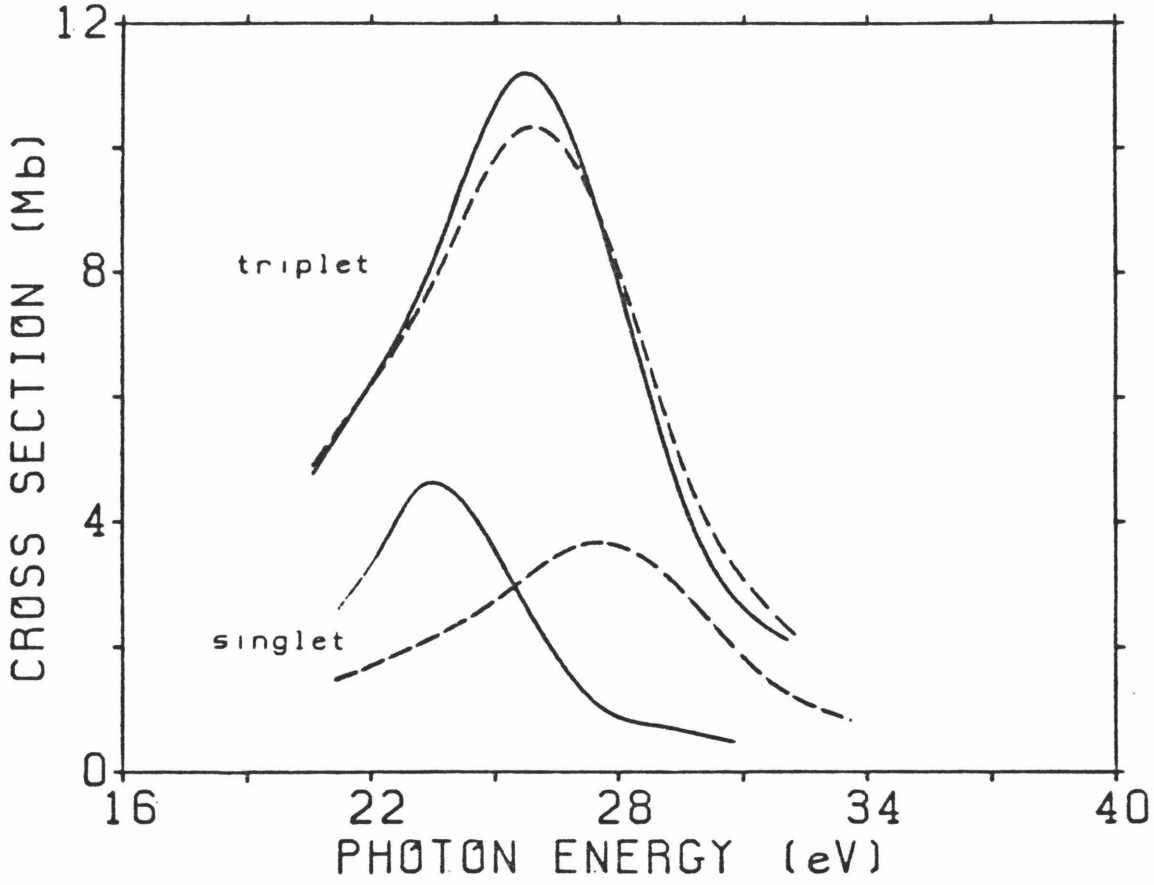
12
8
4
0
CROSS SECTION (Mb)
triplet
singlet
16
22
28
34
40
PHOTON ENERGY (eV)

FIGURE 2.

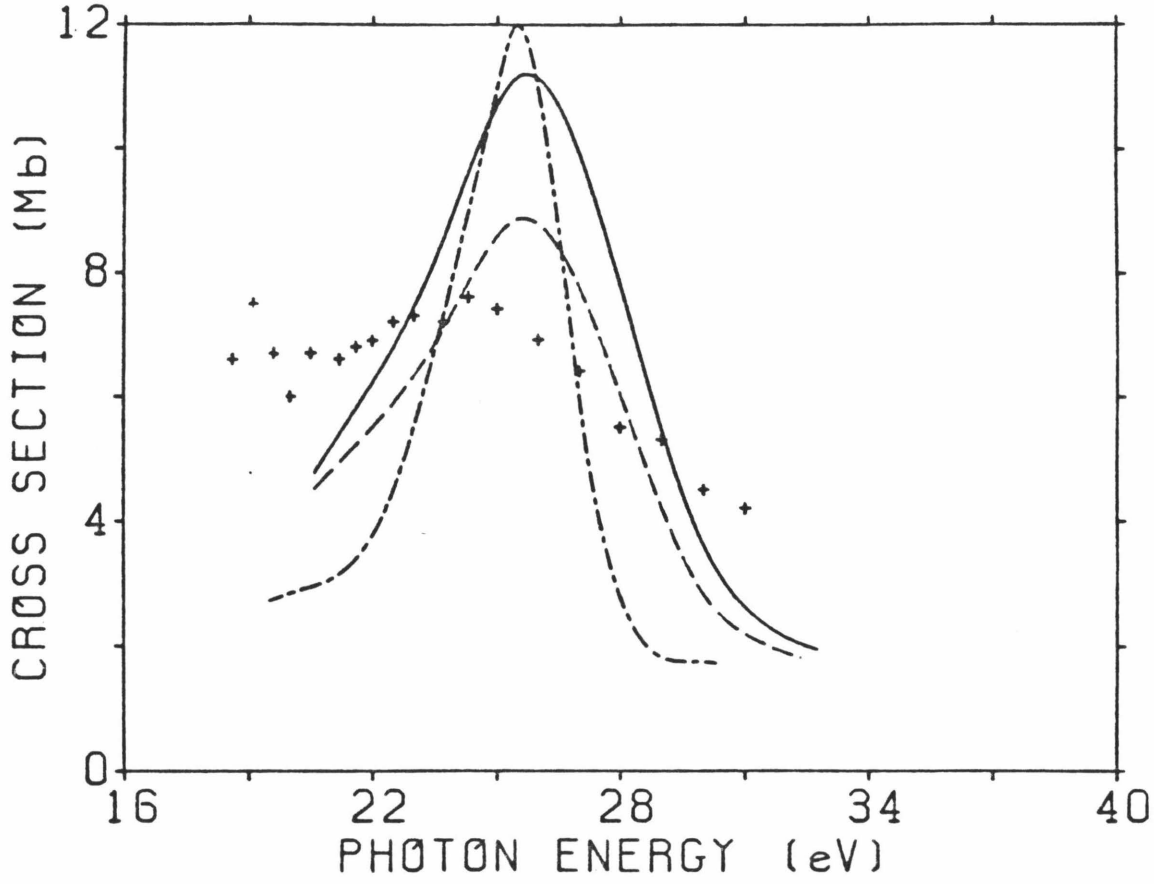

FIGURE 3.

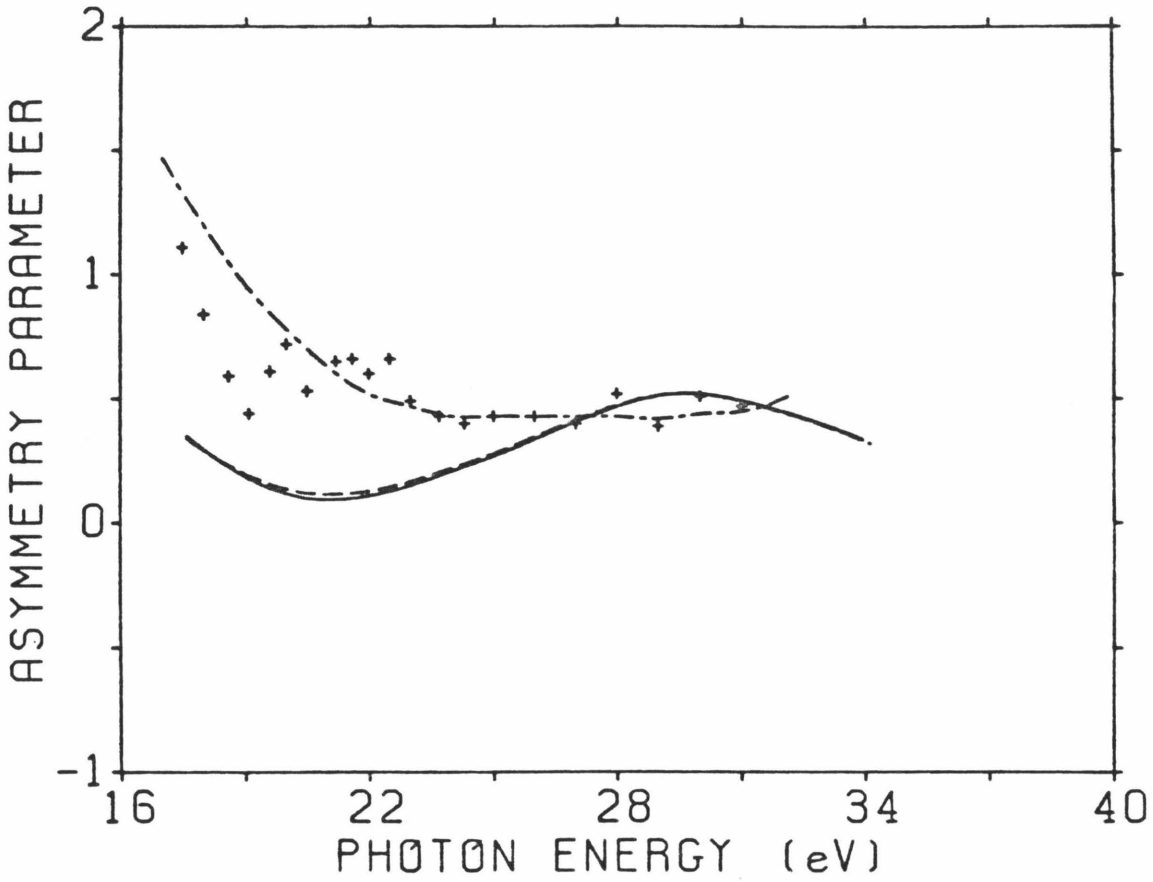

FIGURE 4.

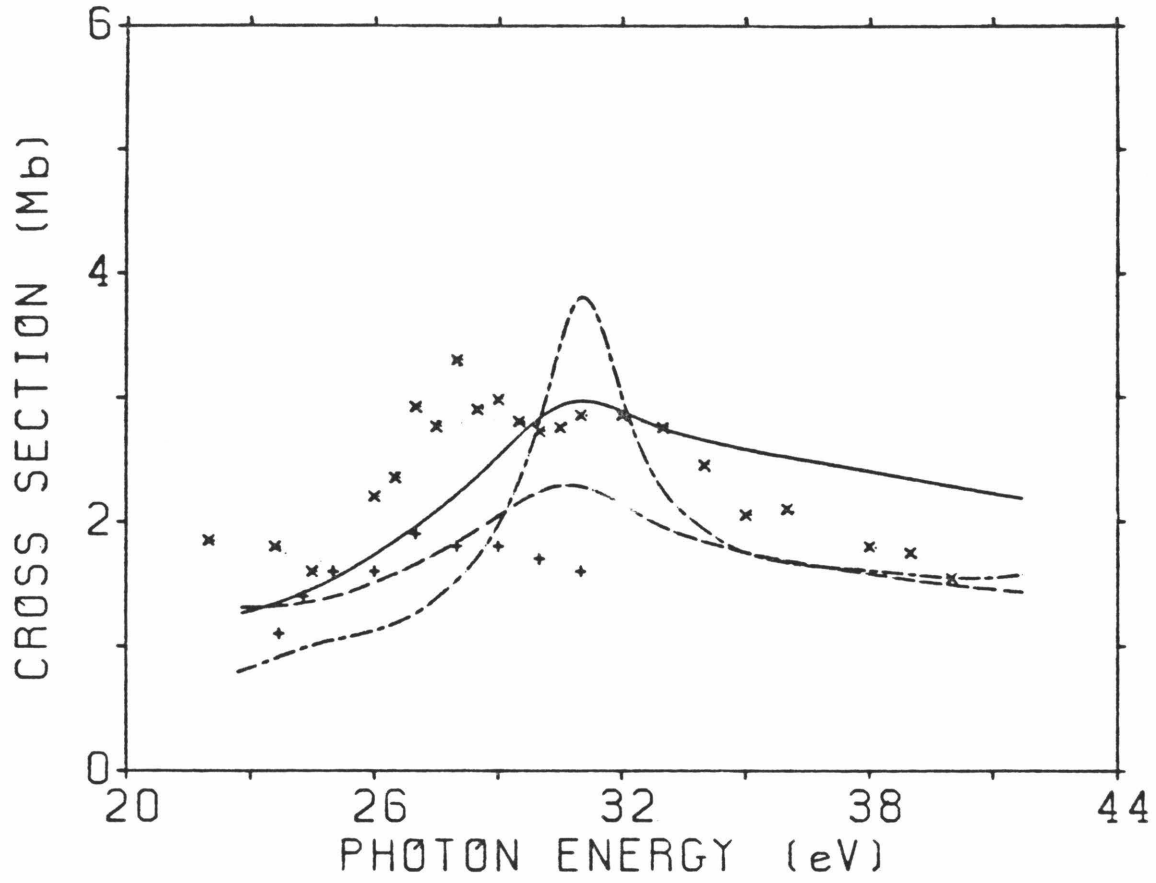

FIGURE 5.

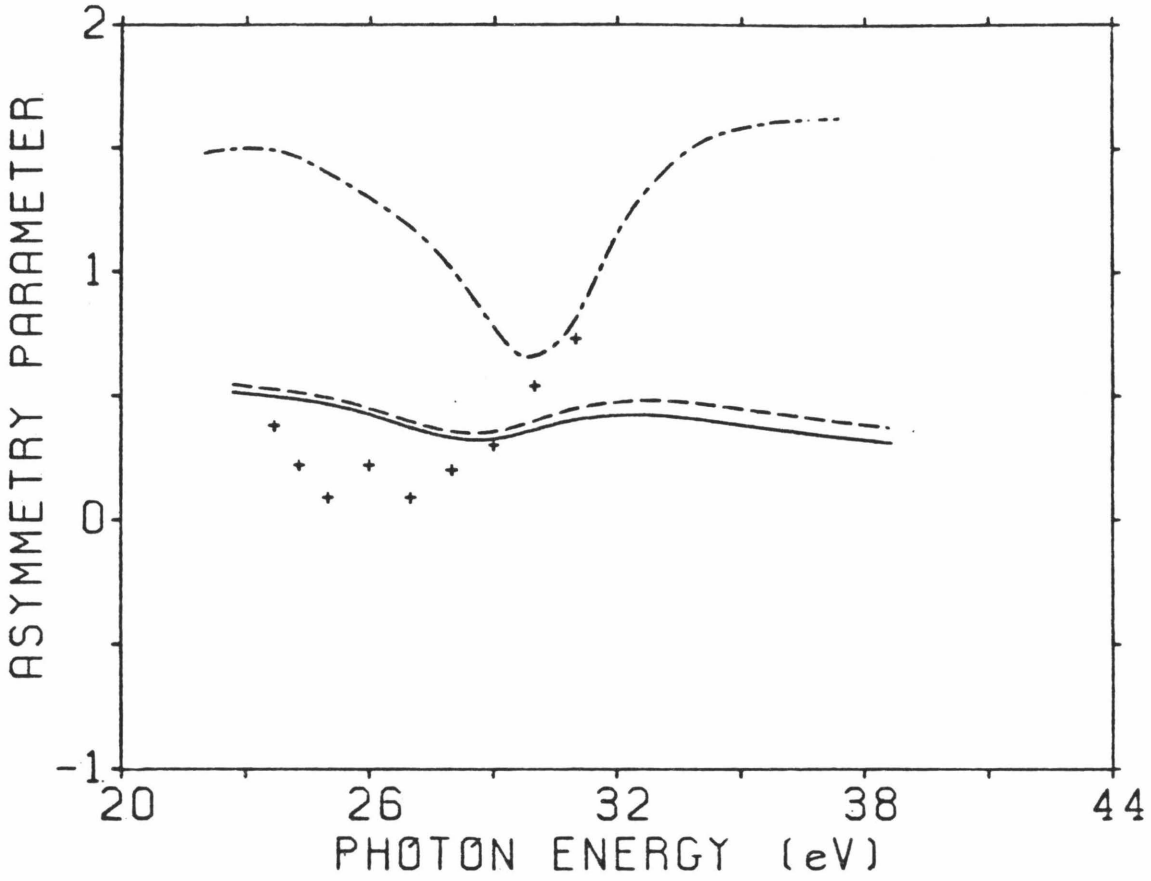

FIGURE 6.

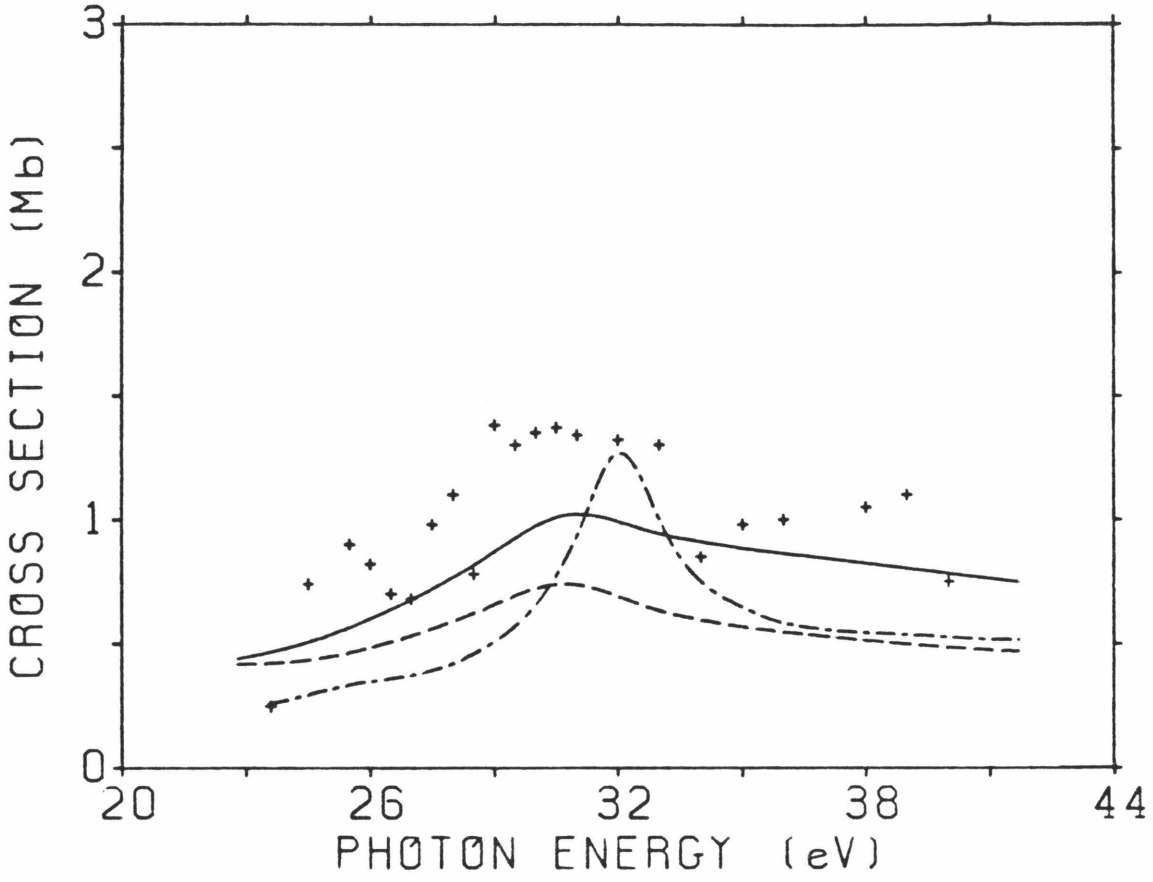

FIGURE 7.

CHAPTER III

A Study of the Vibrational Branching Ratios in the Photoionization of CO ($X^1\Sigma$, v=0) Leading to CO^+ ($A^1\Sigma$, v'=0,1,2)

In recent years there has been a surge of interest in studying the role that a shape resonance plays in molecular photoionization. A shape resonance occurs when an escaping photoelectron is temporarily trapped in the molecular region by a potential barrier formed from a combination of the repulsive centrifugal potential and the attractive electrostatic potential. The photoelectron eventually tunnels through this barrier to escape. This process is manifested in the photoionization spectrum as a broad peak, spread over several volts, and from the width of the resonance the lifetime of the shape resonances can be inferred. A striking consequence of this trapping of the electron is that it causes a strong dependence of the electronic transition moment on the internuclear distance, leading to significant non-Franck-Condon intensities and asymmetry parameters that are strongly dependent upon the final vibrational state of the ion. These effects occur over a much broader spectral range than the resonance width -- often they are seen in a range 10-15 volts long.

One of the earliest studies of vibrationally-resolved cross sections was performed on N_2. The photoionization of the $3\sigma_g$ level leading to the v'=0 and 1 states of the N_2^+ was studied by West et al.[1] Measurements were made in the photon energy range from 20-38 eV and a non-Franck-Condon branching ratio for the production of the v'=1/v'=0 states was observed throughout this energy range. Below 26 eV this behavior can be attributed to autoionization effects, but above this energy it was attributed to the effects of the $3\sigma_g \rightarrow k\sigma_u$ shape resonance. This was corroborated by Dehmer et al.,[2] and by Lucchese and McKoy[3] using theoretical methods. There were considerable differences between these

results however, and this was due to the fact that a muffin-tin multiple-scattering method was used by Dehmer et al. while Lucchese and McKoy used an ab initio method in which the correct static-exchange equation is solved for the continuum orbital. While both calculations showed non-Franck-Condon behavior in the branching ratio, the multiple-scattering method yielded results which were twice as large as those obtained by Lucchese and McKoy, whose results agreed with the experimental data. Lucchese and McKoy also calculated state-specific asymmetry parameters for the v'=0, 1, and 2 states of N_2^+.

More recently attention has focused on the study of carbon monoxide. Stockbauer et al.[4] have measured the branching ratios while Cole et al.[5] have determined vibrationally-resolved photoelectron asymmetry parameters for the photoionization of the 5σ level of CO leading to the $X^2\Sigma^+$ state of CO^+. Their results, like those in N_2, show significant deviations from what would be expected based on Franck-Condon behavior. Stephens et al.[6] attempted a theoretical study of this process, but failed to obtain agreement with the experimental data. This is due in part to the presence of one or more autoionizing states in the spectrum which obscure the effects of the shape resonance, but it is also due to the crude models used to approximate the molecular potential in their multiple-scattering muffin-tin calculations. In this paper we present the results of our studies of this photoionization process. We begin with CO in the ground electronic and ground vibrational state and form the ion in the ground electronic state and the three lowest vibrational states. We present cross sections leading to each vibrational state and the v'=1/v'=0 and v'=2/v'=0 branching ratios. We also

present asymmetry parameters for each final vibrational state. They are quite different from each other and are another example of vibrational state-specific asymmetry parameters.

We first present our calculational details and then our results. We will compare our results to experimental data[4,5] and to those from other theoretical methods.[6]

II. CALCULATIONAL DETAILS

The cross section for photoionization from the ground vibrational state of CO to the n^{th} vibrational state of CO^+ is given by

$$\sigma^{L,V}_{v=0,v'=n} = \frac{4\pi^2 E}{3c} \sum_{\ell m \mu} |\langle \chi_i^{v=0}(R) | I^{L,V}_{\ell m \mu}(R) | \chi_f^{v'=n}(R) \rangle|^2, \quad (1)$$

where χ are the initial and final vibrational wave functions for the molecule and ion, respectively, E is the photon energy, and c is the speed of light. The length and velocity forms of the photoionization transition matrix elements are given by

$$I^{L}_{\ell m \mu}(R) = k^{1/2} \langle \phi_o(r;R) | r_\mu | \phi_{k\ell m}(r;R) \rangle$$

and

$$I^{V}_{\ell m \mu}(R) = \frac{k^{1/2}}{E} \langle \phi_o(r;R) | \nabla_\mu | \phi_{k\ell m}(r;R) \rangle,$$

where ϕ_o is the initial orbital and ϕ_k is the photoelectron continuum orbital. We used the method described elsewhere[7] to calculate the

$\phi_{k\ell m}$'s needed to evaluate these matrix elements. In this method the continuum orbital is expanded in partial waves about a single center and the coupled radial integral equations are solved numerically. A separable potential of the Schwinger type[8] is used to render the nonlocal exchange potential separable. We used the same partial-wave expansion parameters as Lucchese and McKoy[9] in their vibrationally-unresolved study of the photoionization of CO, which should provide converged results.

The transition matrix elements were evaluated at five different internuclear separations R = 1.898, 2.015, 2.132, 2.249 and 2.366 a.u., where the equilibrium internuclear distance of CO is R_e = 2.132 a.u. For this value of R_e, the total energy of the CO molecule was -112.789 a.u. Our SCF wave functions for the molecule at each geometry were those of McLean and Yoshimine[10] and consisted of linear combinations of Slater type orbitals. Our scattering basis, given in Table I, contained seven Cartesian Gaussian functions centered on each nucleus. These basis functions are defined by

$$\phi_{\alpha\ell mnA}(\mathbf{r}) = N(x-A_x)^{\ell}(y-A_y)^{m}(z-A_z)^{n}\exp(-\alpha|\mathbf{r}-\mathbf{A}|^2). \qquad (2)$$

The vibrational wave functions were obtained as solutions to the Schrödinger equation with an RKR potential. The method was outlined by Lucchese and McKoy[3] in their study of N_2. The potential curve for CO was obtained by Tobias et al.[11] and the curve for CO^+ was that of Singh and Rai.[12] With these data we obtained the following Franck-Condon factors: (v=0, v'=0) = 0.9607, (v=0, v'=1) = 0.0391, (v=0, v'=2) = 0.000152.

III. RESULTS AND DISCUSSION

Figure 1 shows the length form of our $(5\sigma)^{-1}$ cross sections for the five values of R at which we performed our calculations. We see that, for large R, the position of the resonance shifts to lower energies and the magnitude of the cross section increases relative to that calculated for the equilibrium value of R. The opposite is true for the small-R cross sections. It is this phenomenon that causes the effects of the shape resonance to be spread over such a broad range of the energy spectrum as mentioned earlier in the introduction.

In Figure 2 we present the cross sections for photoionization leading to the first three vibrational levels of the $X^2\Sigma^+$ state of CO^+. The $5\sigma \rightarrow k\sigma$ shape resonance appears as a very broad feature in the $v=0 \rightarrow v'=0$ transition. This is analogous to the fixed-nuclei calculation and is expected because of its large Franck-Condon factor. Note that the $v'=1$ and $v'=2$ curves are scaled up by factors of 10 and 100, respectively. We see that the position of the resonance moves to higher energy as the final-state vibrational quantum number increases. This is exactly the opposite trend from that predicted by Stockbauer et al.[4] Their prediction was based upon the following argument. The internuclear distance in CO decreases upon photoionization from 1.128Å in the molecule to 1.115Å in the ion.[13] Examination of the overlap of the vibrational wave functions for the neutral molecule and the ion reveals that the large-R part of the transition matrix element in Eq. (1) would be more heavily weighted because of this contraction. As Figure 1 shows, the large-R cross sections have the resonance shifted to lower energies. Thus, it is expected that the

v'=1 and v'=2 cross sections should peak at lower energies than that for v'=0. In the case of N_2, where the bond length expands upon ionization of the $3\sigma_g$ level, the opposite trend would be predicted and indeed the v'=1 and v'=2 cross sections peak at higher energies than the v'=0 cross section.[3] Although this idea is appealing due to its simplicity, it is incorrect as shown in Figure 2. The reason for its failure is that the R-dependence of the transition matrix element in Eq. (1) is equally important in determining the position of the resonance peak. The vibrational wave functions of the neutral molecule and molecular ion are nearly orthogonal due to the small change in bond length upon ionization, and, as a result, the integral in Eq. (1) becomes quite sensitive to the R-dependence of I(R) and so the simple argument of Ref. 4 is not valid.

In Figures 3 and 4 we present the vibrational branching ratios for v'=1/v'=0 and v'=2/v'=0, respectively. They are compared to the data of Stockbauer et al.[4] and to the multiple-scattering results of Stephens et al.[6] Also plotted in these figures are the values of the Franck-Condon branching ratios. The non-Franck-Condon behavior of our branching ratios is induced by the $5\sigma \rightarrow k\sigma$ shape resonance. It extends over a wide range of photon energies for the reasons discussed above. We do not obtain good agreement with the experimental data in the region below 23 eV. This is because there is one or more autoionizing states imbedded in the continuum and the sharp peaks from these resonances are superimposed upon the single-particle spectrum. Our theoretical model does not account for autoionization and so these peaks do not appear in our calculated cross sections. The nature of these autoionizing states is not entirely clear. There is a series which

converges to the $B^2\Sigma^+$ state of CO^+ at 19.5 eV,[11] but the possible autoionizing states occuring near 22-23 eV are not well characterized. Stephens et al.[6] have suggested that the doubly excited $(1\pi^{-1}\ 5\sigma^{-1}\ 2\pi^2)$ configuration mixes with the $(5\sigma k\sigma)$ continuum which results in sharp peaks. While this is not an unreasonable choice for a doubly excited state at this energy, the configuration is of the wrong symmetry to mix with the $(5\sigma\ k\sigma)$ configuration. If this is the doubly excited state leading to autoionization, then it must couple with the $(5\sigma\ k\pi)$ continuum. Because this is a reasonably tight doubly excited state and not a diffuse Rydberg-like state, the magnitudes of the autoionization features in the cross section are sensitive to the final vibrational state of the molecular ion. For this reason the autoionization can be more pronounced in the asymmetry parameters for the v'=2 state in Figure 7 than in the v'=0 state shown in Figure 5.

Because this autoionizing structure obscures our underlying shape resonance, it is difficult to compare our branching ratios in Figures 3 and 4 to the experimental data. Experimental data is clearly needed at energies above 27 eV. This is the region in which we observe significant non-Franck-Condon behavior induced by the $5\sigma \rightarrow k\sigma$ shape resonance. The experimental data between 25 and 27 eV agrees well with our calculated branching ratios and this agreement should persist at higher energies. In similar calculations on the $3\sigma_g$ orbital of N_2, Lucchese and McKoy[3] obtained excellent agreement with experiment. Their branching ratio for v'=1/v'=0 was significantly lower than that obtained from the multiple-scattering method, and this is what we observe in the present

case in Figures 3 and 4.

We observed throughout this study that our results did not agree well with the multiple-scattering calculations. This is due to the different ways that the two methods represent the scattering potential. As stated above, we solve the scattering equations for the continuum orbital in which the exact static-exchange potential is used. The multiple-scattering method employs a local muffin-tin model for the potential, in which over 70% of the potential in the molecular region is approximated by a single constant value. Clearly this will lead to inaccuracies, especially in the case of polar molecules, when one is trying to describe the interactions between the electron and the molecular ion.

Figures 5 through 7 contain our vibrationally-resolved asymmetry parameters along with the experimental data of Cole et al.[5] and the multiple-scattering results of Stephens et al.[6] We note that in Figure 5 the autoionizing peaks are present, but not as pronounced as in Figure 7. As mentioned above this is due to the fact that the autoionization process is sensitive to the final vibrational state of the molecular ion. The transition from the Rydberg-like state at 19 eV into the continuum would be less sensitive than that from the tighter $(1\pi^{-1}\ 5\sigma^{-1}\ 2\pi^{2})$ state where the orbitals depend more strongly upon R, but both appear as very pronounced features in the asymmetry parameters of Figure 7. In Figure 5, which corresponds to v'=0, both theoretical methods are in excellent agreement with the experimental data in the 25-27 eV region, which is the one portion of the experimental data that is not obscured by autoionization. The same is seen for the v'=1 state in Figure 6. Because the autoionization effects are

more pronounced in Figure 7, poorer agreement is obtained for the v'=2 asymmetry parameter. As stated above, experimental data between 27 and 35 eV are clearly needed before any meaningful comparison can be made with our results.

IV. CONCLUSIONS

We have presented branching ratios and vibrationally-resolved asymmetry parameters for photoionization of the 5σ orbital of CO leading to the $X^2\Sigma^+$ state of CO^+ in the v'=0, 1, and 2 states. The experimental data for this process are complicated by the presence of one or more autoionizing states in this region. Beyond the autoionizing region of the spectrum our results are in good agreement with the available experimental data. However, experimental data in the energy range 27-35 eV are needed in order to make a more thorough comparison. We also reported vibrationally-resolved asymmetry parameters which are significantly different for each final vibrational state of the CO^+ ion. Our results are compared with the multiple-scattering results,[6] and, as in a similar study[3] of the photoionization of the $3\sigma_g$ level of N_2, the branching ratios are much higher when obtained by this muffin-tin method. The poor agreement is due to the inaccurate representation of the scattering potential in the multiple-scattering method as discussed previously.

References and Notes

(1) J. B. West, A. C.Parr, B. E. Cole, D. L. Ederer, R. Stockbauer, and J. L. Dehmer, J. Phys. B **13**, L105 (1980).

(2) J. L. Dehmer, D. Dill, and S. Wallace, Phys. Rev. Lett. **43**, 1005 (1979).

(3) R. R. Lucchese and V. McKoy, J. Phys. B **14**, L629 (1981).

(4) R. Stockbauer, B. E. Cole, D. L. Ederer, J. B. West, A. C. Parr, and J. L. Dehmer, Phys. Rev. Lett. **43**, 757 (1979).

(5) B. E. Cole, D. L. Ederer, R. Stockbauer, K. Codling, A. C. Parr, J. B. West, E. D. Poliakoff, and J. L. Dehmer, J. Chem. Phys. **72**, 6308 (1980).

(6) J. A. Stephens, D. Dill, and J. L. Dehmer, J. Phys. B **14**, 3911 (1981).

(7) M. E. Smith, R. R. Lucchese, and V. McKoy, Phys. Rev. A **29**, 1857 (1984).

(8) D. K. Watson and V. McKoy, Phys. Rev. A **20**, 1474 (1979).

(9) R. R. Lucchese and V. McKoy, Phys. Rev. A **28**, 1382 (1983).

(10) A. D. McLean and M. Yoshimine, "Tables of Linear Molecule Wave Functions," IBM San Jose Research Laboratories, San Jose (1967).

(11) I. Tobias, R. J. Fallon, and J. T. Vanderslice, J. Chem. Phys. **33**, 1638 (1960).

(12) R. B. Singh and D. K. Rai, J. Mol. Spectrosc. **19**, 424 (1966).

(13) K. P. Huber and G. Herzberg, Constants of Diatomic Molecules (Van Nostrand Reinhold, New York, 1979).

TABLE I. Scattering Basis Set.[a]

	Center	ℓ	m	n	α
$5\sigma \rightarrow k\sigma$	C	0	0	0	10.0, 4.0, 1.5, 0.5, 0.1,
	C	0	0	1	1.0, 0.1
	O	0	0	0	10.0, 4.0, 1.5, 0.5, 0.1
	O	0	0	1	1.0, 0.1
$5\sigma \rightarrow k\pi$	C	1	0	0	10.0, 4.0, 1.5, 0.5, 0.1
	C	1	0	1	1.0, 0.1
	O	1	0	0	10.0, 4.0, 1.5, 0.5, 0.1
	O	1	0	1	1.0, 0.1

[a]The parameters ℓ,m,n, and α are defined in Eq. (2) of the text.

FIGURE CAPTIONS

Figure 1: Dipole-length cross sections for photoionization of the 5σ level of CO at five different values of the equilibrium distance R.

Figure 2: Vibrationally-resolved photoionization cross sections for v'=0, v'=1, and v'=2 for the $X^2\Sigma$ state of CO^+: ———, dipole-length approximation; ---, dipole-velocity approximation.

Figure 3: Branching ratios for the production of the v'=1/v'=0 vibrational levels of the $X^2\Sigma$ state of CO^+: ———, present results, dipole-length approximation; — — —, MSM results of Ref. 6; Θ, data of Ref. 4; ---, present result for v'=1/v'=0 Franck-Condon ratio.

Figure 4: Branching ratios for the production of the v'=2/v'=0 vibrational levels of the $X^2\Sigma$ state of CO^+. The same labels apply as in Fig. 3.

Figure 5: Photoelectron asymmetry parameters for production of the v'=0 state of $X^2\Sigma$ state of CO^+: ———, present results, dipole-length approximation; ---, MSM results of Ref. 6; Θ, data of ref. 5.

Figure 6: Photoelectron asymmetry parameters for production of the v'=1 state of $X^2\Sigma$ state of CO^+. The same labels apply as in Fig. 5.

Figure 7: Photoelectron asymmetry parameters for production of the v'=2 state of $X^2\Sigma$ state of CO^+. The same labels apply as in Fig. 5.

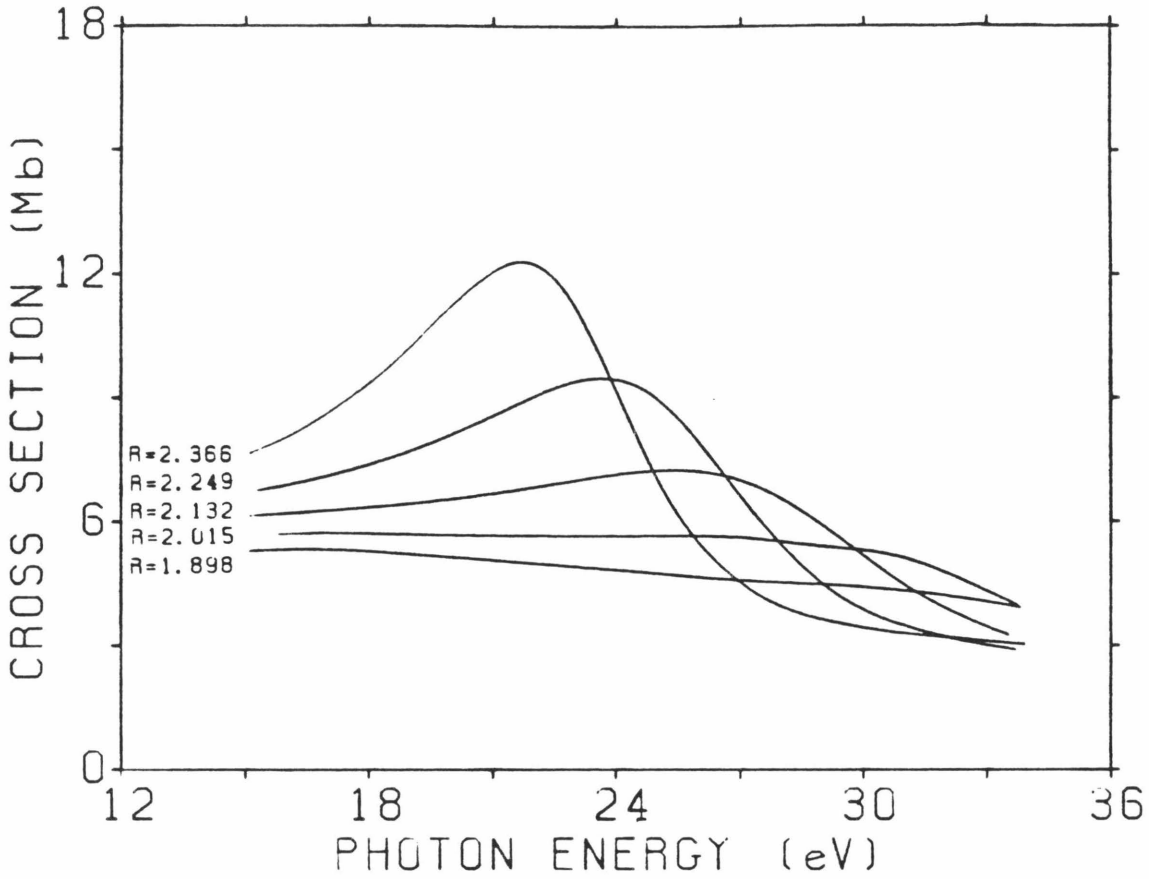
18
12
6
0
CROSS SECTION (Mb)
R=2.366
R=2.249
R=2.132
R=2.015
R=1.898
12
18
24
30
36
PHOTON ENERGY (eV)

FIGURE 1.

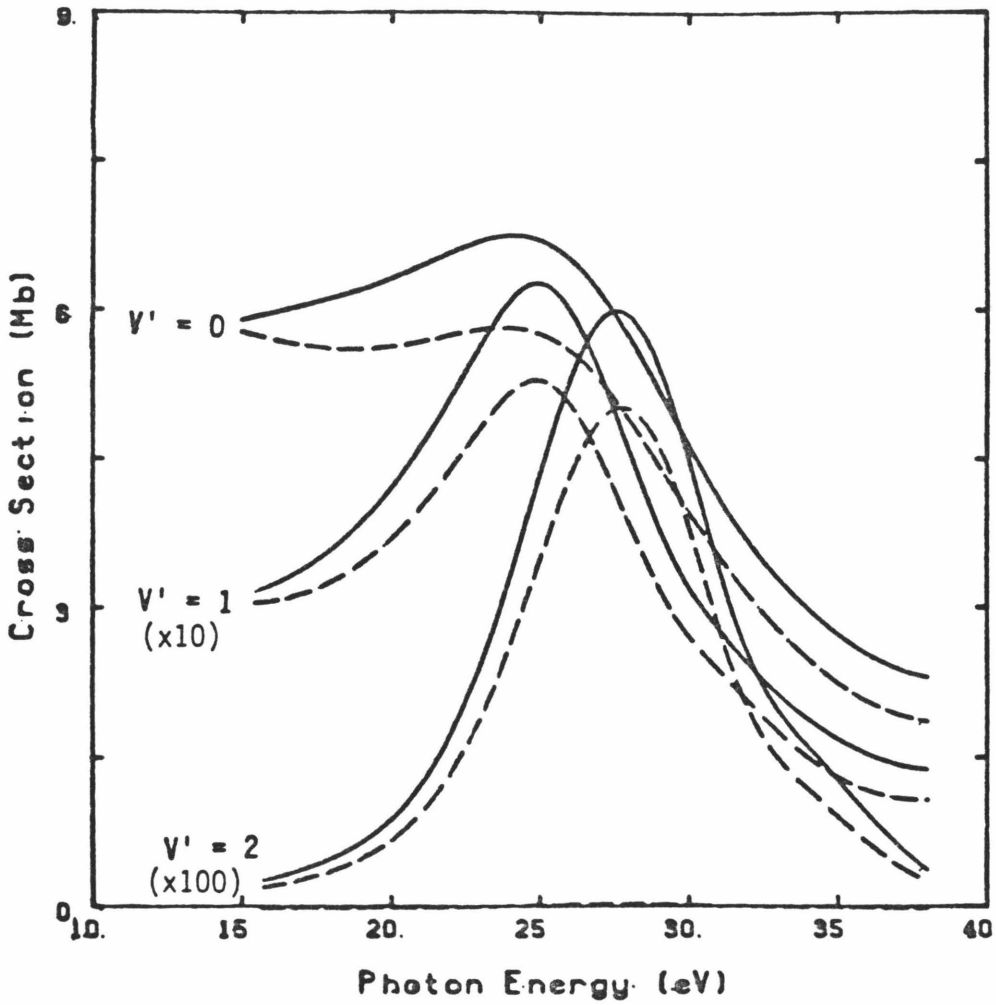
9.
6
3
0
Cross Section (Mb)
V' = 0
V' = 1
(x10)
V' = 2
(x100)
10.
15
20.
25
30.
35
40
Photon Energy (eV)

FIGURE 2.

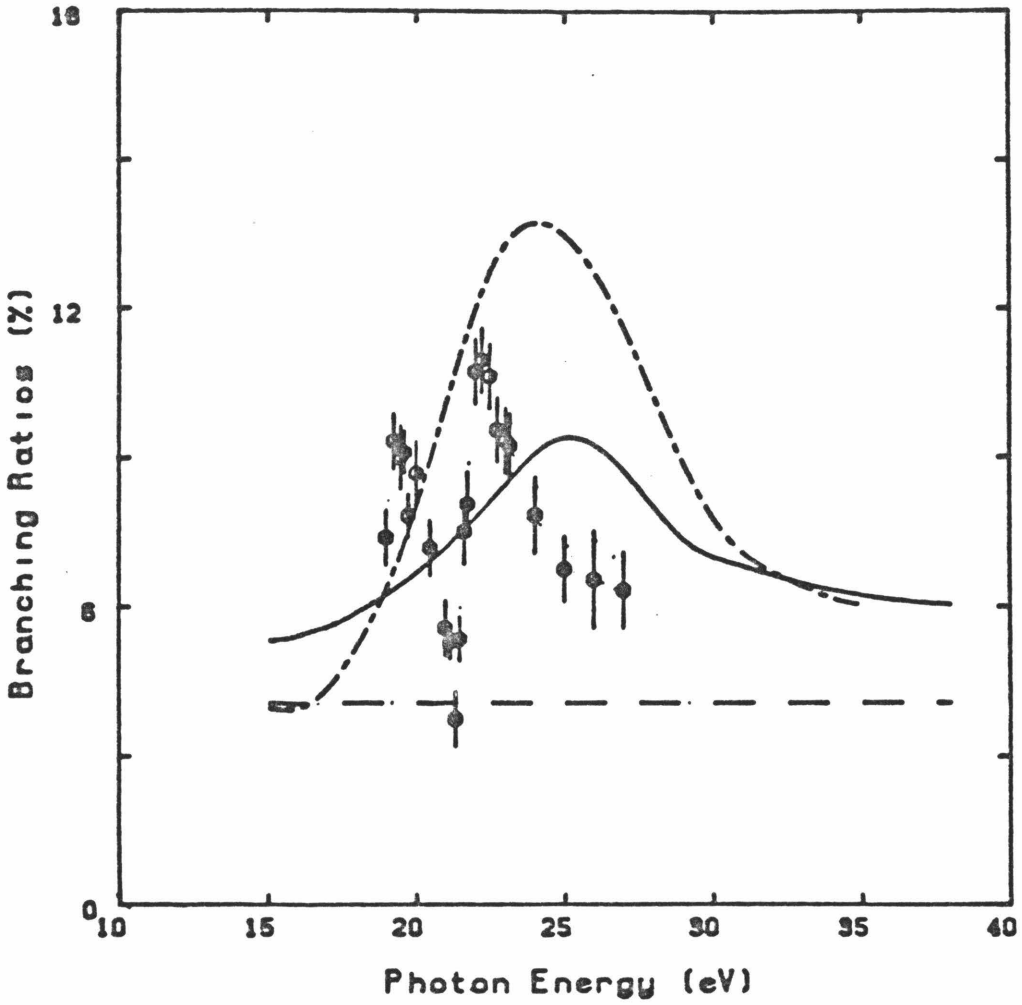

FIGURE 3.

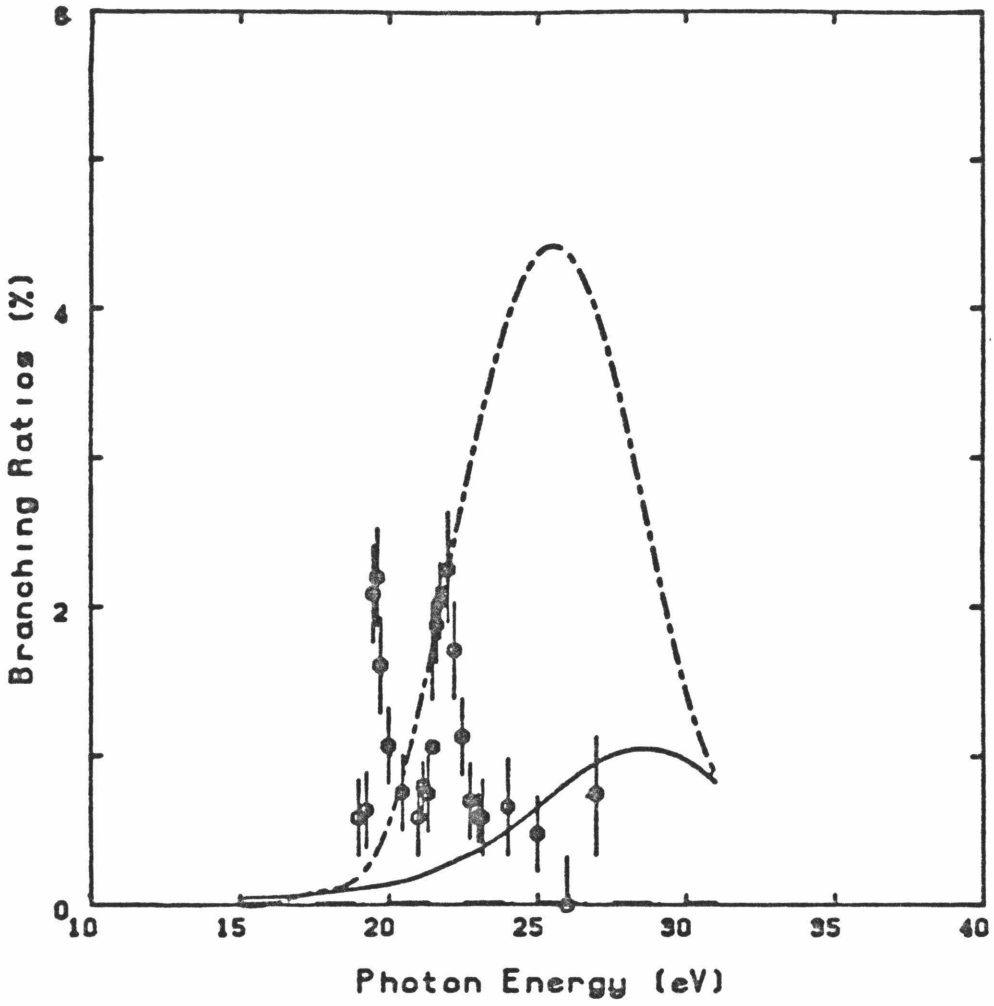

FIGURE 4.

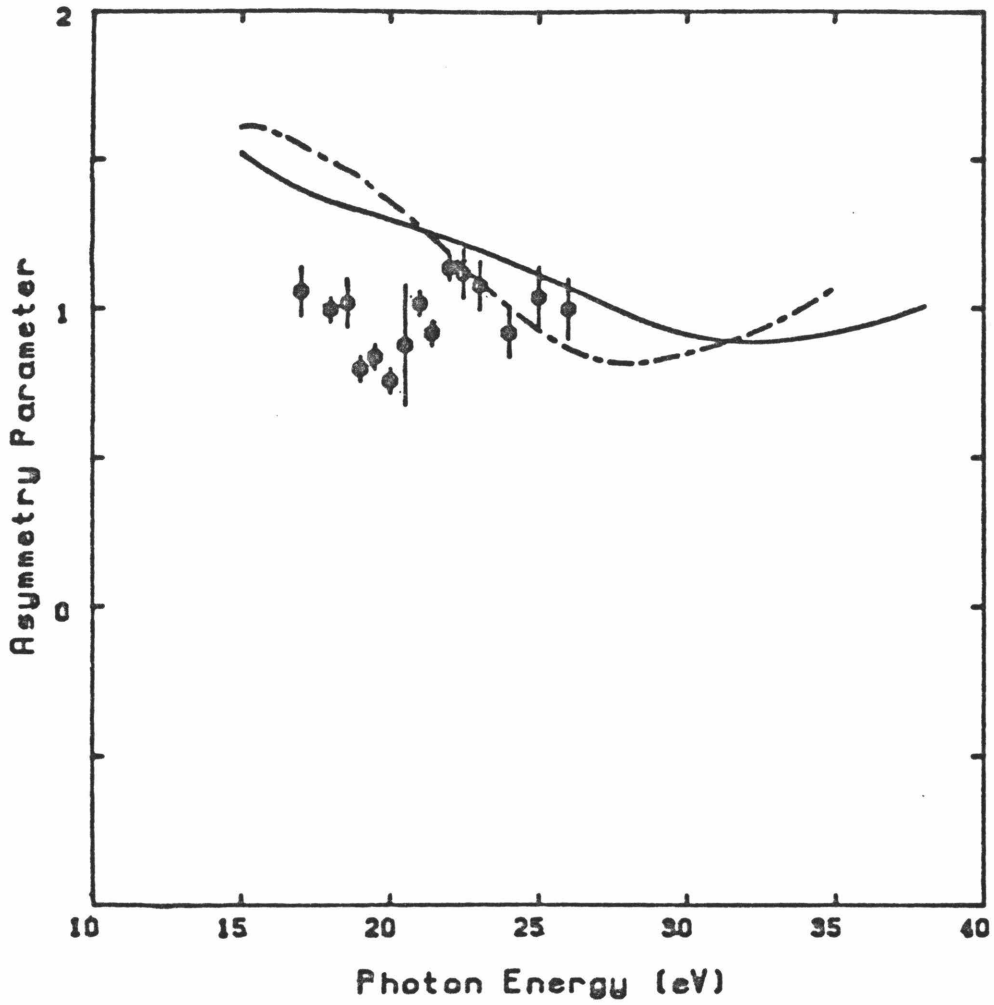

FIGURE 5.

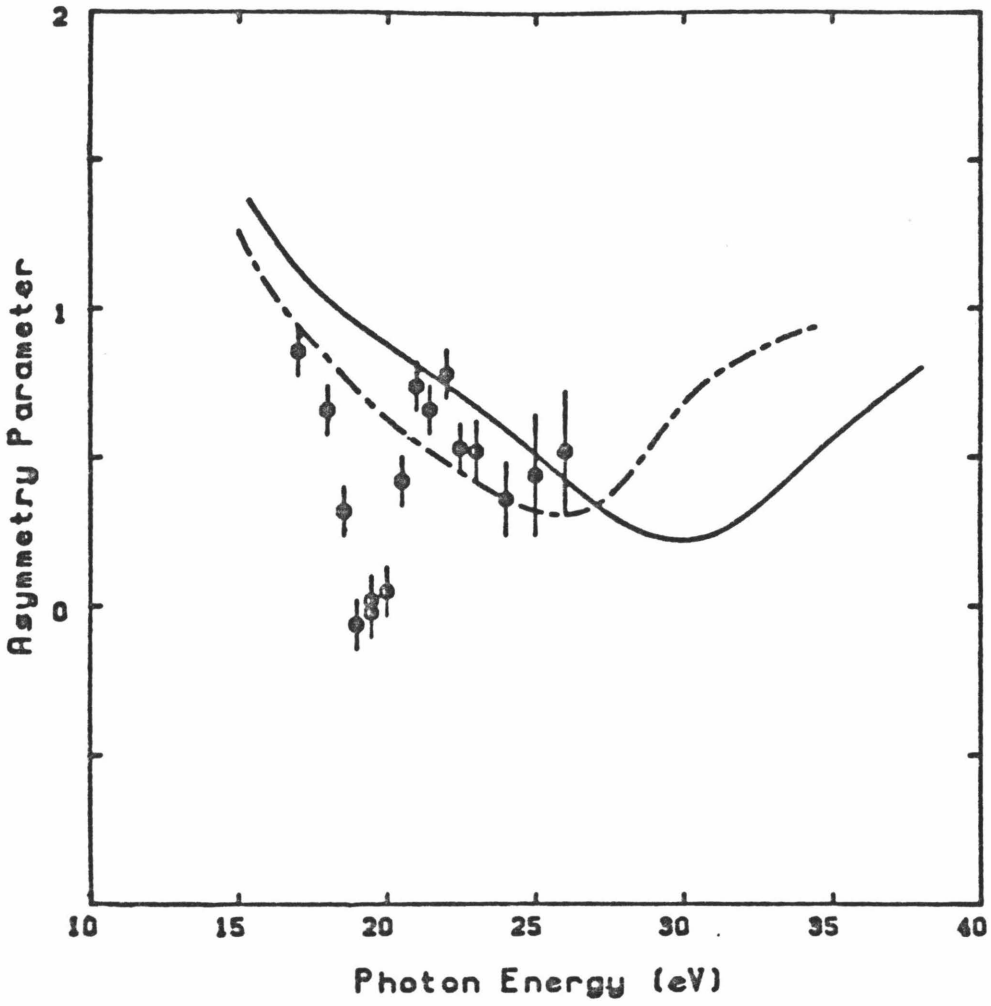

FIGURE 6.

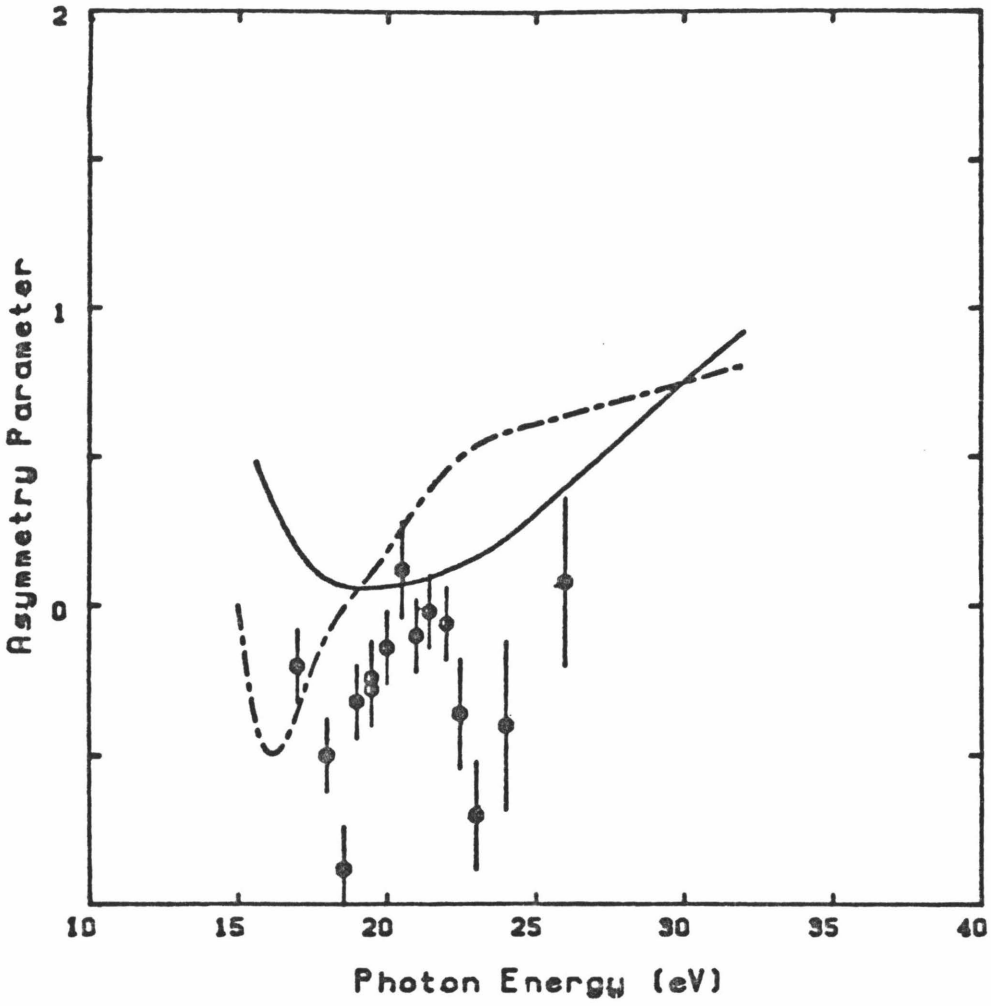

FIGURE 7.

CHAPTER IV

A Theoretical Study of Photoemission of the 5σ Orbital of Carbon Monoxide Adsorbed on a Nickel Surface

I. INTRODUCTION

Photoemission studies of adsorbate molecules on metal surfaces provide unique insights into adsorbate orientation and adsorbate-substrate interactions.[1-4] Comparisons of the photoelectron spectra of the free gas and the adsorbate provide information about the binding energies of the electrons and the perturbations of the molecule induced by the metal surface. This comparison is complicated, even for weakly bound complexes, by the shift to higher kinetic energy of the photoemitted electrons caused by relaxation of the electrons of the substrate around the hole created by photoionization. This shift will not be the same for all orbitals of the adsorbate as each orbital is perturbed differently by the metal. The energy-dependent photoionization cross sections from each of these orbitals play an important role in identifying the energy levels in the adsorbed molecule.

An especially useful facet of a photoemission study of adsorbed molecules is that, if the polarization of the incident light is appropriately oriented, then photoemission will occur only in certain directions for each orbital in the molecule and this is easily predicted from a few simple symmetry rules.[5,6] The effect of this is that the experimenter can resolve photoemission from a pair of nearly degenerate orbitals of a different symmetry simply by placing the detector in two different, appropriately chosen planes -- something which is entirely impossible for a gas-phase molecule. It is even conceivable that by placing the detector in an appropriately chosen plane some autoionization peaks would disappear and simplify the interpretation of the spectrum.

Angle-resolved studies of the above type are based upon initial

knowledge of the bonding geometry of the adsorbate. In the case where this is not known, angle-resolved studies can be used in conjunction with theoretical methods to predict the orientation of the adsorbate. For example, an angular distribution pattern can be measured for an adsorbate-substrate system. Corresponding calculations of this pattern with the adsorbate oriented at different angles should yield a matching pattern when the correct geometry is used. This is a powerful method of determining the adsorbate orientation with respect to a metal surface.[3]

In the past, the angular distribution experiments were performed with fixed-energy light sources. However, with the use of variable energy, highly polarized, synchrotron radiation, these studies become even more powerful. If the angular distribution pattern is obtained at a resonance energy where the photoemission is intense, then the noise is eliminated from these experiments and the angles at which photoemission disappears due to symmetry are quite pronounced. As mentioned earlier, this would be the first case in which a resonant partial channel could be separated out and examined independently of the nonresonant partial channels for the photoionization of a given orbital. This is completely impossible in a gas-phase experimental photoionization study where the molecule is freely rotating.

Of particular interest in this paper is the study of photoemission from carbon monoxide adsorbed on a nickel surface. CO is known to adsorb to the surface at an orientation parallel to the surface normal, with the carbon atom down. Previous photoionization studies have determined the ionization potentials of the valence orbitals,[1] energy-dependent cross sections at various collection angles,[2] and the photoemission intensity as a function of

the angles of polarization and collection for a fixed photon energy.[3-5] Many of these results were compared to the photoionization spectra of free CO[8] and oriented CO.[7]

The photoelectron spectrum of free CO at 40.8 eV[1] exhibits three peaks at binding energies of roughly 14, 17, and 20 eV. These correspond to photoionization of the 5σ, 1π, and 4σ levels, respectively. The 5σ level, a $\sigma 2p$ orbital, is a lone pair on the carbon atom while the 4σ level is a σ^*2s orbital located primarily on the oxygen atom. Hence, the 5σ orbital is expected to be the most perturbed when the CO molecule is adsorbed on a nickel surface. The binding energy spectrum of CO adsorbed on a nickel surface has been more difficult to interpret. The spectrum exhibits two peaks at binding energies of roughly 13 and 16 eV. The original interpretation of this spectrum[9] was that the peak at 13 eV was due to the 5σ-derived orbital (henceforth referred to as the $\overline{5\sigma}$ orbital) and that the $\overline{1\pi}$ orbital gave rise to the peak at 16 eV. However, it was later shown that there was no peak at higher energy which could be attributed to the $\overline{4\sigma}$ level so new assignments were suggested.[1] The low energy peak was assigned to the nearly degenerate $\overline{1\pi}$ and $\overline{5\sigma}$ levels while the higher energy peak was assigned to the $\overline{4\sigma}$ orbital. This assignment is consistent with data from experiments in which energy-dependent cross sections of NiCO[1] were compared to those of free CO.[8]

A theoretical treatment of CO adsorbed on a nickel surface is quite difficult. Incorporating a description of the metal surface and a description of the effects of the surface interactions on the valence orbitals is not easy and is beyond the scope of ab initio theoretical methods. The first attempt[7]

at modeling an adsorbed CO molecule was simply to orient the CO molecule in a fixed direction, just as if it were on the nickel surface. Thus, no surface effects were incorporated into this model, except to fix the direction of orientation. No perturbations of the CO molecule were allowed. These calculations were performed using the continuum multiple-scattering method in which a crude muffin-tin model of the potential is employed. The results of this study were, at best, in poor qualitative agreement with the experimental data.

An oriented CO molecule is clearly a very limited model of adsorbed CO. Such a model includes no effects of the metal on the bonding to the CO molecule. As a first step toward improving these results, a method is needed in which the effects of the metal surface are included. The method used in this study incorporates the effects of the metal surface via a single nickel atom; i.e., we performed a study on the linear, triatomic molecule NiCO. This is a reasonable approximation, especially in light of a recent comprehensive study of many gas-phase metal carbonyls[10] which revealed that a single metal-atom carbonyl complex such as $Ni(CO)_4$ or $Fe(CO)_5$ will reproduce nearly all of the relevant features of the photoionization spectrum of CO adsorbed on a nickel or iron surface, respectively. Similar conclusions can be drawn from a study of $Cr(CO)_6$.[11] Thus, an understanding of small transition metal complexes is a direct step toward understanding adsorbate-substrate interactions.

In this chapter we report the results of our ab initio theoretical study of the photoionization spectrum of the $\overline{5\sigma}$ level of the linear triatomic molecule NiCO. These are the first results presented at the static-exchange

level. We present absolute gas-phase cross sections and asymmetry parameters and compare them to our calculated results for the 5σ level of free CO in order to observe the effects of the nickel atom on the photoemission of this orbital. We also present energy dependent cross sections for the oriented NiCO obtained at fixed collection angles and compare these to our results for oriented CO and to experimental data. The third type of spectrum we present is photoemission intensity as a function of collection angle for a fixed energy source. These results are also compared to our results for free CO, the multiple-scattering results, and the measured data. We first present the calculational details and then our results which we discuss in detail.

II. DETAILS OF THE CALCULATIONS

We performed our scattering calculations at the exact static-exchange level using a method described previously.[12] In this method the wave function is partial-wave expanded about a single center and a set of coupled radial equations is solved. The local contribution to the potential is treated exactly and the nonlocal exchange component is rendered separable by approximating it as a Schwinger separable potential.[13] This method has been applied successfully to the photoionization of the valence orbitals of CO[14] and NO.[15]

Our SCF wave function was composed of a (10s, 5p, 1d) set of Gaussian functions contracted to a (3s, 2p, 1d) set on carbon and oxygen each, with a (14s, 11p, 5d) set contracted to an (8s, 6p, 2d) set on the nickel atom. This set was augmented with diffuse s and p functions on the origin. These diffuse

Gaussian basis functions were necessary in order to obtain the correct long-range behavior of the bound orbital. Earlier studies of the photoionization of carbon monoxide showed that one obtains qualitatively different 5σ cross sections depending upon whether the molecular wave function was composed of Slater type orbitals or Cartesian Gaussian functions. By augmenting the standard Gaussian basis with diffuse Gaussian functions, the cross section is brought into agreement with the one obtained from using Slater orbitals. We chose the C-O bond length to be 2.173 a.u. which is the length of this bond in $Ni(CO)_4$. Likewise, the Ni-C bond was fixed at 3.477 a.u. for the same reason.[16] Because the ground electronic state of NiCO has not been determined definitively, we based our choice of a $^1\Sigma^+$ ground state on theoretical studies.[16,17] We chose this state, in which the nickel atom has an s^0d^{10} configuration, because this is the configuration about the nickel atom in $Ni(CO)_4$. With this choice and the given bond lengths, our SCF total energy was -1618.7383 a.u.

Because we did not approximate the nickel core with an effective potential, we found this part of the NiCO bound orbitals a bit difficult to converge by single-center expansions. However, we obtained converged cross sections to better than 10% by using the same truncation parameters as Lucchese and McKoy in their study of CO.[18] Our scattering basis set consisted of Cartesian Gaussians defined by

$$\phi_{\alpha\ell mnA}(\mathbf{r}) = N(x-A_x)^{\ell}(y-A_y)^{m}(z-A_z)^{n}\exp(-\alpha|\mathbf{r}-\mathbf{A}|^2) \qquad (1)$$

and the functions were centered on each nucleus. Our basis sets for the $5\sigma \rightarrow k\sigma$ and $5\sigma \rightarrow k\pi$ channels are given in Table I.

In this chapter we will discuss differential cross sections for a freely rotating gas molecule and for a molecule oriented with respect to a surface. For the freely rotating molecule the angular distribution is characterized by the asymmetry parameter, β, defined by

$$\frac{d\sigma}{d\Omega_k} = \frac{\sigma}{4\pi} \left(1 + \beta_{\hat{k}} P_2(\cos\Theta)\right) \tag{2}$$

where is the angle between the polarization vector $\hat{n}$ and the direction of the photoelectron, given by $\hat{k}$. The asymmetry parameter is given by[19,20]

$$\beta_{\hat{k}} = \frac{3}{5} \frac{1}{\sum_u D_\mu} \sum_{\substack{\ell m \mu \\ \ell' m' \mu' \\ \mu''}} (-1)^{m-\mu'} I_{\ell m \mu} I^*_{\ell' m' \mu'} \left((2\ell+1)(2\ell'+1)\right)^{1/2}$$

$$\times (1100|20)\ (\ell\ell'00|20)\ (11-\mu\mu'|2\mu'')\ (\ell\ell'm-m'|2-\mu''),$$

where $(j_1 j_2 m_1 m_2 | j_3 m_3)$ is a Clebsch-Gordon coefficient, $I_{\ell m \mu}$ is defined by the expansion of the dipole matrix element in spherical harmonics about $\hat{k}$ and $\hat{n}$

$$I_{k,\hat{n}} = \frac{4\pi}{3}^{1/2} \sum_{\ell m \mu} I_{\ell m \mu} Y^*_{\ell m}(\Omega_{\hat{k}}) Y^*_{1\mu}(\Omega_{\hat{n}}), \tag{3}$$

$$D_\mu = \sum_\ell |I_{\ell, \Delta m-\mu, \mu}|^2,$$

and for linear molecules

$$\Delta m = m\,(\Psi_i) - m\,(\text{ion core}).$$

We note that the expression for the angular distribution in Eq. (2) depends only upon the angle between $\hat{k}$ and $\hat{n}$.

When the molecule is adsorbed on a surface it is no longer free to rotate. Its orientation is fixed and now the angular distribution becomes a function of $\hat{k}$ and $\hat{n}$ which are measured relative to the surface normal. To derive an expression for the angular distribution of the photoelectrons of oriented molecules we begin, as in the case of the randomly oriented molecule, with the doubly differential cross section[19]

$$\frac{d\sigma}{d\Omega_{\hat{k}}\, d\Omega_{\hat{n}}} = \frac{4\pi^2 E}{c} \left| I_{\mathbf{k},\hat{n}} \right|^2.$$

We insert the partial wave expansion of Eq. (3) into this expression to obtain

$$\frac{d\sigma}{d\Omega_{\hat{k}}\, d\Omega_{\hat{n}}} = \sum_{\substack{\ell m \mu \\ \ell' m' \mu}} I^*_{\ell' m' \mu'} I_{\ell m \mu} Y_{\ell' m'}(\Omega_{\hat{k}}) \times Y_{1\mu}(\Omega_{\hat{n}}) Y^*_{\ell m}(\Omega_{\hat{k}}) Y^*_{1\mu}(\Omega_{\hat{n}}).$$

The expression is then converted from the body-fixed frame into the laboratory frame by using the rotation matricies. Unlike in the case of the freely rotating gas-phase molecule, we do not average over all polarization angles. Thus, after considerable algebra we obtain a general form for the

differential cross section

$$\frac{d\sigma}{d\Omega_{\hat{k}}\, d\Omega_{\hat{n}}} = \frac{4\pi^2 E}{c} \sum_{\substack{\ell m \\ \ell' m'}} B_{\ell m \ell' m'} Y_{\ell m}(\Omega_{\hat{k}}) Y_{\ell' m'}(\Omega_{\hat{n}}). \qquad (4)$$

This form is applicable to a linear molecule adsorbed at an angle $\hat{R}$ with respect to the surface normal (z-axis). For this case we have

$$B_{hijk} = \left[(2h+1)(2j+1)\right]^{-1/2} (1100|j0)$$

$$\times \sum_{\substack{\ell m \mu \\ \ell' m' \mu'}} (-1)^{m+\mu} \left[(2\ell+1)(\ell'+1)\right]^{1/2} I^*_{\ell' m' \mu'} I_{\ell m \mu}$$

$$\times (\ell\ell' 00|h0)(\ell\ell' -mm'|h\ m'-m)(11-\mu\mu'|j\ \mu'-\mu)$$

$$\times \sum_{n} (hj\ m'-m\ \mu'-\mu|n0)(hjik|n\ i+k) D^n(R)_{i+k,0}. \qquad (5)$$

This general form will simplify if the molecule is adsorbed parallel to the z-axis. In the case in which it does not assume this geometry, an averaging must be performed to take into account all possible orientations of a molecule with a given polar angle with the z-axis. We will make use of the differential cross sections of Eqs. (2) and (4) to obtain information about NiCO.

III. RESULTS AND DISCUSSION

In this section we discuss our results for photoionization of the $\overline{5\sigma}$ level of NiCO. In Figure 1 we present the gas-phase cross sections for this system and compare it to our gas-phase cross section for the photoionization of the 5σ level of CO obtained in an earlier study. We use the experimental ionization potentials of 13.5 and 14.01 eV, respectively[1,8] to fix these curves on the energy axis. We see that the broad 5σ shape resonance is shifted to higher energy and becomes more pronounced when this orbital is perturbed by the metal. Thus, we see immediately that the results have been improved significantly by the inclusion of only one nickel atom. In Figure 2 are the corresponding asymmetry parameters. The usual characteristic structure is present which is observed in the photoionization of valence sigma orbitals. This type of flat, broad asymmetry parameter is seen in the 4σ and 5σ levels of NO[13] and the $3\sigma_g$ level of N_2.[19] These spectra are presented in order to observe some of the effects of the nickel atom on the 5σ orbital. To obtain results which can be meaningfully compared to experiment, we now orient the NiCO molecule. Figure 3 shows our coordinate system for a molecule oriented along the z-axis. In our discussion, the light will always be incident in the yz-plane so that the polarization vector **A** can be broken into two perpendicular components, one in the yz-plane making an angle Θ_A with the z-axis and the other parallel to the x-axis and not shown in the figure. Collection is made in the plane containing the z-axis and the momentum vector **k**. The position of the detector is defined by the angles Θ and ϕ.

In Figure 4 we present energy-dependent cross sections for photoioni-

zation of oriented CO and NiCO. The light is assumed to have a polarization component only in the yz-plane at $\Theta_A = 45^o$ and collection was made along the z-axis. We note that the cross section for the $\overline{5\sigma}$ orbital is roughly five times as large as that for the 5σ orbital. In light of other evidence, this large enhancement of the photointensity is expected. In Figure 5 we plot the data for the same polarization and collection angles, but this time we plot our cross sections for photoionization of the 4σ and 5σ levels of oriented CO, along with the experimental data for the $\overline{4\sigma}$ and $\overline{5\sigma}$ levels[2] of adsorbed CO. The experimental data have been normalized so that the peak heights of the 4σ and $\overline{4\sigma}$ levels coincide. We expect these levels to exhibit somewhat similar photoionization spectra because the $\overline{4\sigma}$ level is not perturbed nearly as much as the $\overline{5\sigma}$ in adsorbed CO. With this normalization, we see that the photoemission intensity of the $\overline{5\sigma}$ level is roughly five times that of the 5σ level of oriented CO. The experimental data of Williams et al.[4] in a fixed-energy angular distribution experiment, when combined with our 4σ and 5σ data for oriented CO, also suggests a large enhancement in the $\overline{5\sigma}$ cross section relative to the 5σ cross section for observation along the z-axis.

With this observation, we have normalized the unnormalized experimental cross sections for $\overline{5\sigma}$ photoionization[2] to our results of the $\overline{5\sigma}$ level of NiCO and included these in Figure 4. We note that the position of resonance has shifted to higher energy as expected, due to the screening of the ion by the metal electrons. We also observe that the experimental resonance is quite broad. This is due to several factors. There is a weak

$(\overline{1\pi})^{-1}$ cross section included in this band which would have the effect of broadening the resonance on the high-energy side. This band is not resolved from the $(\overline{5\sigma})^{-1}$ band because they have similar ionization potentials and hence cannot be easily resolved. This band may also be broadened due to surface effects such as photoemisison or reflection.

In Figure 6 we present angular distribution patterns for unpolarized light incident at 45° and collection made in the yz-plane (θ_A = 45°, 0° $\leq \theta \leq$ 90°, and ϕ = 0° in Fig. 3). We present our calculated results for oriented CO and NiCO and compare them to the experimental data for the $\overline{5\sigma}$ orbital[4] which we have normalized to match the peak height of our $\overline{5\sigma}$ angular distribution. The energy of the incident photon was 40.8 eV. We see that the angular distribution of oriented NiCO is quite different from oriented CO, reflecting the perturbation of the $\overline{5\sigma}$ level by the nickel atom. Our agreement with the experimental data is fair, at best. The reasons for the discrepancy are not obvious. It could be due to the choice of an s^0d^{10} configuration about the nickel atom. Certainly an ion with an s^1d^9 or s^2d^8 configuration would yield a different pattern. Angular distributions should be obtained at other photon energies, preferably at an energy where photoemisison is more intense, to see if closer agreement results.

In Figure 7 we compare our theoretical results for photoionization of the 5σ and $\overline{5\sigma}$ levels to those obtained using the continuum multiple-scattering model.[5] The photoemisison intensity is seen to increase for the $\overline{5\sigma}$ level in our calculations, while the opposite is true in the multiple-scattering results. As we have discussed, experiments have confirmed that

the photoemission intensity from this orbital increases upon adsorption, so the correct trend is predicted by our calculations. The differences between our results and the multiple-scattering results are due simply to the inaccuracies which arise from representing the potential by a local muffin-tin approximation. In this model, the potential is approximated by a constant value in over 70% of the molecular region. The choice of the size of each muffin-tin sphere is arbitrary, and a recent report[21] has shown that the cross sections for photoionization change radically both in magnitude and position when the sizes of the spheres are changed.

IV. CONCLUSIONS

We have presented results for the photoionization of the $\overline{5\sigma}$ level of the linear triatomic molecule NiCO. When the orientation of this molecule is fixed, this becomes an excellent model of CO adsorbed on a nickel surface. We have presented both energy-dependent cross sections at a fixed collection angle for polarized light and angular distributions for a fixed photon energy. Our results indicate that inclusion of a nickel atom in the calculations brings about significant changes in the cross sections and angular distributions relative to those for oriented CO.

The most useful part of the study of adsorbed molecules is obtained when full advantage is taken of the fact that the angle of incidence can be specified, unlike the case of gas-phase molecules. This allows for the resolution of partial channels if the polarization and collection directions are correctly chosen. It also affords the determination of the bonding geometry if this is unknown. Clearly the photoionization of adsorbed species is a much

more powerful probe of the system than for the same molecule in the gas phase.

References and Notes

(1) T. Gustafsson, E. W. Plummer, D. E. Eastman, and J. L. Freeouf, Solid State Commun. **17**, 391 (1975).

(2) C. L. Allyn, T. Gustafsson, and E. W. Plummer, Chem. Phys. Lett. **47**, 127 (1977).

(3) G. Apai, P. S. Werner, R. S. Williams, J. Stöhr, and D. A. Shirley, Phys. Rev. Lett. **37**, 1497 (1976).

(4) P. M. Williams, P. Butcher, J. Wood, and K. Jacobi, Phys. Rev. B **14**, 3215 (1976).

(5) J. Davenport, J. Vac. Sci. Technol. **15**, 433 (1978).

(6) J. Hermanson, Solid State Commun. **22**, 9 (1977).

(7) J. W. Davenport, Phys. Rev. Lett. **36**, 945 (1976).

(8) E. W. Plummer, T. Gustafsson, W. Gudat, and D. E. Eastman, Phys. Rev. A **15**, 2339 (1977).

(9) D. E. Eastman and J. K. Cashion, Phys. Rev. Lett. **27**, 1520 (1971).

(10) E. W. Plummer, W. R. Salaneck, and J. S. Miller, Phys. Rev. B **18**, 1673 (1978).

(11) G. Loubriel and E. W. Plummer, Chem. Phys. Lett. **64**, 234 (1979).

(12) M. E. Smith, R. R. Lucchese, and V. McKoy, Phys. Rev. A **29**, 1857 (1984).

(13) D. K. Watson and V. McKoy, Phys. Rev. A **20**, 1474 (1979).

(14) D. L. Lynch, M. E. Smith, and V. McKoy (manuscript in preparation). This work is reported in Chapter III of this thesis.

(15) M. E. Smith, R. R. Lucchese, and V. McKoy (submitted for publication). This work is reported in Chapter II of this

thesis.

(16) A. B. Rives and R. F. Fenske, J. Chem. Phys. **75**, 1293 (1981).

(17) S. P. Walch and W. A. Goddard, J. Am. Chem. Soc. **98**, 7908 (1976).

(18) R. R. Lucchese and V. McKoy, Phys. Rev. A **28**, 1382 (1983).

(19) R. R. Lucchese, G. Raseev, and V. McKoy, Phys. Rev. A **25**, 2572 (1982).

(20) J. W. Davenport, Ph.D. Thesis, University of Pennsylvania (1976).

(21) A. Schiel, D. Menzel, and N. Rösch, Chem. Phys. Lett. **105**, 285 (1984).

TABLE I. Scattering basis sets for photoionization of the 5σ level of NiCO.[a]

Partial Channel	Center	ℓ	m	n	α
$5\sigma \rightarrow k\sigma$	Ni	0	0	0	32.0, 16.0, 6.0, 2.0, 0.6, 0.2
		0	0	1	8.0, 2.0, 0.5
		0	0	2	2.0, 0.5
	C	0	0	0	10.0, 4.0, 1.5, 0.5, 0.1
		0	0	1	1.0, 0.1
		0	0	2	1.0
	O	0	0	0	10.0, 4.0, 1.5, 0.5, 0.1
		0	0	1	1.0, 0.1
		0	0	2	1.0
$5\sigma \rightarrow k\pi$	Ni	1	0	0	32.0, 16.0, 6.0, 2.0, 0.6, 0.2
		1	0	1	8.0, 2.0, 0.5
	C	1	0	0	10.0, 4.0, 1.5, 0.5, 0.1
		1	0	1	1.0, 0.1
	O	1	0	0	10.0, 4.0, 1.5, 0.5, 0.1
		1	0	1	1.0, 0.1

[a]The basis functions are defined in Eq. (1).

FIGURE CAPTIONS

Figure 1: Cross sections for photoionization of the 5σ and $\overline{5\sigma}$ levels of CO and NiCO in the gas phase: (——), dipole-length form; (— —), dipole-velocity form.

Figure 2: Asymmetry parameters for photoionization of the 5σ and $\overline{5\sigma}$ levels of CO and NiCO in the gas phase: (——), dipole-length form; (— —), dipole-velocity form.

Figure 3: The coordinate system used in our calculations. The molecule is oriented along the z-axis as shown. Photons are incident in the yz-plane. The polarization vector A has a component in the yz-plane, making an angle Θ_A with the z-axis. The other component is parallel to the x-axis and is not shown. The point of collection is defined by the angles Θ and ϕ.

Figure 4: Cross sections for photoionization of the 5σ and $\overline{5\sigma}$ levels of oriented CO and NiCO: (——), dipole-length form for CO; (— —), dipole-length form for NiCO; (Δ), experimental data of ref. 2 for CO adsorbed on nickel. The polarization and collection angles, defined in Figure 3, are $\Theta_A = 45^o$, $\Theta = 0^o$, and $\phi = 0^o$.

Figure 5: Cross sections for photoionization of the 4σ and 5σ levels of oriented CO along with the corresponding experimental data for CO adsorbed on nickel from ref. 2: (——), dipole-length form for the 5σ level of CO; (— —), dipole-length form for the 4σ level of CO; (Δ), experimental data for the $\overline{5\sigma}$ orbital; (X), experimental data for the 4σ orbitals. The polarization and collection angles, defined in Figure 3, are $\theta_A = 45^o$, $\theta = 0^o$, and $\phi = 0^o$.

Figure 6: Angular distribution for photoionization of the 5σ and $\overline{5\sigma}$ levels of oriented CO and NiCO, along with the experimental data for CO adsorbed on a nickel surface from ref. 4: (——); dipole-length form for oriented CO; (— —), dipole-length form for oriented NiCO; (Δ), experimental data for CO adsorbed on nickel. The light is unpolarized, incident in the yz-plane at 45^o to the normal. Thus, the polarization and colleciton angles are $\theta_A = 45$, $0 < \theta < 90$, and $\phi = 90^o$.

Figure 7: Angular distribution for photoionization of the 5σ and $\overline{5\sigma}$ levels of oriented CO and NiCO: (——), present results, dipole-length form for CO; (–––); present results, dipole-length form for NiCO; (---), multiple-scattering results of ref. 7 for CO; (— —), multiple-scattering results of ref. 5 for NiCO.

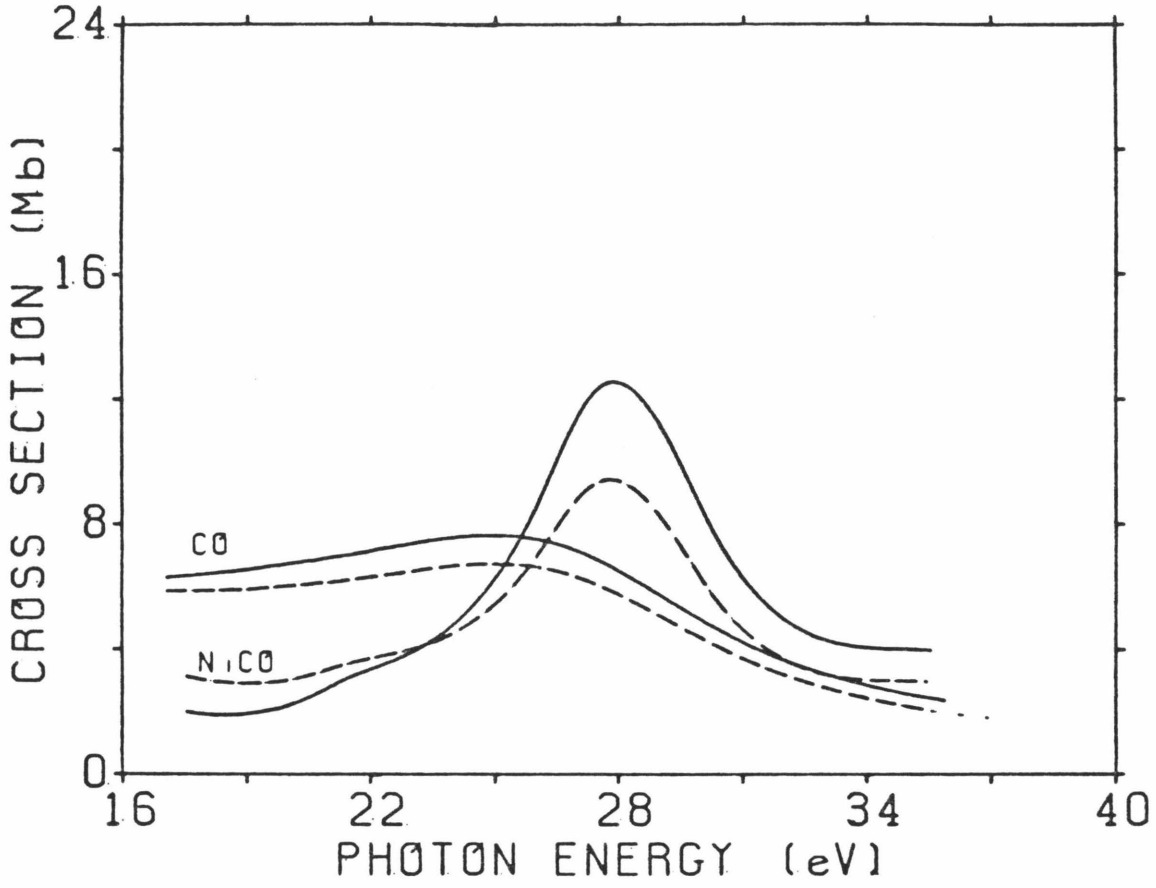
24
16
8
0
CROSS SECTION (Mb)
CO
N2CO
16
22
28
34
40
PHOTON ENERGY (eV)

FIGURE 1.

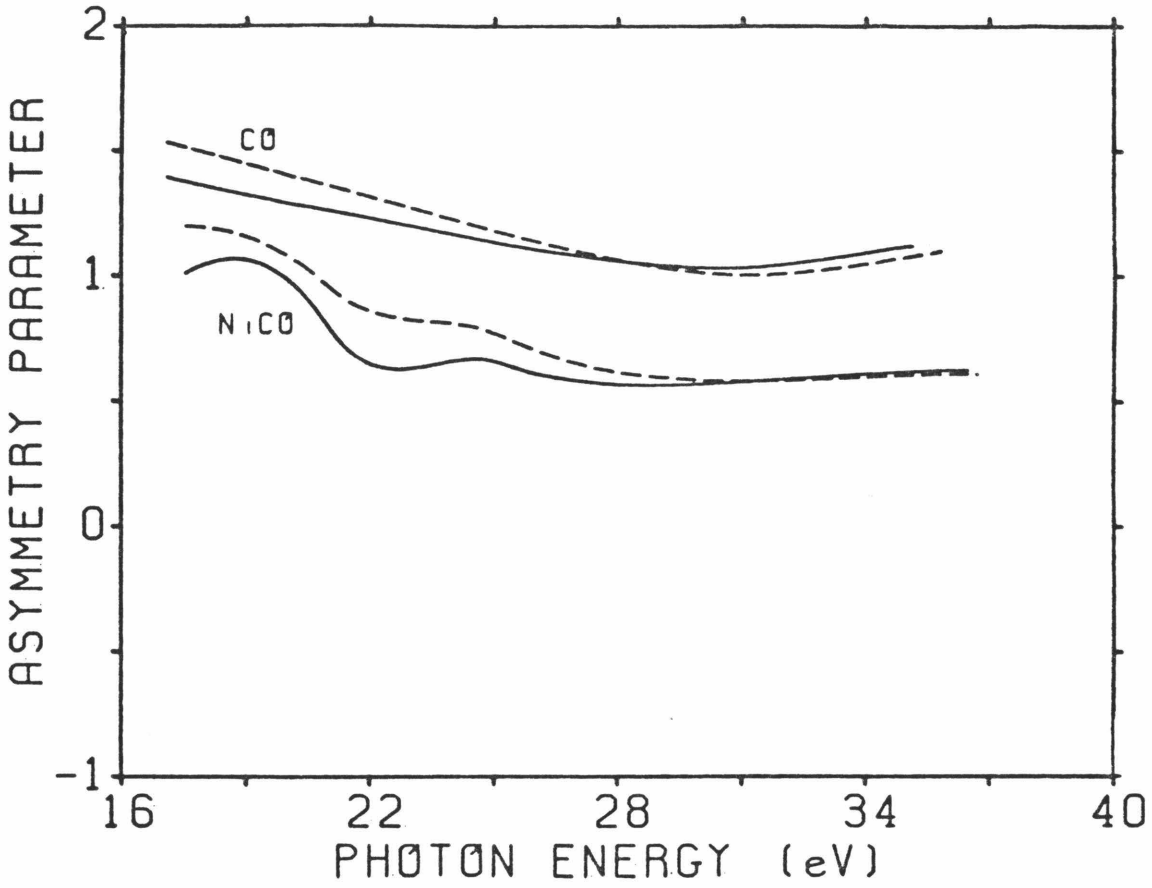
2
1
0
-1
ASYMMETRY PARAMETER
CO
N2CO
16
22
28
34
40
PHOTON ENERGY (eV)

FIGURE 2.

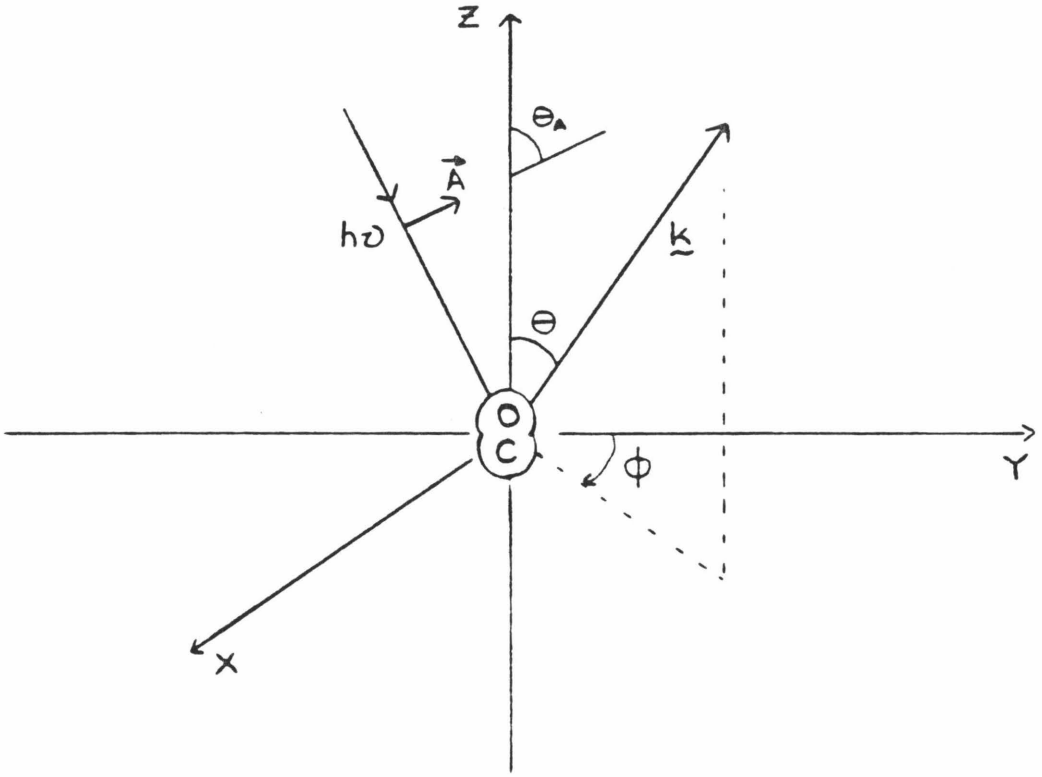

FIGURE 3.

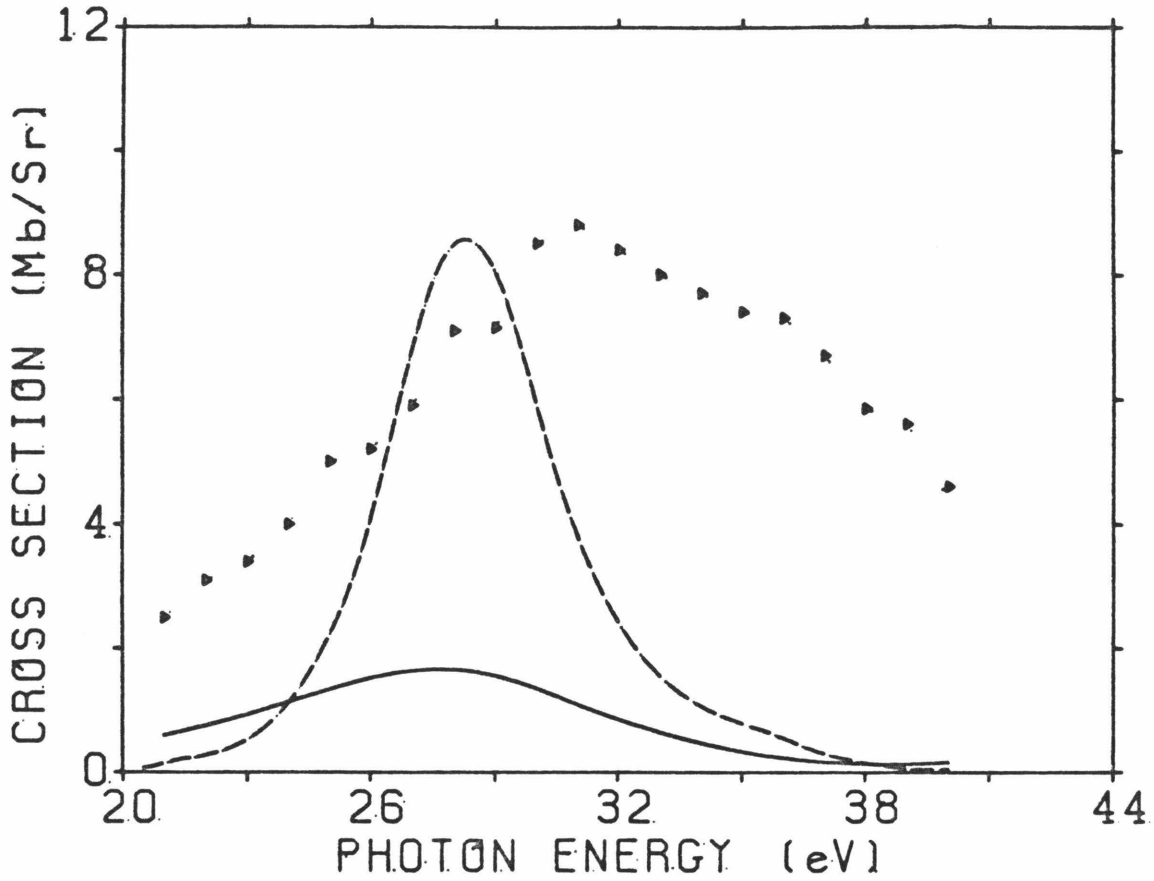

FIGURE 4.

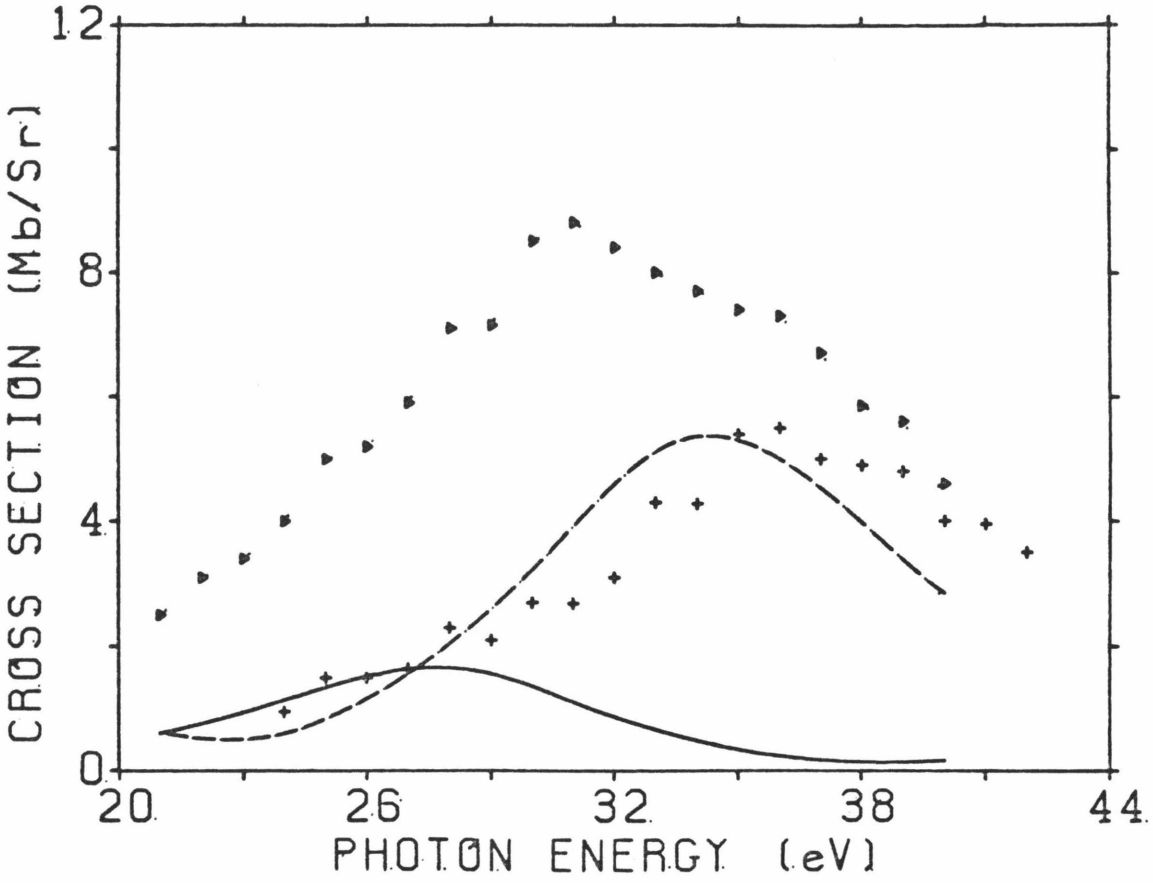

FIGURE 5.

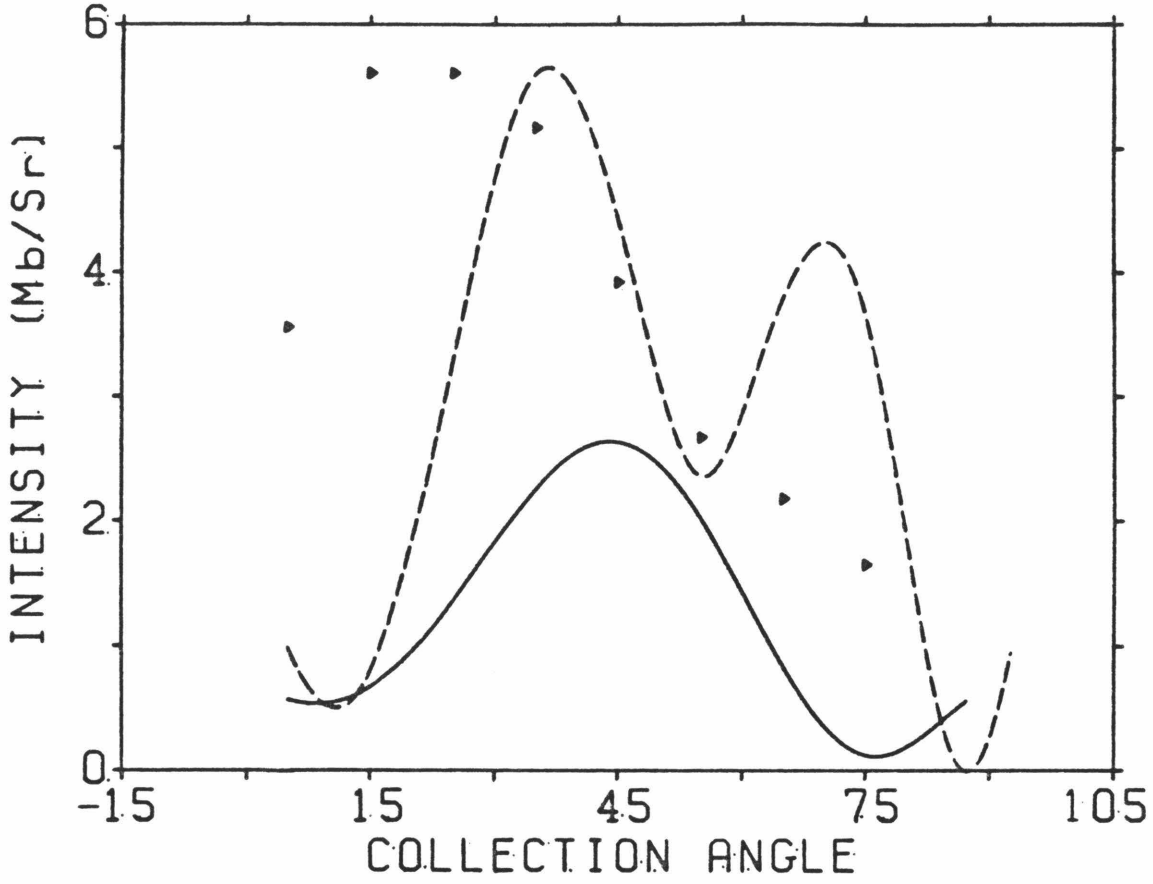

FIGURE 6.

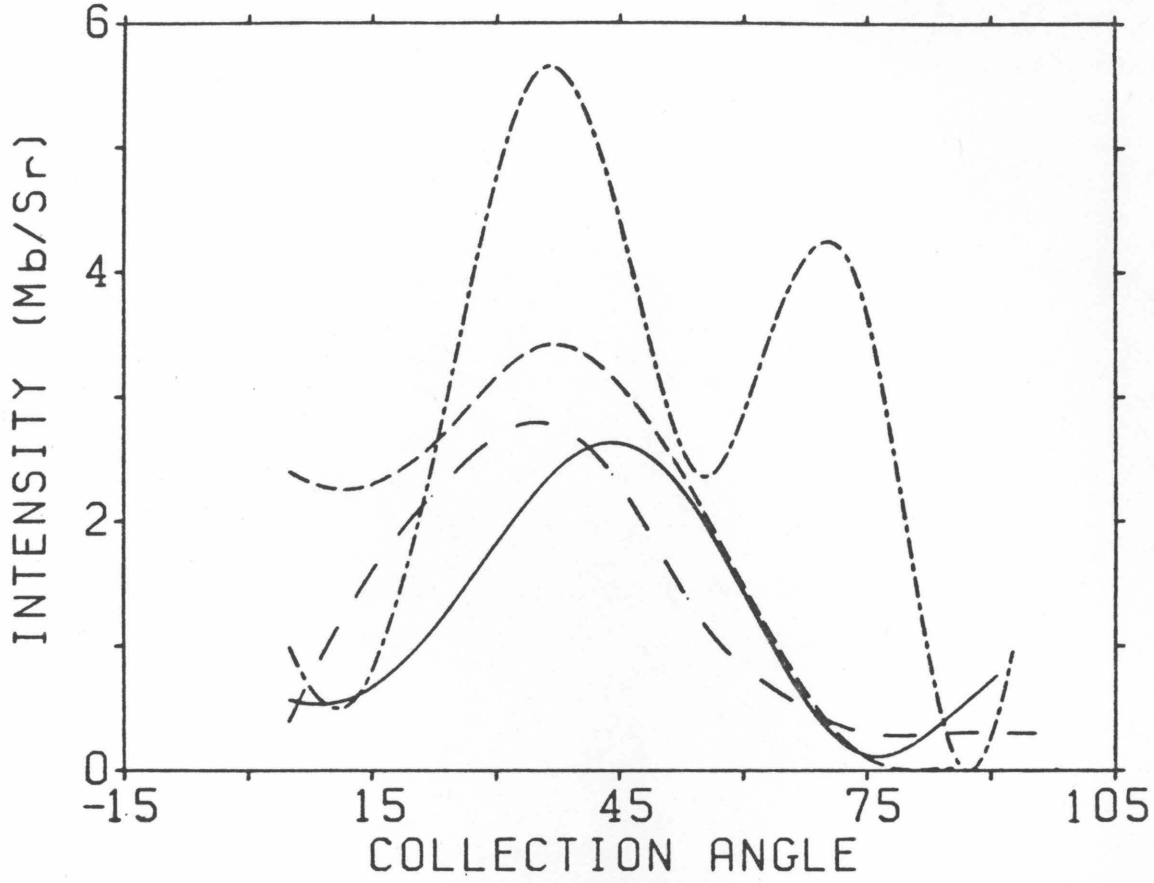

FIGURE 7.